DISSERTATION

submitted to the
Combined Faculty of Natural Sciences and Mathematics
of the Ruperto Carola University Heidelberg, Germany
for the degree of
Doctor of Natural Sciences

Presented by
Anupriya Chatterjee, Master of Biological Sciences
born in: Dhanbad, India
Oral examination: 15th November 2019

The role of Tie-2 and protein O-GlcNAcylation in Ang-2 regulation in NDPK-B deficiency - a vasoregressive model

Referees: Prof. Dr. Thomas Wieland

PD Dr. Yuxi Feng

Acknowledgement

This thesis sees 4 years of hard work condensed into 110 pages. It has been a long, tortuous and yet a remarkable journey. The guidance I have received, the knowledge I gleaned, and the memories I made are incomplete without the people that made it possible.

I would like to thank Prof. Dr. Thomas Wieland for providing me with the opportunity to work on this project and guiding the completion of my project. I am grateful to him for providing me with the encouragement to collaborate and broaden my understanding of science.

A heartfelt mention goes to my supervisor Dr. Yuxi Feng for being an incredible advisor and boosting my morale in difficult times. I thank her for mentoring me with competent expertise and patience, for her untiring support, and for instilling in me the invaluable benefits of seamless teamwork.

Our technician Heike Rauscher deserves commendation for aiding me with the animal experiments. Without her expertise, I may have found it hard to finish in a timely fashion. I thank our other technicians Heinz, Zenon, Tina, Sabine, and Doris for their invaluable support in the smooth running of the lab.

They say great colleagues are those who make work seem like play. I was blessed with the best co-workers who have now moved on to become close friends. My memories of my PhD would be incomplete without Yi, Joost, Rachana, Philipp, Santosh, Alex, and Shenliang. Our animated discussions of science, the news, fan fiction, and our frequent forays into ethnic cooking will remain with me for years to come.

I would like to acknowledge DIAMICOM, and particularly Prof. Dr. Hans-Peter Hammes, for making it possible for me to partake, learn, and impart knowledge in the arena of diabetic microvascular complications and enabling me to connect to my fellow peers. I also thank Dr. Gernot Poschet and Dr. Thomas Fleming for their assistance and generous help with my findings and Dr. Kerstin Wilhelm for taking the time to mentor me.

This acknowledgement would be incomplete without a shout out to my friends and family. My parents Dr. Swati Chakrabarty and Prashant Shirpurkar, for their undying moral support and for making me who I am today. I thank Ian Bumbalough for his ever-enduring patience in times, when I ran out of mine. Last but not the least, I thank Dr. Krishna Rakesh Sharma for her keen scientific eye and for always being in my corner.

Table of Contents

List of Figures

List of Tables

Summary

Similar to high glucose (HG) levels, ablation of nucleoside diphosphate kinase B (NDPK-B) causes a diabetic retinopathy-like vascular pathology. NDPK-B deficient retinae and endothelial cells (ECs) showed increased levels of Angiopoietin 2 (Ang-2) and protein O-GlcNAcylation. In this study we investigated the regulation of the Ang-2 receptor, Tie-2, the Hexosamine Biosynthesis Pathway (HBP), and the protein O-GlcNAc removing enzyme O-GlcNAcase (OGA) in NDPK-B deficiency.

The Ang-2 elevation in NDPK-B$^{-/-}$ retinae was found to be crucial for the development of vasoregression. The regulation of Tie-2 was observed in NDPK-B$^{-/-}$ retinae, specifically in the deep capillary layer. In vitro, the upregulation of Tie-2 was mirrored in NDPK-B-depleted ECs from different origins, whereas no alteration of Tie-2 expression was observed by HG treatment. Tie-2 enrichment occurred at the endothelial plasma membrane upon NDPK-B depletion. Similar to HG, NDPK-B depletion blunted Tie-2 receptor phosphorylation. Although both HG and NDPK-B deficiency elevated the secretion of Ang-2, intracellular and released Ang-2 was higher in NDPK-B depleted ECs. Interference with Tie-2 expression and Ang-2-binding attenuated NDPK-B depletion-induced, but not HG-induced Ang-2, upregulation. Mimicking NDPK-B depleted conditions, the overexpression of recombinant Ang-2 promoted the upregulation of Tie-2 in ECs.

NDPK-B deficiency induced an increase in protein O-GlcNAcylation. Mass spectrometry measurements showed that NDPK-B depletion in ECs elevated the HBP end product, UDP-GlcNAc, without changes in glycolysis, indicating a shift from glycolysis to the HBP. Although NDPK-B accounted for about 20% of the total NDPK activity in ECs and 35% in retinae, its ablation did not alter nucleotide triphosphate levels. NDPK-B depletion led to an increase in the protein content of glutamine:fructose-6-phosphate amidotransferase (GFAT), the rate-limiting enzyme of the HBP, accompanied by an EC-specific suppression of OGA activity. Both together resulted in an increase in protein O-GlcNAcylation and Ang-2 levels which was independent of the catalytic activity of NDPK B. It was similarly rescued by adenoviral re-expression of either wild type or a catalytically inactive mutant of NDPK-B.

In summary, NDPK-B depletion directly influences the participation of the HBP in glucose metabolism via alteration of GFAT levels and suppression of OGA activity, which subsequently further increases protein O-GlcNAcylation and upregulates Ang-2. NDPK-B deficiency additionally induces an increase in Tie-2 levels which further supports Ang-2 production and secretion in a positive feedback loop. As enhanced Tie-2 expression was detected on the vasculature of NDPK-B-deficient mice, showing early stages of pathological vasoregression, it likely contributes together with enhanced protein O-GlcNAcylation to this Ang-2-driven pathology leading to vasoregression.

Zussamenfassung

Ähnlich wie ein Hyperglykämie, verursacht die Ablation der Nucleosiddiphosphatkinase B (NDPK-B) eine der diabetischen Retinopathie-ähnliche Gefäßpathologie. Sowohl die Retina als auch Endothelzellen (ECs) mit vermindertem NDPK-B-Gehalt zeigen erhöhten Angiopoietin 2-Gehalt (Ang-2) - und verstärkte Protein-O-GlcNAcylierung. In dieser Arbeit untersuchten wir die Regulation der Ang-2-Rezeptors Tie-2- und der Protein-O-GlcNAcylierung bei NDPK-B-Mangel.

Wie in der Hyperglykämie, erwies die Erhöhung von Ang-2 in der NDPK-B$^{-/-}$ Retina als maßgeblich für die Entwicklung der Vasoregression. Eine Hochregulation von Tie-2 trat insbesondere in der tiefen Kapillarschicht der Retina von NDPK-B$^{-/-}$ Mäusen auf. In vitro konnte die Hochregulation von Tie-2 in ECs aus verschieden Teilen des Gefäßbetts durch Depletion der NDPK-B induziert werden, während eine Behandlung mit hohen Glukosekonzentrationen (HG)-Behandlung keine Veränderung in Tie-2 hervor rief. Bei NDPK-B-Mangel konnte eine Anreicherung von Tie-2- in der Plasmamembran beobachte werden. Ähnlich wie HG reduzierte eine NDPK-B-Depletion die Phosphorylierung des Tie-2-Rezeptors. Obwohl sowohl HG- als auch NDPK-B-Mangel die Sekretion von Ang-2 erhöhten, war der Anstieg an intra- und extrazellulärem Ang-2 in ECs nach NDPK-B-Depletion deutlich stärker ausgeprägt. Durch Verminderung der Funktion bzw. Expression von Tie-2 konnte die durch NDPK-B-Depletion, nicht aber die HG-induzierte Ang-2-Hochregulation. Ähnlich wie die NDPK-B-Depletion, erhöhte die Überexpression von rekombinantem Ang-2 in ECs die Ang-2-Sekretion und förderte die Hochregulation von Tie-2.

In vorausgegangen Arbeiten unseres Labors, in denen ein durch NDPK-B-Verlust bedingter Anstieg der Protein-O-GlcNAcylierung beobachtet werden. Durch massenspektrometrische Analysen konnte hier nachgwiesen werden, dass ein NDPK-B-Verlust mit einem Anstieg in der Menge des Endprodukts des Hexosamin-Biosynthesewegs (HBP), UDP-GlcNAc, einhergeht, ohne dass es dabei zu Veränderungen Glykolyserate -kam. Dies deutet was auf eine Verschiebung des Metabloismus von der Glykolyse zum HBP hin. Obwohl NDPK-B etwa 20% bzw. 35% der gesamten NDPK-Aktivität in ECs und Retinae ausmachte, änderte deren Verlust nichtsam Nukleotidtriphosphatgehalt. Die NDPK-B-Depletion führte dagegen zu einer Erhöhung des Proteingehalts der Glutamin:Fructose-6-phosphat-Amidotransferase (GFAT), dem geschwindigkeitsbestimmenden Enzym des HBP, die mit einer EC-spezifischen Reduktion der Aktivität der die O-GlcNAc-Modifkation reduzierenden O-GlcNAcase (OGA) einherging. Die daraus resultierende Zunahme der Protein-O-GlcNAcylierung modifizier war unabhängig von der katalytischen Aktivität der NDPK-B, da sie in ähnlicher Weise durch adenovirale Reexpression entweder des Wildtyps oder eines

katalytisch inaktiven Mutanten von NDPK-B ausgeglichen wurde. Zusammenfassend induziert ein NDPK-B-Verlust eine Erhöhung des Glucosestoffwechsel HBP durch Anstieg in GFAT, welcher zusammen mit der Reduktion der OGA-Aktivität die Protein-O-GlcNAcylierung erhöht und damit Ang-2 hochreguliert. Expression verändert und anschließend die unterdrückt Die Zunahme in Tie-2 verstärkt die Produktion und Sekretion von Ang-2 in einer positiven Rückkopplungsschleife weiter. Da eine Zunahme sowohl von Tie-2 als auch der Protein-O-GlcNAcylierungin den retinalen Gefäßen von NDPK-B-defizienten Mäusen festgestellt wurde, die bereits frühe Stadien der pathologischen Vasoregression aufwiesen, trägt wahrscheinlich beides zu dieser Ang-2-induzierten Pathologie und damit zur Vasoregression bei.

Abbreviations

2-DG	2-Deoxy Glucose
AC	Acellular Capillaries
AMP	Adenosine MonoPhosphate
ADP	Adenosine DiPhosphate
Akt	Protein Kinase B (PKB)
Ang	Angiopoietin
ANOVA	Analysis Of Variance
APS	Ammonium Peroxide Sulphate
ATP	Adenosine Triphosphate
BSA	Bovine Serum Albumin
CO_2	Carbon Dioxide
DAPI	4',6-Diamidino-2-Phenylindole
dH2O	Distilled Water
DM	Diabetes mellitus
DMEM	Dulbecco´s Modified Eagles Medium
DMSO	Dimethyl Sulphoxide
DNA	Deoxyribonucleic Acid
DR	Diabetic Retinopathy
ECAR	Extracellular Acidification Rate
ECBM	Endothelial Cell Basal Medium
ECGM	Endothelial Cell Growth Media
ECs	Endothelial Cells
eNOS	Endothelial Nitric Oxide Synthase 3

FCCP	Trifluoromethoxy CarbonylCyanide Phenylhydrazone
FCS	Fetal Calf Serum
FITC	Fluorescein Isothiocyanate
FoxO1	Forkhead Box Protein O1
GDP	Guanosine DiPhosphate
GFAT	Glutamine: Fructose-6 Phosphate Amidotransferase
GPCR	G Protein-Coupled Receptor
GTP	Guanosine Triphosphate
HBP	Hexosamine Biosynthesis Pathway (Never mentioned below)
HCl	Hydrochloric Acid
HE	Heterozygous
HRMVECs	Human Retinal Microvascular Endothelial Cells
HMECs	Human Microvascular Endothelial Cells
HUVECs	Human Umbilical Vein Endothelial Cells
IP	Immunoprecipitation
KCl	Potassium Chloride
KD	Knockdown
KH_2PO_4	Potassium Dihydrogen Phosphate
KO	Knockout
MBMECs	Murine Brain Microvascular Endothelial Cells
NaCl	Sodium Chloride
NaOH	Sodium Hydroxide
NDP	Nucleoside DiPhosphate
KD	Knockdown

NTP	Nucleoside TriPhosphate
OCR	Oxygen Consumption Rate
OGA	O-GlcNAcase
O-GlcNAc	O-Linked N-Acetylglucosamine
OGT	O-GlcNAc-Transferase
PAGE	PolyAcrylamide Gel Electrophoresis
PCR	Polymerase Chain Reaction
PCs	Pericytes
RT	Room Temperature
SDS	Sodium Dodecyl Sulfate
sWGA	succinylated Wheat Germ Agglutinin
TMG	Thiamet G
UDP-GlcNAc	Uridine DiPhosphate N-Acetyl-Glucosamine
WB	Western Blotting
WT	Wild Type

Unit

µl	Microliter
g	Gram
mg	Milligram
M	Molar
mM	Millimolar
mol	Mole
µmol	Micromole
pmol	Picomole
cm	Centimeter
µm	Micrometer
cm^2	Centimeter Squared
mm^2	Millimeter Squared
h	Hour
min	Minute
kDa	KiloDalton
V	Volt
rpm	Revolutions Per Minute
hpt	Hours Post Transfection
p	Passage Number

1. Introduction

1.1 Diabetes and diabetic retinopathy

1.1.1 Diabetes mellitus

Diabetes mellitus (DM) is a long-standing metabolic disorder that has reached epidemic proportions. The fundamental feature of DM is hyperglycemia resulting from defects in insulin secretion and action [1]. Statistics indicate that more than 425 million individuals worldwide suffer from diabetes. Current and past statistics predict the dramatic rise of diabetes to 629 million individuals (48% increase) by the year 2045 (**Fig.1**)

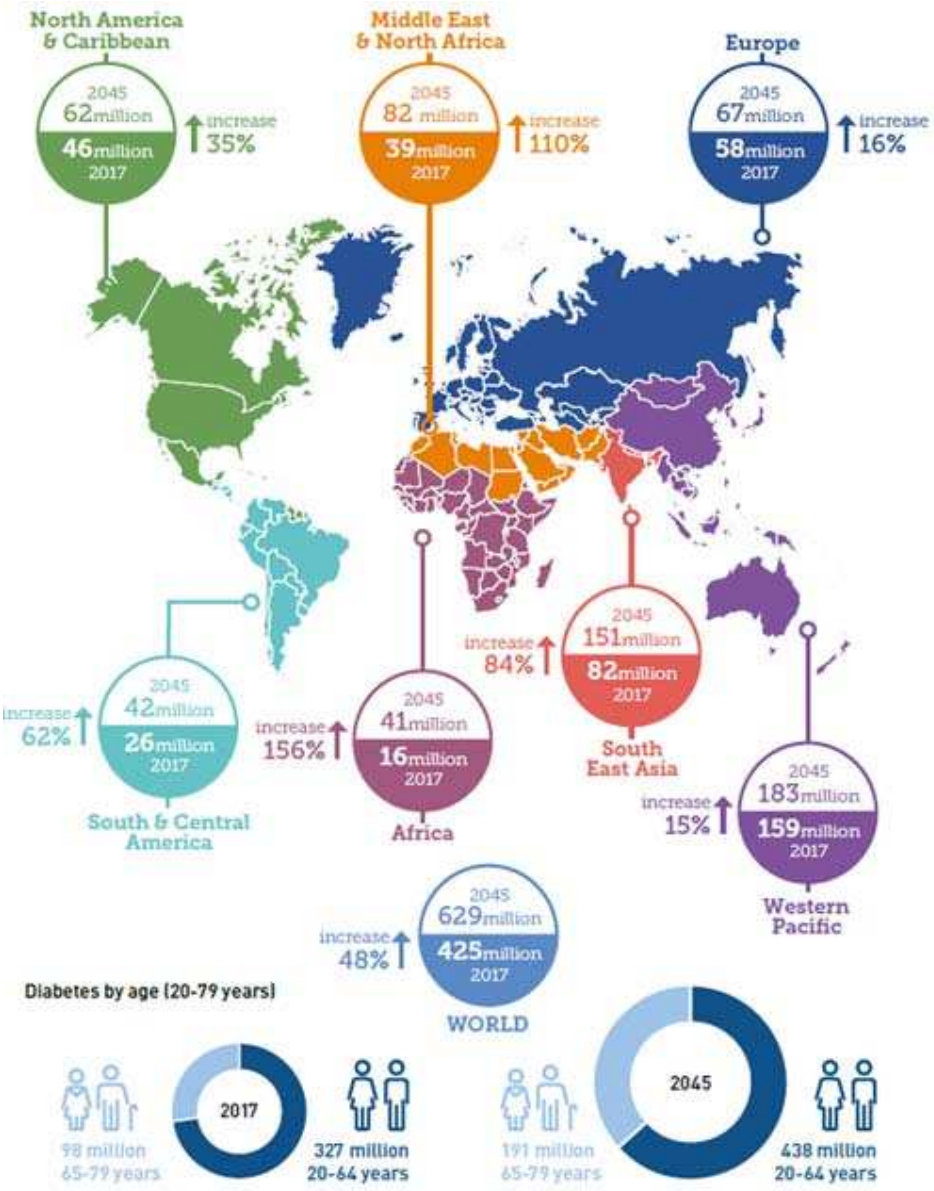

Fig. 1: Global prevalence of diabetes from 2017 to 2045. *Adapted from IDF Diabetes Atlas 2017, International Diabetes Federation [2]*

DM was categorized in 1980 by the World Health Organization (WHO) and subsequently subdivided into several types, the most common being Type 1 and Type 2 DM. Type 1 DM refers to the elevation of blood glucose due to a loss of insulin production as a result of autoimmune destruction of pancreatic β-cells or genetic inheritance [1]. Type 2 DM (T2DM) makes up 90-95% of DM cases. In this subtype, the disease develops due to a combination of impaired production of insulin and resistance to insulin action [3]. Some of the influencing factors for the development of T2DM are obesity, due to poor diet or sedentary lifestyle, and genetic background. The common symptoms of hyperglycemia are polyuria, thirst, blurred vision and weight loss. These symptoms vary with duration and intensity of the disease. Long-term complications of diabetes vary from microvascular in nature, such as, retinopathy, neuropathy and nephropathy to macrovascular, such as coronary heart disease, heart failure, hypertension, peripheral arterial disease, and stroke [4].

1.1.2 Diabetic retinopathy (DR)

Amongst the eye-related late-stage complications of diabetes are retinopathy (DR), macular edema, cataracts, and glaucoma. DR is one of the most prevalent complications of DM, affecting 100 million people worldwide leading to visual impairment and eventually blindness [4, 5]. DR is currently the 5th leading cause of blindness and is predicted to increase to 191 million people by 2030, making it one of the leading causes of acquired vision loss [6]. Although DR currently ails 35% of people worldwide, there has been a decline in retinopathy and its sight-threatening stages due to early detection and new treatment options [7, 8]. Screening for DR in Europe uncovered that over 13% of newly diagnosed type 2 diabetics showed signs of DR, indicating that at the point of diagnosis, the disease is well-advanced and tackled only via glucose lowering therapy [9-11]. The costs of treatment and development of technologies for effective treatment and diagnostic screening for DR in diabetic patients makes it not only a public health burden but also an economic burden [8, 12]. Apart from chronic hyperglycemia, certain genetic and inflammatory markers, sex of the patient, duration of the disease; blood pressure and lipids provide associations with the development of DR and have been studied intensively [12-14]. DR also leads to pathologies in various important cells types of the retina such as the neurons and glial cells, making it larger than only a microvascular disease [15].

1.2 Development and pathogenesis of DR

1.2.1 The classification of DR

The vasculature starts to develop in the late embryonic stage in humans and postnatally in mice allowing for study of initial angiogenesis in animal models. The astrocyte macroglia produce a VEGF gradient that directs the formation of the first plexus in the retina. The endothelial cells (ECs) specialize into three different subtypes to carry out angiogenesis; of which pre-quiescent stalk and quiescent phalanx ECs attract pericytes (PCs) and remain in contact with them [16-19]. Retinal vasculature may be easily visualized by quantitative retinal morphometry and shows similar structural phenotype of EC and PC interaction across species (**Fig. 2**) [20].

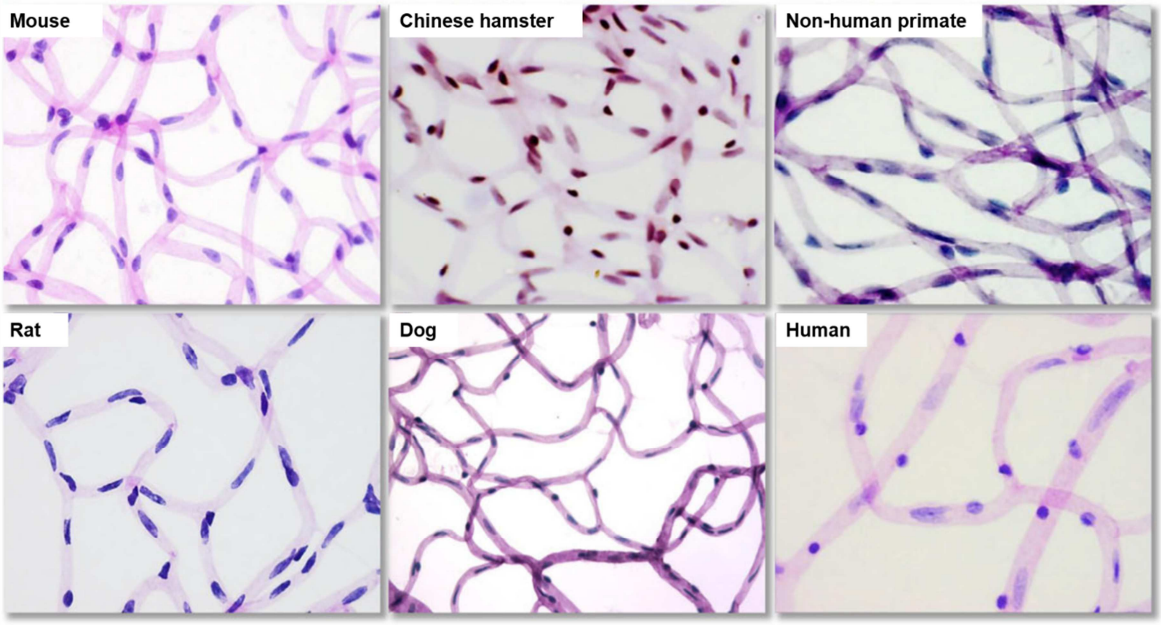

Fig. 2: Retinal digest preparations from several species depicting standard EC and PC interactions phenotype. *Adapted from Dietrich, Methods Mol. Biol. 2012 [20].*

1.2.2 The pathogenesis of DR

The disease severity scale developed for DR was based on findings of Early Treatment of Diabetic Retinopathy Studies (ETDRS) and Wisconsin Epidemiologic Study of Diabetic Retinopathy (WESDR) [21-24]. It is as follows:

Table 1: Classification of observable diabetic retinopathy stages according to ETDRS and WESDR [21-24]

Severity level	***Observable findings***
No apparent retinopathy	No changes found
Mild NPDR	Few microaneurysms
Moderate NPDR	Microaneurysms, hemorrhaging and venous beading
Severe NPDR	Any of the following (4:2:1 rule): • More than 20 intraretinal hemorrhages in each of 4 quadrants • Venous beading in 2 or more quadrants • Intraretinal microvascular abnormalities in 1 or more quadrant
PDR	One or more of the following: Neovascularization of the retina, iris, disc, angle Vitreous hemorrhaging

The microvascular and neuronal changes that classify the development of DR occurs in two broad stages:

- **Non-proliferative diabetic retinopathy (NPDR):**
  This stage marks the importance of PCs in predicting the incidence of vascular damage in DR [25]. Extensive animal studies show that the hallmark of this stage is the loss of two major cell types: the PCs and the ECs. Biochemical changes in ECs cause the loss of PCs, which are essential for vessel quiescence and maturity. PC dropout is, therefore, by far the earliest morphological change seen in DR, occurring 2 months after the onset of diabetes [26-28]. Normally, PC recruitment is mediated by the PDGFB receptor and the Ang-2-Tie-2 system. Dysfunction of these recruiting pathways generates DR-like phenotype, indicating the indispensability of PCs [29, 30]. In the absence of the stabilizing effect of the PCs, ECs die or deteriorate leaving behind a husk of a vessel that does not support blood flow. Acellular capillaries (AC), occur around 6 months after onset of diabetes and can be quantified in retinal digest preps of the retina and represent the degree of vasoregression. Apart from the disintegrating neuro-vascular unit (NVU), other features of this stage are microaneurysms, hemorrhaging, abnormal glial activity and lipid exudates from damaged capillaries [5, 28]. Neurodegeneration begins at 6 weeks and can be measured via electroretinography [31].
- **Proliferative diabetic retinopathy (PDR):**

The non-perfusion of the NPDR stage leads to an ischemic buildup in the retina leading to the release of pro-angiogenic factors such as VEGF and the formation of neovascularizations. Aberrant formation of immature blood vessels in combination with the degeneration of pre-existing vessels, cause vascular leakage into the vitreous and hemorrhages. In certain cases, tractional retinal detachment occurs, leading to blindness [5, 28]. Curiously, no animal models with PDR have been established so far [32].

The pathogenesis of DR cannot be singularly isolated. Intensive research over the years have uncovered several mechanisms such as inflammatory responses, gliosis, altered neural responses, the loss of protective cell-cell interactions and an increase in vessel permeability due to barrier breakdown that lead to DR development. DR is now considered a disease of the NVU instead of a disease of the vasculature alone [33, 34]. The Muller glia (MC) form a link between the neurons and the vasculature and are indispensable for the tightness of the blood-retinal barrier (BRB) and the survival of the neurons and blood vessels (**Fig. 3**). The microglia form immunological gatekeepers and defend against inflammatory signals [35, 36]. Together the micro- and macroglia support the vasculature to form the NVU [14, 37]. Initial chemical changes originating from high blood glucose can be further examined by investigating cellular biochemical pathways in response to high glucose fluxes.

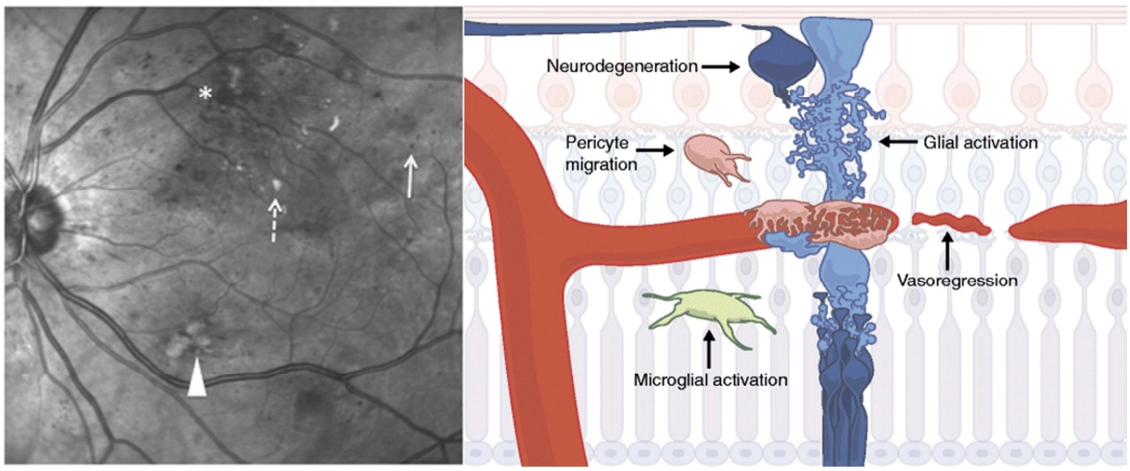

Fig. 3: DR and the retinal microenvironment. *Left panel: The microaneurysms (solid arrow), haemorrhages (asterisk) and hard (dashed arrow) and soft (arrowhead) exudates are as depicted. This stage is classified as severe NPDR. Right panel: Hyperglycemia induced changes to the neurovascular unit in STZ-induced rat retina involving vasoregression due to pericyte dropout/migration, microglia and macroglia activation and neurodegeneration. Adapted from Hammes, Diabetologia 2018 [7]*

1.3 Biochemical mechanisms of diabetes

1.3.1 Hyperglycemia and ROS production

Different cell types respond varyingly to hyperglycemia via their glucose transporters. This determines the susceptibility of the cell to glucose-mediated metabolic changes [38, 39]. Cells susceptible to hyperglycemia showed consistently high reactive oxygen species (ROS) levels than resistant cells [40-42]. Post-TCA cycle, electrons donors NADH and $FADH_2$ enable the transport of electrons from Complex I to II, II and IV in the electron transport chain ETC to be finally converted and reduced to water (**Fig. 4**). The transmembrane pumping of electrons by complexes I, II and IV generates a membrane potential required for ATP production. Excess intracellular glucose drives the flux through the ETC causing the membrane potential to reach a threshold beyond which the ETC is arrested at complex III. The buildup of electrons in coenzyme Q results in electron donation to the oxygen available for production of water, making superoxide instead. *Hyperglycemia therefore drives increased ROS production.*

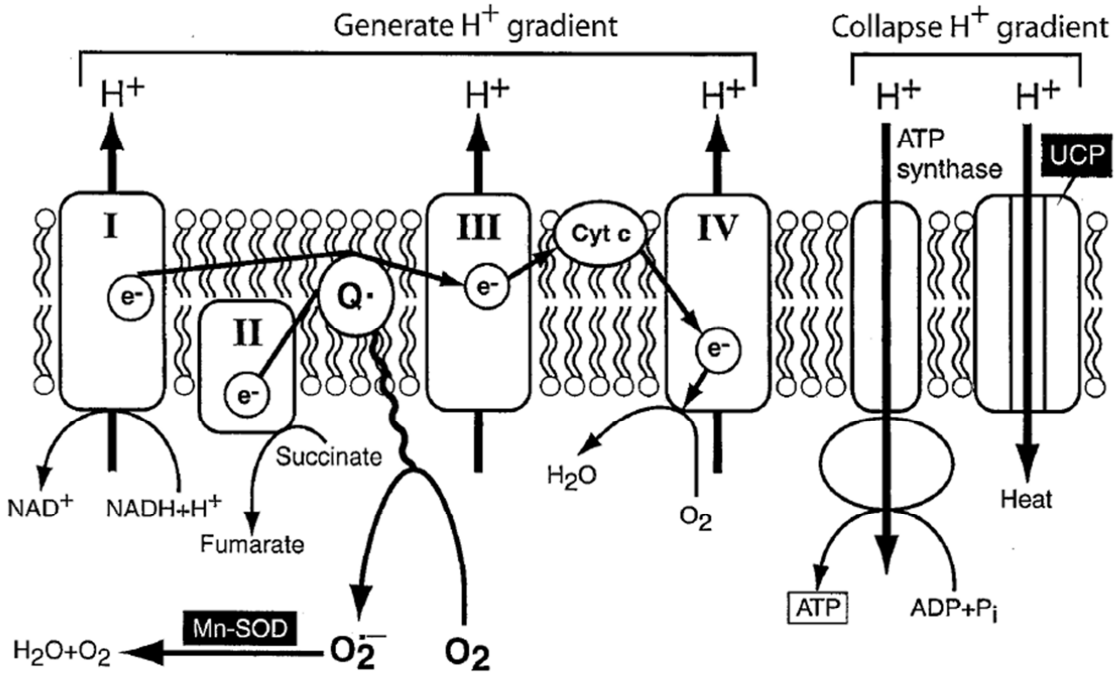

Fig. 4: Hyperglycemia-induced production of ROS. *Excessive glucose increases flux through the ETC, which proceeds until threshold membrane potential is reached. Subsequent blockade of the ETC at complex III generates electron buildup at coenzyme Q, which donates electrons to O_2 for superoxide production resulting in elevated ROS. Adapted from Brownlee, Diabetes 2005 [43]*

1.3.2 Hyperglycemia and GAPDH activity

The crucial enzyme glyceraldehyde-3-phosphate dehydrogenase (GAPDH) catalyzes the formation of 1-3-diphosphoglycerate. Diabetes consistently dampens GAPDH activity in cells and animals with the exception of those without the ability of ROS production [40]. ROS production induces DNA damage that activates PARP, which subsequently dampens the activity of nuclear GAPDH. *Thus, there is a link between increased ROS and lower GAPDH activity.*

1.3.3 Pathways activated by hyperglycemia

Prior research highlights four cardinal mechanisms that are altered intracellularly (**Fig. 5**).

i. ***Polyol pathway:*** focuses on the conversion of high amounts of intracellular glucose to fructose by aldose reductase, a reaction that requires NADPH [44]. By utilizing NADPH for countering excess glucose, it depletes the reserves for the production of the antioxidant, reduced glutathione, thereby increasing susceptibility to oxidative stress. Treatment with aldose reductase inhibitor prevented diabetes mediated cell damage [45].

ii. ***AGE pathway:*** increased advanced glycation end products (AGEs) form as a result of increased intracellular glucose can damage cells on transcriptional level via alteration of gene transcription, modification of extracellular matrix post-secretion and via modification of plasma proteins which then bind to AGE receptors and initiate secretion of inflammatory cytokines [46-50]. The damage caused due to multi-faceted effect of excessive AGEs can be mitigated upon AGE inhibition indicating their prevalence in mediating diabetic disorders [51].

iii. ***PKC activation:*** hyperglycemia-mediated elevation in diacylglycerol (DAC) promotes the activation of PKC isoforms. These in turn mediate the regulation or multiple factors transcriptionally. Regulation of vessel tone via eNOS inhibition, increased endothelial permeability via VEGF and heightened inflammation via NF-κB are among the few PKC-mediated outcomes. Targeting PKC has been shown to prevent vascular dysfunctions in diabetic retina and mesangial cells [52].

iv. ***Hexosamine pathway:*** Fructose-6-phosphate is partially utilized by GFAT for the production of UDP-GlcNAc which, not unlike phosphorylation, modifies nuclear and cytoplasmic proteins on serine and threonine residues. Modification by O-GlcNAc changes functionality and stability of altered proteins [53]. High glucose-mediated modification of transcription factor Sp3 causes decreased binding to repressive elements in Ang-2 promoter, thereby increasing Ang-2 expression in microvascular endothelial cells [54].

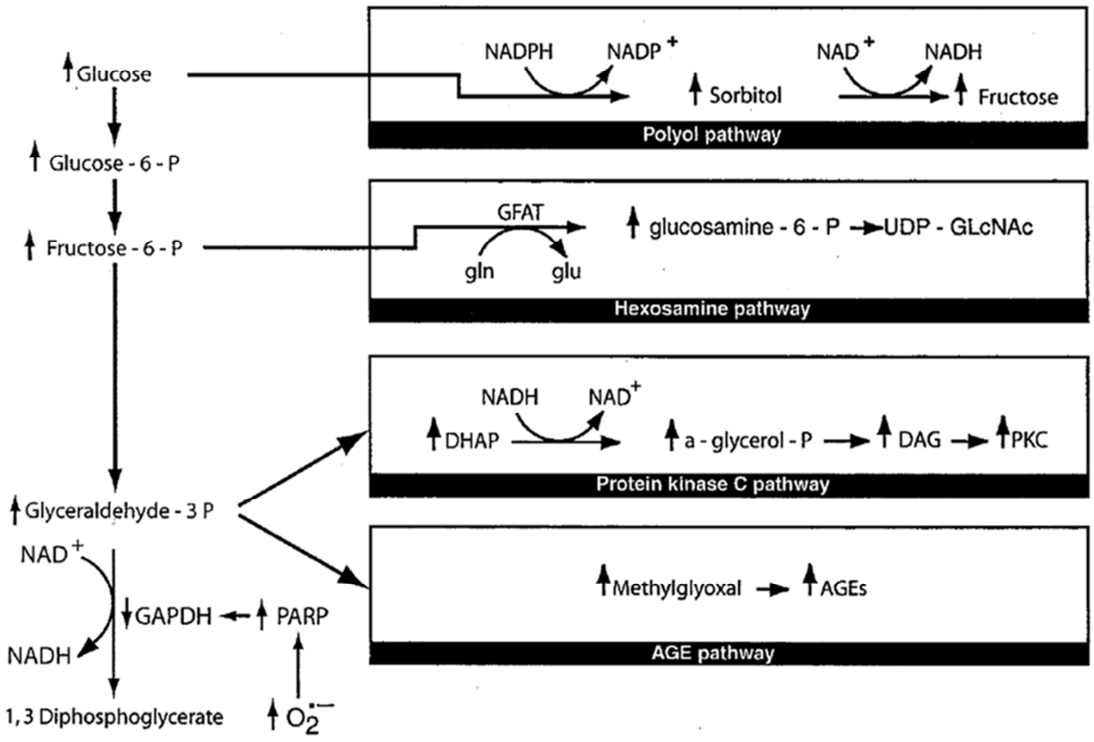

Fig. 5: Four pathways activated by intracellular hyperglycemia: *polyol pathway, hexosamine pathway, protein C kinase pathway and AGE pathway all combined under the unifying hypothesis that excessive ROS-mediated reduction in GAPDH activity enables accumulation of glycolytic intermediates providing substrates for the four pathways. Adapted from Brownlee, Diabetes 2005 [43].*

Lowered GAPDH activity purports accumulation of glycolytic intermediates, thereby providing substrates for increased flux through the four pathways [55]. *This provides a unifying mechanism for the intracellular metabolic effects of hyperglycemia.*

Recent findings show, that the altered bioavailability of the gastrotransmitters iNOS, CO and H_2S, induce oxidative stress by lowering the protective effects of vasodilation, ROS scavenging and survival signaling, in response to hyperglycemia [56]. Although hyperglycemia is an antecedent in the development of DR, several factors unaffected by high glucose contribute to the pathogenesis of DR. AGE precursor methylglyoxal (MG) depends, not on glucose, but on generation and detoxification by the glyoxalase 1 and 2 systems for its production. Administration of MG, leads to DR-like vasoregression, NVU breakdown and neuronal dysfunction [57, 58].

1.4 The Hexosamine Biosynthesis Pathway (HBP) and Protein O-GlcNAcylation

1.4.1 O-GlcNAc modification and HBP

Protein O-GlcNAcylation is a reversible posttranslational modification, resulting in the alteration of a wide range of proteins and their activity, interactions, and functions [59-62]. It was discovered in the 1980s and occurs exclusively in nuclear and cytoplasmic fractions. It differs from canonical glycosylation by being reversible, not elongated or modified to complex structures [63] , and regulates transcription and cell signaling dynamics [59, 61].

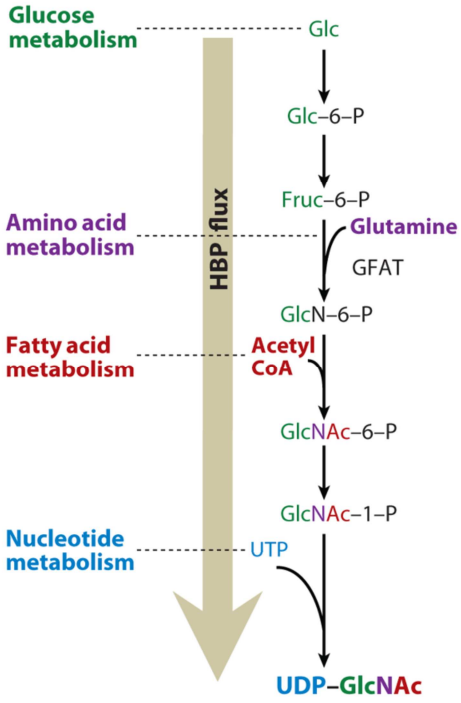

Fig. 6: The hexosamine biosynthesis pathway (HBP) *assembling glucose intermediates, glutamine, fatty acids and UTP in the manufacture of UDP-GlcNAc for modification of protein with O-GlcNAc residue. Adapted from Hart, Annu Rev Biochem 2011 [64].*

The hexosamine biosynthesis pathway (HBP) is an offshoot of glycolysis, normally accounting for just 2-5% of glucose metabolism. Glycolysis intermediate fructose-6-phosphate (F-6-P) is utilized to generate HBP end product UDP-GlcNAc [65-67]. Amongst the components of the HBP, the key enzyme is glutamine:fructose-6-phosphate amidotransferase (GFAT), which catalyzes the formation of glucosamine-6-phosphate (GlcN-6-P) in a rate limiting step and controls UDP-GlcNAc availability [68, 69]. In addition to glucose metabolism, fatty acid and amino acid metabolism also contribute to the generation of the HBP end product, UDP-GlcNAc (**Fig. 6**) [66, 67] [65]. Externally supplied glucosamine may bypass the rate-limiting reaction and is directly converted to glucosamine-6-phosphate,

thereby altering UDP-GlcNAc levels. The HBP is therefore, in essence, a nutrient-sensing pathway. There are several factors regulating the HBP. A moderate change in HBP can result in significant changes in O-GlcNAcylation [69].

1.4.2 Glutamine: fructose-6-P-amidotransferase (GFAT)

GFAT is the rate-limiting enzyme of the HBP and controls UDP-GlcNAc availability. The isoform GFAT1 is ubiquitously expressed while GFAT2 is expressed primarily in the central nervous system (CNS), heart, lung, skeletal muscles and placenta [70]. Although GFAT activity is robustly regulated by its expression, prior research illustrates phosphorylation of GFAT by cAMP-dependent PKA and AMP-kinase (AMPK) in a manner of regulating its activity [71-73]. Endothelial GFAT activity is dampened by AMPK-mediated phosphorylation in response to VEGF stimulation [73, 74]. GlcN-6-P and UDP-GlcNAc amounts also serve as regulators of HBP and inhibit GFAT allosterically [68].

1.4.3 The expression, structure, localization and regulation of the enzymes regulating O-GlcNAc cycling: OGA and OGT:

UDP-GlcNAc serves as a substrate for the O-GlcNAc cycling enzymes, O-GlcNAc transferase (OGT) and O-GlcNAcase (OGA) (**Fig. 7**). Unlike phosphorylation, O-GlcNAcylation is cycled reversibly by this single pair of enzymes.

i. OGT catalyzes the reversible attachment of the GlcNAc moiety to serine/threonine residues of proteins. Although OGT active site appears to lack a specific substrate recognition motif, it does show preference for Ser/Thr residues flanked by residues in extended peptide conformations. Additional specificity is achieved by certain structural confirmations on fully-folded proteins or TPR binding sites that allow access to the active site [75, 76]. Three isoforms of OGT; ncOGT (nucleocytoplasmic), sOGT (short) and mOGT (mitochondrial) can be found in the respective cellular compartments. OGT activity is promoted by increasing amounts of substrate UDP-GlcNAc. Low GlcNAcylated proteins can become better acceptors at high UDP-GlcNAc levels indicating that UDP-GlcNAc levels can also dictate OGT selectivity. Other factors influencing OGT selectivity are multimerizations, splicing, and post-translational modifications such as the phosphorylation or O-GlcNAcylation of its own catalytic domain [77].
ii. OGA catalyzes the detachment of the GlcNAc moiety from the proteins. Highly conserved in sequence, it is enriched in brain, pancreas and thymus. Two isoforms, namely, ncOGA (nucleocytoplasmic) and sOGA (short) are localized in the nucleo-cytoplasmic fractions and in the endoplasmic reticulum, respectively. OGA

localization is however predominantly cytoplasmic. The specificity of OGA is rather uncomplex when compared to OGT. Analyses of crystal structure and docking simulations show that OGA binding to O-GlcNAcylated proteins involves interaction with the peptide backbone and sugar moiety only with the least interference from the side chains, similar to the action of global phosphatases [76].

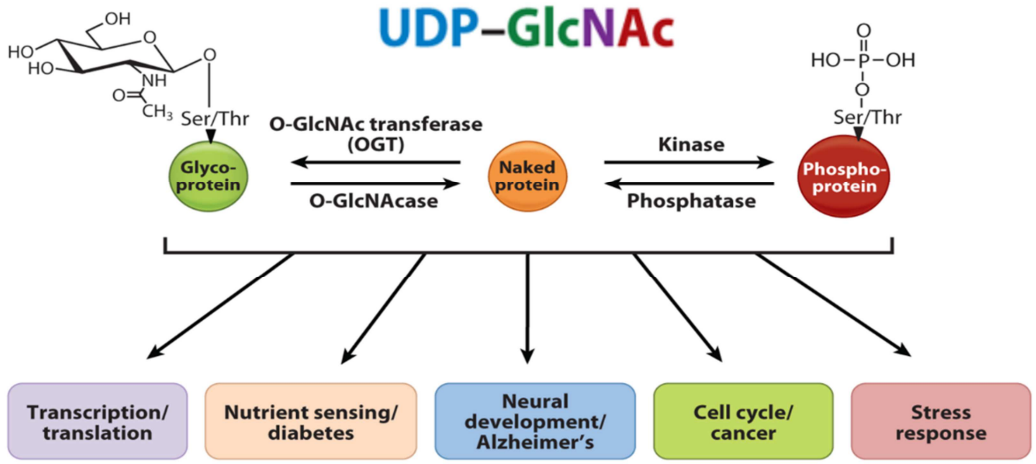

Fig. 7: The regulation of O-GlcNAcylation by O-GlcNAc cycling enzymes. *OGT and OGA enzymes catalyze the attachment and detachment of GlcNAc group based on the availability of UDP-GlcNAc from the HBP. The modification of proteins alters several cellular pathways. Adapted from Hart, Annu Rev Biochem 2011 [64].*

1.4.4 Functions of O-GlcNAcylation:

Unlike canonical glycosylation that exists in the Golgi, endoplasmic reticulum and the extracellular environment, O-GlcNAcylation is rather ubiquitous and thereby plays many roles.

i. **Transcription:** The prevalent localization of OGT in the nucleus indicates a role in regulation of transcription. Several transcription factors such as FoxO1, NF-κB and Sp3, have been reported to be modified by O-GlcNAc thereby influencing glucose metabolism, lymphocyte activation and angiogenesis, respectively [54, 60, 78]. The modification alters the functions of transcription factors such as DNA binding, stabilization via inhibition by ubiquitination and transactivation [62]. In diabetes research, Yao et al. show that hyperglycemia promotes methylglyoxal modification of mSin3A in ECs, triggering the increased O-GlcNAcylation of Sp3 via recruitment of OGT [54]. Modification of Sp3 diminishes its binding to the glucose-responsive GC box of the Ang-2 promoter, thereby permitting increased Ang-2 expression.

ii. **Epigenetics:** The modification of Pol II and transcription factors as well as the discovered association of OGT with HDAC corepressor complex implicates O-GlcNAcylation in parallel with histone deacetylation playing a role in gene silencing [79].

iii. **Regulation of cell signaling:** GlcNAc groups on Ser/Thr residues not only alter the function and specificity of susceptible proteins but also compete with other modifications such as phosphorylation and ubiquitination. Elevation of O-GlcNAcylation of Akt prevents its phosphorylation on insulin treatment, thereby inhibiting associated survival pathways. The reduction of Akt O-GlcNAcylation reverses the process. Since phosphorylation and O-GlcNAcylation of Akt occur on the same Ser/Thr residues, competition and balance between the two modifications affects major survival related cellular functions [80, 81].

iv. **O-GlcNAcylation in diabetes and DR:** Transcription factors regulating insulin; NeuroD1 and Pdx-1 possess O-GlcNAcylation sites, and increasing modification causes nuclear translocation and elevated insulin expression [82, 83]. Since the prevalence of O-GlcNAc in pancreatic β cells is higher than in surrounding cell types, the HBP is crucial to normal insulin production but in excess turns deleterious by raising oxidative stress, β cell toxicity and apoptosis [84-87]. Members of the insulin signaling pathway are also modified by O-GlcNAc [80, 88-90]. Incidentally, O-GlcNAcylation of IRS-1 and Akt blunts their phosphorylation. Elevated levels of O-GlcNAc therefore cause dysregulated glucose cycling and eventually glucose toxicity.

In diabetic retinopathy (DR), retinal Ang-2 is elevated and promotes pericyte dropout from the retinal microvasculature under hyperglycemia. In the absence of the protection of pericytes, the microvasculature is susceptible to vasoregression [28, 91, 92]. O-GlcNAcylation is heightened in the retinae of diabetic mice [93]. Furthermore, retinal ECs and pericytes show increased O-GlcNAcylation in response to high glucose in a dose dependent manner. Retinal ECs exposed to HG also show enhanced migratory capacity without changes in viability [94]. O-GlcNAc is maintained by a balance in activity of OGT and OGA. Both are O-GlcNAcylated and thereby subject to regulation by the modification they oversee [95-97]. OGT overexpression studies recapitulated the diabetic phenotype where as OGA overexpression reversed cardiomyopathic phenotypes [98-100]. Single nucleotide polymorphism of OGA gene is associated with the risk of T2DM in Mexican-American population studies. Ablation of OGA in *C. elegans* produces metabolic changes reminiscent of insulin resistance in humans. Gurel et al. demonstrate the regulation of OGT/OGA gene and protein expression in healthy and diabetic mouse retinae [93]. Pharmaceutical inhibition of OGT with Alloxan blocked the hyperglycemia-mediated elevation in O-GlcNAc in retinal PCs and promoted PC migration. Similar results were seen upon treatment with GFAT inhibitor DON. In

contrast, treatment with OGA inhibitor PUGNAc or Thiamet-G heightened O-GlcNAc levels similar to HG and hampered PC migration. These findings show how protein O-GlcNAcylation in DR can be modulated at several checkpoints in the HBP.

Endothelial cells are susceptible to changes in blood glucose levels and hence serve as an excellent tool for metabolic studies. Elevated blood glucose prompts increased flux through the HBP in ECs [101, 102]. O-GlcNAcylation of eNOS can induce endothelial dysfunction via inhibition of its phosphorylation [103, 104]. Several publications highlight the crosstalk between O-GlcNAcylation and other modifications such as tyrosine phosphorylation, methylation, acetylation, ubiquitination and methylglyoxal modification [77]. The crosstalk between O-GlcNAcylation and AMPK stress signaling is outlined in reports showing phosphorylation of endothelial GFAT by AMPK and the subsequent reduction in enzymatic activity [73, 74]. The spontaneous O-GlcNAcylation of proteins on exposure to extracellular stress implicates O-GlcNAcylation in survival and stress signaling [63, 74]. Reports, however, claim that O-GlcNAcylation is modified not only by nutrient availability but also by substrate regulation via modification of OGT and OGA specificity [105, 106]. The complicated mechanisms and intimate crosstalk between O-GlcNAcylation and other pathways make it a master regulator and influencer of nutrient and stress-driven signaling.

1.5 Angiopoietin-2-Tie-2 system

Two processes mediate the development of vasculature in any organism. Vasculogenesis is the formation of a primitive vasculature in response to external signals and progenitors. The formed blood vessels mature and acquire quiescence. The supply of blood is expanded throughout the tissue and organs via angiogenesis, the development of blood vessels from pre-existing vasculature [107]. Endothelial cells form the basis of any vasculature. They migrate and assemble to form monolayers of tight intracellular contacts. Perivascular cells such as pericytes and smooth muscle cells support the assembly of endothelial cells into blood vessels such as veins, arteries and capillaries. The complex crosstalk that enables vascularization is carried out by autocrine and paracrine signaling of vascular ligands (VEGF, Ang-1, Ang-2) and their respective receptors (VEGFR-2 and Tie-2/1) [107].

1.5.1 The Angiopoietins and their receptor Tie-2

The structure of the angiopoietins consists of an N-terminal angiopoietin specific domain and a coiled-coil domain responsible for multimerization, a linker peptide and a C-terminal fibrinogen domain essential for receptor binding (**Fig. 8**) [108, 109]. The angiopoietins use their fibrinogen-like domain to bind to their receptor Tie-2. Ang-1 and Ang-2 share 60% homology and are located side-by-side on chromosome 8 p22 and 23, respectively [110,

111]. Ang-1 is incorporated into the extracellular matrix of the ECs and is primarily secreted by perivascular cells such as pericytes. Ang-2 on the other hand is stored in Weibel-Palade bodies, which are secretory vesicles in the endothelial cytoplasm and is released in response to inflammatory stimuli [112, 113]. The mediator of Angiopoietin signaling is the membrane-bound receptor tyrosine kinase Tie-2, which is predominantly expressed in ECs and mediates functions such as survival and maintenance of vascular integrity, angiogenesis and vasoregression [114-118].

Tie-2 and Tie-1 form a family of receptor tyrosine kinases. They consist of an extracellular multidomain of three EGF-like motifs between two Ig-like loops [119]. Genetic ablation studies show that both Tie-$2^{-/-}$ and Tie-$1^{-/-}$ mice are embryonic lethal with vascular defects. Tie-$2^{-/-}$ mice have fewer ECs, supporting PCs and SMCs, and poorly organized vasculature with fewer branches. Additionally, Tie-2 plays a crucial role in developmental hematopoiesis [120-123]. Tie-1 on the other hand is not crucial for hematopoiesis but Tie-$1^{-/-}$ mice lose vessel integrity resulting in widespread edema and embryonic death. Both receptors however do not partake in the initial assembly of the vasculature [124, 125].

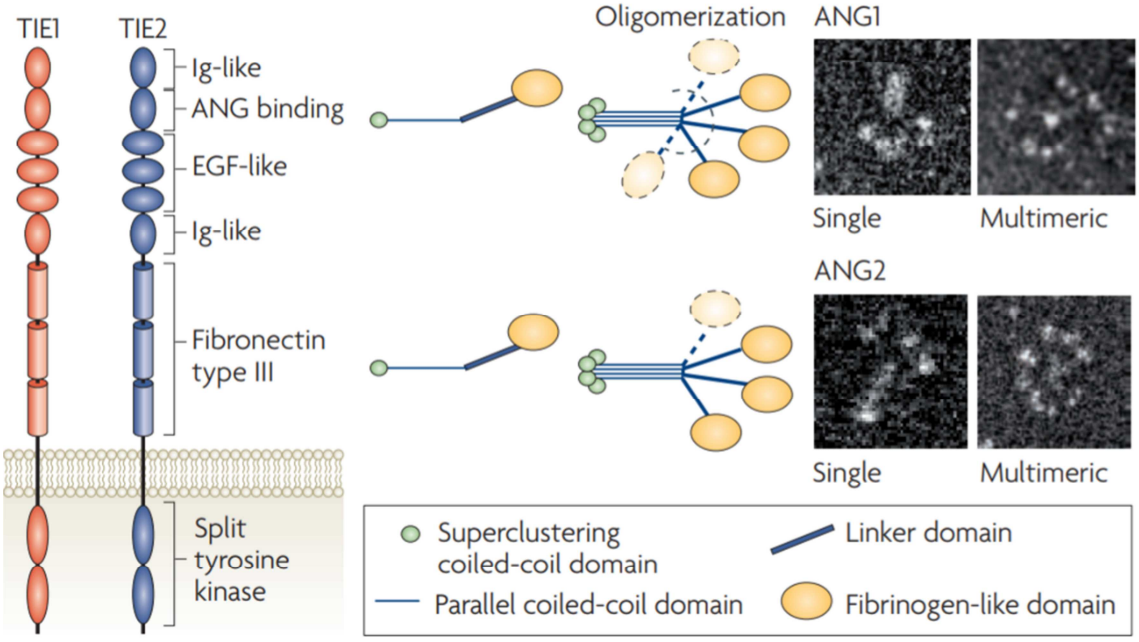

Fig. 8: Structure of Tie-2 receptors and Angiopoietin ligands. *The Tie-2 receptor consists of N-terminal Ang binding domain and C-terminal receptor tyrosine binding domain. Rotatory shadow techniques show the possible multimerizations of Angiopoietin ligands. Adapted from Augustin, Nat Rev Mol Cell Biol 2009 [16].*

The characterization of Tie-1/2 led to genetic ablation studies of their ligands. Ang-$1^{-/-}$ mice phenocopy Tie-$2^{-/-}$ mice and are embryonic lethal. This led to the characterization of Ang-1 as the primary ligand of Tie-2 that mediates critical vascular functions distinct from VEGF [126]. Endothelial cells of Ang-$1^{-/-}$ mice are rounded and loosely attached to the ECM indicating the importance of Ang-2-Tie-2 in EC-ECM interactions. Development of Ang-$2^{-/-}$ mice proceeds unhindered although certain genetic backgrounds report postnatal death. C57BL/6 background mice show transient postnatal chylous ascites, making it possible to investigate Ang-2 in knockout animals [127, 128]. Although Ang-2 deficient mice are viable, detailed researches show consequences in various vascular beds. Ang-2 is dispensable for vascularization at development and gains importance postnatally. Angiogenesis is best studied in the retina. Ang-$2^{-/-}$ mice show non-regressing hyaloid vessels of the embryonic lens and perturbed retinal and renal vasculature [129-131]. Knock-in of Ang-1 into Ang-2 locus rescues lymphatic abnormalities in Ang-$2^{-/-}$ but not blood vessel defects indicating rudimentary roles of Ang-1 and Ang-2 in lymphatic vasculature and ligand-specific roles in the formation of blood vessels [132].

Conversely, gain-of-function (GOF) experiments have also shed light on the Ang-1/2-Tie-2 functions. Ang-1 overexpression promotes dermal hypervascularization, whereas delivery of recombinant Ang-1 counters VEGF-induced hyperpermeability and inflammation due to VEGF-induced release of inflammatory adhesion molecules. A series of findings conclude the crucial function of Ang-2 in promoting vessel maturation and quiescence via increased signaling through Tie-2 [117, 133, 134]. Contrary to expectations Tie-2 overexpression does not phenocopy Ang-1 overexpression and leads to venous malformations and dilated blood vessels. This proves the significance of Tie-2 signaling via both ligands and not just its preferential binding to Ang-1 [135]. Ang-2 overexpressing mice demonstrate contradictory phenotypes and similar vascular defects as seen in Ang-1 and Tie-2 null mice. Hence, Ang-2 is popularly regarded as the Tie-2 antagonist [134]. Ang-2 GOF has been associated with barrier-opening effects in brain endothelial cells thereby increasing permeability to solutes, prompting no compensatory elevation response from Ang-1. Furthermore, disrupted glycocalyx in GOF brain ECs indicates the anti- EC-ECM action of Ang-2 antagonizing the effect of Ang-1-Tie-2 signaling [136].

1.5.2 The Ang-1/Ang-2 Tie-2 signaling axis

Ang-1 and Ang-2 bind with equal affinity to Tie-2. Angiopoietin 1 (Ang-1), the canonical agonist of Tie-2, is released by perivascular cells and binds to Tie-2 to promote endothelial survival, adhesion, and quiescence [108]. Upon the binding of Ang-1, Tie-2 is phosphorylated, which further activates survival signaling via phosphorylation of PI3K, Akt,

and FoxO1 [137]. The activation of Akt prompts survival pathways such as eNOS and inhibition of inflammatory and apoptotic pathways. Akt subsequently phosphorylates FoxO1, a transcriptional activator of Ang-2, causing its nuclear exclusion and inactivation (**Fig. 9**). Ang-1-Tie-2 signaling also inhibits vessel permeability via the sequestration of Src, which mediates VEGF-induced redistribution, and internalization of VE-cadherin, an adherens junction protein [138]. Tie-2 activation is also known to recruit smooth muscle cell migration and recruitment to ECs and restore survival in developing retinal models with disrupted peri-endothelial interactions [139, 140]. Via the recruitment of Tie-2 to basal plasma membrane of ECs and activation of Erk1/2 and Dok-R pathways, Ang-1 promotes EC-ECM adhesion. Ang-1 also stimulates the production of collagen IV, thereby promoting EC-EC contact, stability, maturity and quiescence of the endothelium [141, 142] (**Fig.10**).

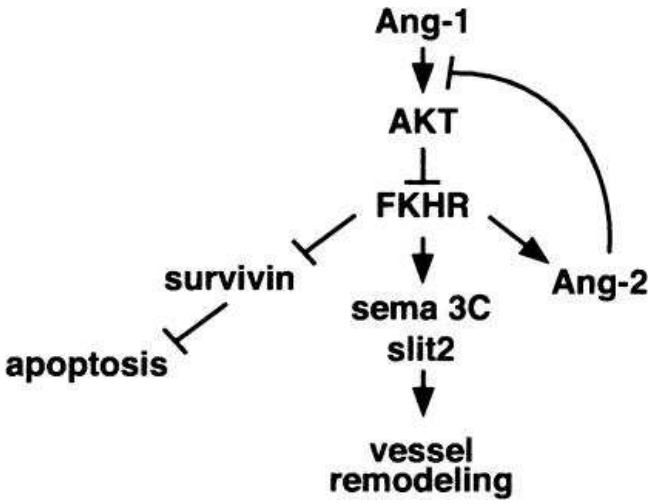

Fig. 9: The interplay between Ang-1 and Ang-2 via receptor Tie-2. *The Ang-1-Tie-2 signaling promotes inhibition of FoxO1 (FKHR) and the subsequent suppression of Ang-2. Adapted from Daly, Genes Dev 2004 [137].*

Ang-2 is predominantly expressed in ECs and released upon stimulus from vesicles [113]. Thereafter, it binds in an autocrine fashion to Tie-2 on the ECs. [143-145]. Hampering the Ang-1/Tie-2 signaling axis maintains active FoxO1 in the nucleus, purporting unchecked Ang-2 production (**Fig. 9**) [137, 146]. The binding of Ang-2 to Tie-2, however has context-dependent outcomes [147]. As an antagonist, it perturbs Ang-1/Tie-2 signaling and promotes vascular remodeling via the loosening of matrix contacts. It supports the effects of the vascular endothelium-derived growth factor (VEGF) in inducing angiogenic responses. In the absence, or at low VEGF levels, excessive Ang-2 however leads to vasoregression [109].

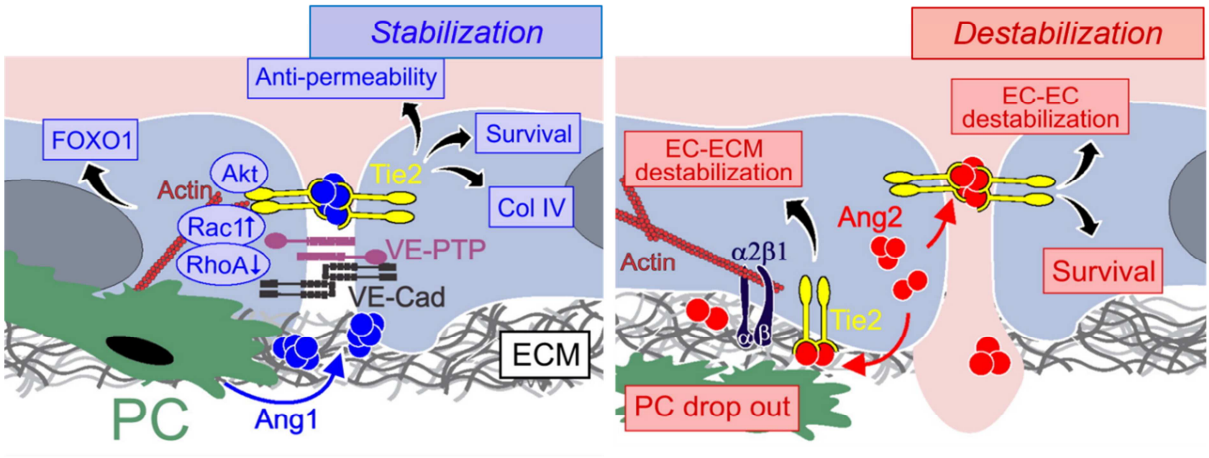

Fig. 10: The contrasting outcomes of Ang-1 and Ang-2 binding to Tie-2. *Ang-1 binding promotes vessel stability and integrity whereas Ang-2 binding promotes destabilization and remodeling. Adapted from Eklund, Exp Cell Res 2013 [132].*

Paradoxically, several reports indicate that Ang-2 might be a weak agonist of Tie-2, promoting its phosphorylation and hence, vascular survival and angiogenesis [148-150]. However, in the presence of Ang-1 it reverts to its antagonist role, inhibiting Ang-1-Tie-2 action in a dose-dependent manner, thus highlighting the complex interplay between the angiopoietins and their receptor Tie-2 (**Fig. 10**) [109, 150-152]. The effects of Ang-2 are vastly amplified in the presence of inflammatory cytokines [153, 154]. Under pulmonary infection conditions, Ang-2 acts as Tie-2 antagonist and suppresses its phosphorylation and promotes FoxO1 expression. The effect was mimicked by excessive exogenous Ang-2, anti-Tie-2 reagents and suppressed by exogenous Ang-1-mediated activation of Akt survival pathways. In contrast, under pathogen-free conditions, Ang-2 plays the agonist and mediates vascular remodeling via Tie-2 phosphorylation and suppressed FoxO1 activation [148]. Thereby, Ang-2 plays a complex role in the regulation of vascular remodeling and angiogenesis.

1.5.3 The regulation of Ang-2 in diabetes and diabetic retinopathy

DR is the most prevalent microvascular complication of diabetes [5]. Naturally, the angiogenic factors play a large role in its development. In the developing retina, the tip and stalk ECs guide the vessel growth along a VEGF gradient with the aid of VEGFR-2. The role of VEGF becomes prevalent in the later PDR stage [155, 156]. Once the vessels are formed and mature, they are sheathed in pericytes. Healthy pericyte coverage is the mark of a quiescent mature vessel. Pericyte-secreted Ang-1 is a mediator of survival signaling in the ECs and along with TGF-β1 contributes to the final maturation of the vasculature [157]. As postulated by Hanahan and Hammes, the complex interplay between Ang-1/2 and VEGF determines the fate of the vasculature [28, 147]. In hypoxic tissues with high VEGF and high Ang-2/Ang-1 ratio, vascular remodeling and angiogenesis is promoted. In the absence of hypoxia, Ang-2 upregulation leads to vascular regression. The synergistic remodeling effect of Ang-2 and VEGF is commonly seen in later stages of DR where hypoxic demand builds in a retina with non-perfused vessels (**Fig. 11**) [28, 147].

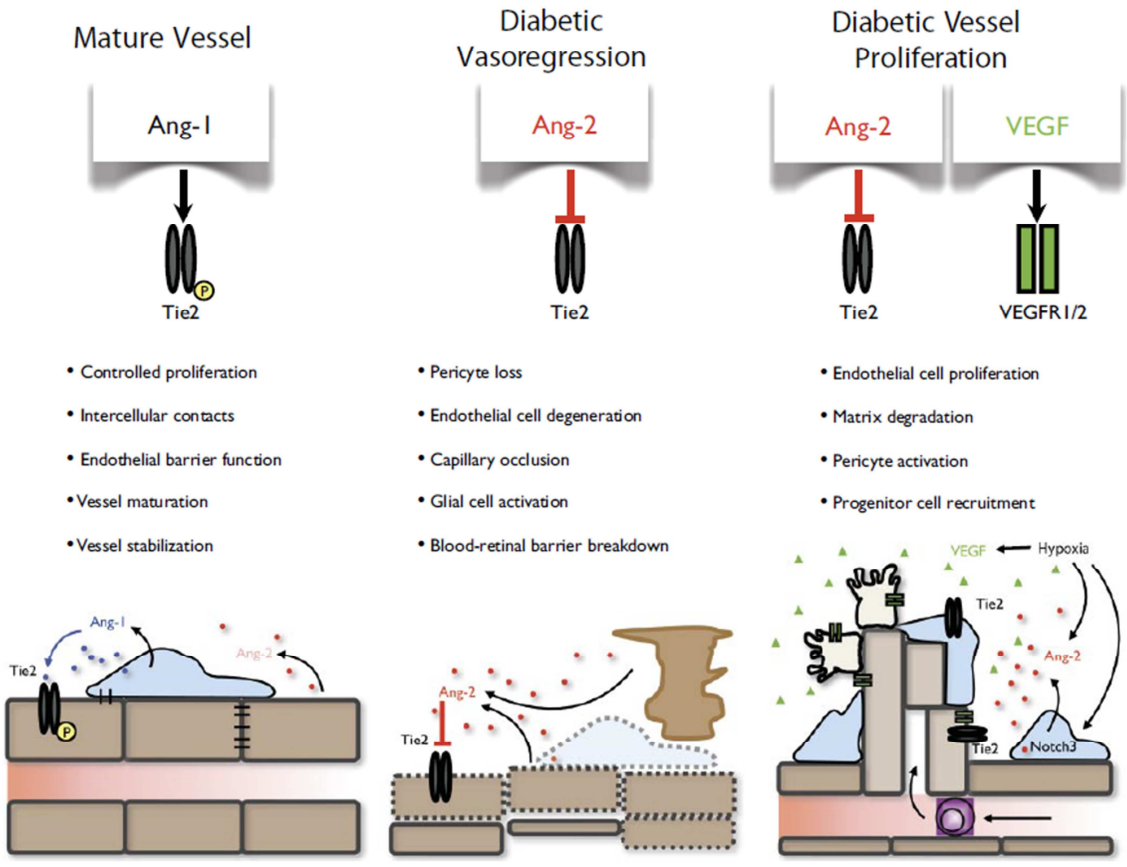

Fig. 11: The mechanism of vascular destabilization in DR. *In a mature vessel, pericyte-derived Ang-1 binds to endothelial Tie-2 to phosphorylate it and promote quiescence. In the absence of hypoxia and in low VEGF conditions, Ang-2 upregulation drives vasoregression. In ensuing hypoxia,*

VEGF and Ang-2 destabilize the endothelium to promote vascular remodeling and angiogenesis. Adapted from Hammes, Diabetes 2011 [28].

The very first morphological change in DR is pericyte dropout. This is preceded by an elevation of retinal Ang-2 [91]. Intravitreally-injected recombinant Ang-2 in non-diabetic rats promoted pericyte dropout similar to DR. Animal models overexpressing human Ang-2 in the mouse retina, showed significant pericyte loss and formation of non-perfused capillaries, the hallmark of retinal vasoregression. Moreover, heterozygous expression of Ang-2 was sufficient to prevent DR-mediated pericyte dropout, implying that Ang-2 is undoubtedly mediating the development of DR [91, 92]. In endothelial cells, hyperglycemia-induced formation of methylglyoxal modifies transcriptional co-repressor mSin3A which then recruits OGT to mSin3A-Sp3 complex. The O-GlcNAcylation of transcriptional factor Sp3 eases its binding to the repressor complex of the Ang-2 promoter, thereby increasing Ang-2 expression [54]. In DR, an elevated Ang-2/Ang-1 ratio inhibits Akt-mediated FoxO1 inactivation. Increasingly activated FoxO1 allows transcription of Ang-2 which in turn destabilizes the vasculature leading to DR. Furthermore, several reports claim that, Ang-2 may destabilize the vasculature in low-Tie-2 conditions by binding integrins and promoting pericyte apoptosis [158-162].

1.6 Nucleoside diphosphate kinase B (NDPK-B)

1.6.1 The NDPK family and its members

NDPK-B belongs to the family of NDPKs that were discovered around the 1950s in yeast and pigeon breast muscle [163, 164]. NDPKs are housekeeping enzymes that are primarily involved in the catalytic transfer of γ-phosphate between a nucleoside 5'-triphosphate (NTP) and a nucleoside 5'-diphosphate (NDP) via a ping-pong mechanism which involves the formation of a high energy phosphate intermediate, e.g. on Histidine118 of NDPK-B [165, 166].

$$NDP + ATP \rightleftharpoons NTP + ADP$$

The NDPK/Nme/NM isoforms are ubiquitously present throughout the cells, the various isoforms localized in one or more cellular compartments. The localization of the isoforms dictates their functionality [167-169]. The NDPK family consists of 10 isoforms, highly conserved across the taxonomies, of which vertebrates possess 8-10 isoforms. In mammalian tissues, the isoforms form heterohexamers of size 17-21kDa [170, 171]. The

NDPKs are divided into two groups. Group I consists of NDPK A→D. These isoforms retain enzymatic activity unlike the rest and share 58-88% sequence homology. Group II proteins share only 25-45% homology. The only exception is Nm23-H6 from group II which retains its NDPK activity [168, 170, 172]. Besides their canonical function, an increasing number of publications show additional functions and highlight the moonlighting character of several isoforms [173-178]. Amongst Group I NDPKs, A and B are well-investigated. At first the cDNA of NDPK-A was found to be heavily downregulated in a metastatic murine melanoma cell line. Deeper investigation produced mouse models that developed heightened metastatic potential when crossed with an NDPK-A deficient transgenic line [179, 180].

1.6.2 NDPK-B and signal transduction

i. GPCR independent G-protein activation:

G-protein coupled receptors (GPCRs) are transmembrane proteins that are coupled to G-proteins, which act as molecular switches in mediated internal signaling. The heterotrimeric G-proteins consist of three subunits namely α, β, γ, of which βγ form a stable dimeric complex [181, 182]. The GDP bound G-proteins are maintained in an inactive state. During GPCR dependent activation of G-proteins, agonist binding dissociates the GDP on Gα and the naturally occurring excess GTP binds to the Gα nucleotide pocket, causing a conformational change that dissociates Gα from Gβγ. Both subunits bind downstream effectors [183]. The hydrolysis of GTP to GDP returns Gα to its inactive state.

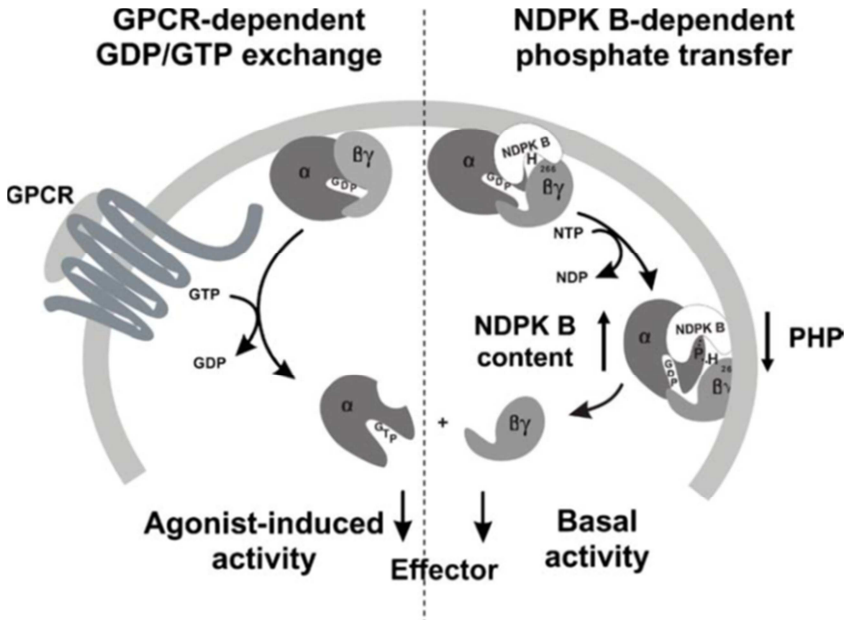

Fig. 12: GPCR-agonist independent activation of G-proteins by NDPK-B. *Adapted from Wieland, 2007 [184].*

NDPK-B and not NDPK-A was found to bind Gβγ and activate G-proteins independent of GPCRs. The spontaneous conversion of GDP to GTP in the presence of an NTP phosphorylates the His residue on Gβγ, which then converts the dissociating GDP from Gα to GTP. Therefore, the binding of this GTP causes activation of G-proteins in a manner that does not require an extracellular agonist for the GPCRs (**Fig. 12**) [185-187]. NDPK-B also mediates membrane targeting of G-proteins, a function that is independent of its histidine kinase activity [188]. MEFs isolated from NDPK-A/B knockout embryos possess depleted G-proteins at the membrane [188, 189]. Recent reports show that another isoform, NDPK-C, interacts with NDPK-B at the membrane where it facilitates NDPK-B-G-protein complex formation. The NDPK-B/C complex synergistically mediates G-protein activation [186, 190]. One of the downstream functions of G-protein activation is the production of cAMP, which has made NDPK-mediated GPCR-independent G-protein activation of interest in cardiovascular research. Knockdown of NDPK-B has been published to diminish cAMP levels and induce cardiac contractile dysfunction and overexpression of NDPK-C increases cAMP production and elevates cardiomyocyte contractility, thereby reinforcing the concept of NDPK-B/C heterohexamers in G-protein signaling [191].

ii. Histidine phosphorylation:

Most signaling pathways involve regulation of proteins via phospho/de-phosphorylation mediated by kinases and phosphatases on Ser/Thr residues of proteins. A relatively unknown method of protein activation/deactivation is by histidine kinases and phosphohistidine phosphatases (PHP). The role of NDPKs as histidine kinases emerged with their ability to phosphorylate enzyme ATP citrate lyase (ACL) [192]. Phosphorylation targets of NDPK-B includes the conductance potassium channel KCa3.1 and the Ca^{2+}-conducting TRP channel, TRPV5 and annexin I [193-195]. The activation of KCa3.1 is required for T cell activation and TRPV5 is required for efficient Ca^{2+} reabsorption in nephron tubules [196]. Mice lacking NDPK-B phenocopy KCa3.1$^{-/-}$ have defective T cell activation, thereby, making them susceptible to autoimmune diseases.

1.6.3 NDPK-B and caveolae

Caveolae are lipid-raft-like membrane invaginations that house components of signaling complexes. They conduct a myriad of functions including cholesterol homeostasis and operating as signaling platforms. The caveolin (Cav) proteins form building components of the caveolae and the isoforms Cav-1 and Cav-3 have been identified to interact with NDPK-

B. Several loss-of-function animal and cellular models for Cav and NDPK-B show overlapping phenotypes and co-dependency for expression. Several Cav-1 deficient models also show impaired angiogenic potential, a phenotype observed in NDPK-B deficient mice. This implicates NDPK-B in playing a role in angiogenesis as well as the maintenance of caveolae formation. Caveolae are also known to house angiogenic master regulators such as VEGFR-2 [197-201].

1.6.4 NDPK-B and diabetes

Kowluru et al., conducted analyses of GTP in rat retina and established the functional deterioration of G-proteins during streptozotocin-induced diabetes (T1DM) [202]. Based on prior reports of NDPKs enabling GTP-mediated agonist-independent activation of G-proteins, NDPK activity was analyzed in diabetic rat retina and found to be unchanged [203]. Similar investigations in pancreatic islet β-cells implicated NDPK enzymatic activity to be necessary for glucose-stimulated insulin secretion [204]. Additionally, a rat model for T2DM showed reduced NDPK expression and activity in in pancreatic islet β-cells [205]. *In vitro* exposure of β-cells to glucotoxicity as well as glucolipotoxicity caused marked reduction in NDPK-A and B expression and activity, implicating the NDPKs in impaired insulin secretion under glucolipotoxicity via dysregulated G-protein activation [206].

1.7 Role of NDPK-B in angiogenesis and DR

1.7.1 NDPK-B KO model

Loss-of-function mouse models have been a popular and indispensable tool for identifying protein function. Global knockout models have been developed for the NDPK genes, specifically, NDPK-A [207], NDPK-B [196] and NDPK-A/B [208, 209]. NDPK-$A^{-/-}$ and NDPK-$B^{-/-}$ mice are physiologically normal and retain normal life span and fertility. NDPK-$A/B^{-/-}$ develop smaller than WT mice in the embryonic stage and die perinatally due to defective erythroid cell maturation and severe anemia [209, 210]. NDPK-$B^{-/-}$ mice have a normal phenotype but possess defective K^+ KCa3.1 channel activity and thereby defective cytokine production in Th1 and Th2 CD4 T cells [196, 211]. Aside from the global KO model, NDPK-B has been manipulated in the zebrafish via a morpholino-induced knockdown (MO). MO-mediated KD of NDPK-B, and not NDPK-A, severely decreased cardiac contractility, lowered cAMP production, depleted Gβγ subunits and Cav-1 and 3 [189, 191]. NDPK-B depleted zebrafish embryos also possessed malformed blood vessels which were rescued upon NDPK-B re-expression establishing its role in angiogenesis [198].

1.7.2 Role of NDPK-B in angiogenesis and PDR

NDPK-B has been investigated for its role in angiogenesis through a multi-model approach. The hindlimb ischemia model in the KO mice demonstrated delayed blood flow recovery and lower capillary density in the gastrocnemius muscles as compared to WT littermates [198]. Proliferative DR late stages comprise of primarily uncontrolled angiogenesis and elevated VEGF-VEGFR-2 signaling. To investigate the role of NDPK-B in PDR, oxygen-induced retinopathy (OIR) model was implemented, where mice were introduced postnatally to hyperoxia and later returned to room air, inducing relative hypoxia. This mounted an angiogenic response in the retina and led to neovascularization. NDPK-B KO retinae showed far fewer neovascularization and decreased VEGFR-2 expression than the WT retinae. siRNA-mediated gene knockdown of NDPK-B in ECs showed impaired VEGF-mediated VEGFR-2 recruitment to the membrane, elevated permeability due to altered VE-cadherin spatial arrangement and stunted EC sprouting in response to VEGF. Cav-1 was found to interact with adherens junction proteins such as β-catenin. β-catenin phosphorylation by c-Src was found to be essential for barrier breakdown in ECs. Collectively, NDPK-B enabled angiogenic responses via the correct localization of caveolae at the endothelial membrane and c-Src-mediated Cav-1 phosphorylation (**Fig. 13**) [212].

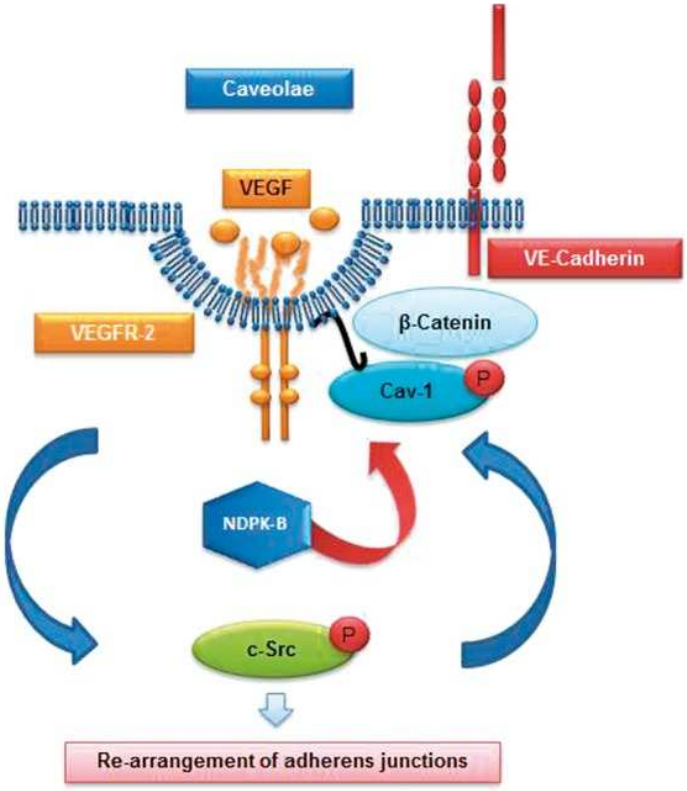

Fig. 13: The mechanism for elevation of permeability in NDPK-B deficient ECs via p-c-Src-mediated phosphorylation of Cav-1 causing re-arrangement of AJ proteins. *Adapted from Gross, J Cereb Blood Flow Metab. 2017 [212].*

1.7.3 NDPK-B KO model and DR

As NDPK-B plays a role in the regulation of angiogenesis, its possible involvement in the regulation of microvascular complications should be considered. Additionally, the primary function of NDPK-B is the catalysis of NTP from NDP. UTP is utilized for the generation of UDP-GlcNAc as described in Section 1.4. UDP-GlcNAc is a substrate for protein O-GlcNAcylation and mediates increased expression of Ang-2 [54]. Ang-2-mediated development of DR, a microvascular complication has been described in Section 1.2. The hypothesis that NDPK-B plays a role in DR development was investigated.

Diabetes was induced via streptozotocin injection. NDPK-B KO animals were found to be normoglycemic, possess normal HbA1c levels and body weight in contrast to the diabetic animals [213]. Retinal analysis of NDPK-B KO mice showed poor PC coverage and large number of AC similar to WT diabetic retinae. The concomitant increase in retinal Ang-2 and protein O-GlcNAcylation similar to WT diabetic retina imply that NDPK-B normoglycemic retinae mimicked WT diabetic retinae. The symptoms of vasoregression were exacerbated in KO diabetic retinae indicating a cumulative effect of NDPK-B KO and diabetes, although no such accumulative increase was seen in KO diabetic Ang-2 and O-GlcNAc as compared to KO non-diabetic groups at the protein level.

DR develops due to the elevated levels of Ang-2 that initiate vasoregressive effects [91, 92]. Both, endothelial cells and Muller cells were identified as one of the major sources of Ang-2 in the retina [54, 214]. The analysis of retinal cross-sections showed glial activation in normoglycemic KO and diabetic WT and KO mice. Ang-2 co-localized with the Muller glia and is elevated in normoglycemic KO and diabetic WT and KO mice [215]. Normoglycemic NDPK-B deficient ECs mirrored the retina in exhibiting elevated Ang-2 and protein O-GlcNAcylation similar to HG treated ECs. [213]. These findings signify the parallels between NDPK-B deficient and diabetic systems and implicate NDPK-B in the development of DR-like vasoregression.

1.7.4 Intracellular mechanisms for vasoregression in NDPK-B deficiency

FoxO1 is a transcription factor regulating Ang-2 expression [162]. NDPK-B deficient Muller cells and ECs exhibited elevated FoxO1 protein expression in comparison to controls [215, 216]. Shan et al. and Qiu et al. demonstrated that, FoxO1 is required for basal expression of Ang-2 as well as NDPK-B deficiency-induced upregulation of Ang-2 in Muller cells and ECs.

Immunofluorescence images showed elevated FoxO1 and O-GlcNAc levels in NDPK-B deficient ECs that partially overlap, implying the possible modification of FoxO1 by O-GlcNAc. While NDPK-B depletion did not induce any changes in FoxO1 phosphorylation, it increased FoxO1 O-GlcNAcylation, which was essential for Ang-2 elevation in comparison to controls. These findings highlight not only a novel mechanism for Ang-2 regulation in NDPK-B deficient ECs via FoxO1, but also shed light on the consequences of elevated protein O-GlcNAcylation on existing pathways (**Fig. 14**).

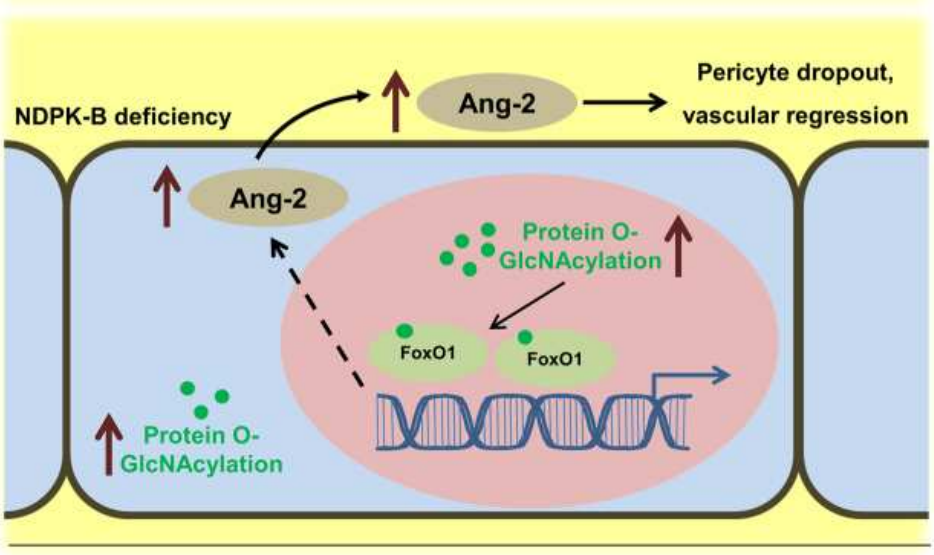

Fig. 14: Protein O-GlcNAcylation of FoxO1 mediates NDPK-B deficiency induced vasoregression via Ang-2 in ECs. *Adapted from Shan, Sci Rep 2018 [216].*

2. Aims of the study

Retinal vasoregression is a common consequence of endothelial damage caused by hyperglycemia or NDPK-B deficiency. Recent findings indicated, that both hyperglycemia and NDPK-B deficiency promote protein O-GlcNAcylation and elevation of Ang-2 [213]. Prior research provided evidence that hyperglycemia-induced O-GlcNAcylation of transcription factors elevates Ang-2, being the causative factor in retinal vascular regression [54, 91]. The underlying mechanism of protein O-GlcNAcylation and Ang-2 regulation in the NDPK-B deficient models are still unclear. In the current study, we focus on the regulation of Ang-2 by its receptor Tie-2 and O-GlcNAcylation in NDPK-B deficiency-driven retinal vasoregression.

Aim 1: The importance of Ang-2-Tie-2 signaling in HG and NDPK-B deficiency-mediated vasoregression: In this part of study, we explore, the importance of Ang-2 in vascular regression in NDPK-B$^{-/-}$ retinae, and the role of Tie-2 in the upregulation of Ang-2-mediated vascular regression in NDPK-B deficiency and high glucose conditions.

Aim 2: The importance of protein O-GlcNAcylation in NDPK-B deficiency: In this part of the study, we explore glucose metabolism in NDPK-B deficiency by examining the HBP and protein O-GlcNAcylation, and the regulation of Ang-2 via O-GlcNAcylation by NDPK-B.

3. Materials

3.1 Cell culture

3.1.1 Cell culture medium and supplements

Table 2: Cell culture medium and supplements

Components (500ml)	**Catalog number**
Endothelial cell basal medium (ECBM)	C-22110; PromoCell
Endothelial supplements	C-39210; PromoCell
Endothelial cell growth media (ECGM)	ECBM + Supplements
Microvascular ECGM (ECGM MV)	ECBM + Hydrocortisone: 1 µg/ml, ECGS: 40 µg/ml, PenStrep: 1%, EGF: 5ng/ml
FCS	F7524; Sigma
DMEM (1000 mg/ml glucose)	D-6546; Sigma-Aldrich

3.1.2 Cell isolations and cell lines

Table 3: Cell isolations and cell lines

Cell type	**Catalog number**
HUVECs	Self-isolated from umbilical cords (Section 4.2.1.1)
HMECs	INS-CI-1008; inSCREENex
HRMVECs	PB-CH-160-8511; Pelobiotech
MBMECs	Self-isolated from murine brain (Section 4.2.1.4)

3.1.3 siRNA

Table 4: siRNA

siRNA	Sequence
Control siRNA (Eurofins)	5´- AGG UAG UGU AAU CGC CUU G -3`
NDPK-B siRNA (Eurofins)	5´- AAC UGG UUG ACU ACA AGU CUU -3`
Tie-2 siRNA (Qiagen)	SI00604912
OGT siRNA (Qiagen)	SI02631412
OGA siRNA (Qiagen)	SI04187043
Allstars negative control (Qiagen)	SI03650318

3.1.4 Cell culture reagents and enzymes

Table 5: Cell culture reagents and enzymes

Reagents	Company	Catalog number and details
Lipofectamine RNAiMAX	Invitrogen	13778-075
OptiPRO^{TM} SFM	Invitrogen	12309-019
EDTA Trypsin 0.05%	Sigma-Aldrich	T3924
Dispase II	Roche	04942078001
Puromycin	Sigma	P7255
Collagenase/Dispase	Sigma	10269638001
DNaseI	Sigma-Aldrich	11284932001

Rat-tail Collagen	Self-made	1mg/ml (Section 4.2.1.4)
Collagenase II (CLS2)	Worthington	4177
Penicillin/Streptomycin	Sigma	P4333

3.2 Buffers and chemicals

3.2.1 Cell culture buffers

Table 6: Cell culture buffers

Buffer	**Catalog number**
PBS	D-5652; Sigma-Aldrich

3.2.2 Protein analysis buffers

Table 7: Protein analysis buffers

Buffer	**Contents**
Ponceau. S (100 ml)	5 ml acetic acid; 95 ml H_2O; 0.2 g Ponceau
Protein Loading buffer (4x) (50 ml)	25 ml 50% Glycerol; 5 ml 10% 2-Mercaptoethanol; 5 ml 10% 2-Mercaptoethanol; 0.25% Bromophenol Blue; 5 ml H_2O
RIPA buffer	150 mM NaCl; 1.0% Triton X-100; 0.5% sodium deoxycholate; 0.1%SDS; 50 mM Tris, pH 8.0
Cell lysis buffer	RIPA buffer; Protease inhibitor (Roche) (1 tablet/10 ml)
NDPK assay buffer	50 mM Tris-HCl pH 7.5; 2 mM MgCl2; 1 mM DTT; 0.01% BSA

SDS-PAGE Electrophoresis buffer (5X SDS)	0.125 M Tris; 1.25 M Glycine; 0.5%SDS; 500 ml H_2O
TAE buffer (50X)	2 M Tris; 5.7% Acetic acid; 0.05 M EDTA pH 8.0 in 1 L H_2O
TBS (10x) TBST (1000 ml)	100 mM Tris; pH: 7.4; 1.5 M NaCl 100 ml 10x TBS; 890 ml H_2O, 10 ml; 1 ml Tween 20
Tris Buffer for stacking gel	1 M Tris, pH: 6.8
Tris Buffer for separating gel	1.5 M Tris, pH: 8.8
Western Blot transfer buffer (WB) (10x)	32.5 g Tris; 144 g Glycine; 1000 ml H_2O

3.2.3 Immunoprecipitation buffers

Table 8: Immunoprecipitation buffers

Buffer	**Contents**
Tie-2 IP buffer	50 mM Tris-HCl pH 7.4, 150 mM NaCl, 1% Triton X-100, PhosSTOP and Protease inhibitor (Roche) (1 tablet/10 ml, each)
sWGA IP buffer	50 mM Tris-HCl pH7.4, 100 mM NaCl; 1% Triton X-100, Protease inhibitor
sWGA wash buffer	50 mM Tris-HCl pH7.4, 100 mM NaCl; 0.1% Triton X-100, Protease inhibitor

3.2.4 Immunofluorescence buffers

Table 9: Immunofluorescence buffers

Buffer	**Contents**
Fixation buffer	4% PFA in PBS (for retina fixation) 4% Roti®-Histofix (for ECs fixation)
Permeabilization/Blocking buffer	1x PBS; 2% BSA; 0.5% Triton™ X-100 (Retina) 1x PBS; 2.5% BSA; 0.3% Triton™ X-100 (ECs)
Antibody Dilution Buffer	1x PBS; 1% BSA; 0.5% Triton™ X-100
Wash buffer	1x PBS
DAPI	0.1-10 µg/ml

3.3 Chemicals

Table 10: Chemicals

Chemicals	**Company**	**Catalog number**
2-Mercaptoethanol	Serva	28625
Absolute ethanol	Riedel-de Äen	32205
APS	Merck	1.012.010.100
Bromophenol Blue	Chroma-Gesellschaft	4F057
BSA	Sigma-Aldrich	A9418-5G

BSA	Sigma-Aldrich	B-4287
Chloroform	Merck	2447
DMSO	Sigma-Aldrich	D8418
DAPI	Life Technologies	1603428
D-(+)-Glucose	Sigma-Aldrich	SLBF1738V
Ethanol	Richter Chemie	V-126
EDTA	Roth	8040.1
Entellan	Merck	107961
Gelatin from porcine skin	BD	214340
Glycerol	Sigma-Aldrich	G9012
HCl	Sigma-Aldrich	H1758
Roti histofix	Roth	P087.4
KCl	Sigma-Aldrich	P9333
Luciferase (ATP-dependent)	Promega-Kinase-GLo	V6711
Methanol	Roth	4627.5
NaCl	Sigma-Aldrich	M7439
$NaHCO_3$	Sigma-Aldrich	S5761
NaOH	Merck	106498
PFA	Merck	1.040.031.000

PhosSTOP™	Sigma-Aldrich	4906845001
Ponceau S	Sigma-Aldrich	P-3564
Protease inhibitor	Roche	5892970001
Protein marker	ROTH	T8512
Protein A/G beads	Santa Cruz	sc-2003
Roti-Block	Roth	A151.1
Roti-Mount FluorCare	Roth	HP19.1
Rotiphorese Gel 30	Roth	3029.1
SDS	Sigma-Aldrich	74255
SuperScript IV VILO Master Mix	Thermofischer	11755050
sTie-2 Fc chimera human	Promokine	B-68028
Succinylated Wheat Germ Agglutinin coated agarose beads (sWGA)	Vector Laboratories	AL-1023S
TEMED	Roth	T7024
Thiamet G (TMG)	Sigma	SML0244
Tris	Serva	37181
Triton-X-100	Merck	1.080.031.000
Tween 20	Sigma-Aldrich	P-7949
1,2-Propanol	Sigma-Aldrich	134368

3.4 Antibodies

3.4.1 Primary antibodies for western blot (WB) and immunofluorescence (IF)

Table 11: Primary antibodies

Antibody	**Catalog number; Company**	**Dilution**
Ang-2 (WB)	sc-7017; Santa Cruz	1:500
	sc-74403; Santa Cruz	1:500
FoxO1 (WB)	2880; Cell Signaling	1:1000
Gβ (WB)	Sc-378; Santa Cruz	1:1000
GFAT (WB)	Prof. Weigert, Tübingen	1:3000
Histone H3 (WB)	sc-8654; Santa Cruz	1:1000
Isolectin-TRITC	L5264; Sigma	1:50
NDPK-B (WB)	MC-412; Kamiya	1:1000
N1-phospho-histidine	MABS1330; Millipore	1:1000
NG-2 (IF)	AB5320; Millipore	1:200
O-GlcNAc (WB)	ab2739; Abcam	1:2000
OGT (WB)	O6264; Sigma	1:1000
OGA (WB)	SAB4200267; Sigma	1:1000
PECAM-1 (IF)	sc-1506-R; Santa Cruz	1:200
Phospho-GFAT1 (WB)	s343c; MRC-PPU	1:150
Phospho-Tyrosine 4G10	05-321; Millipore	1:1000

Tie-2 (IP)	AF313; R&D systems	2µg/IP
Tie-2 (IF ECs)	sc-324; Santa Cruz	1:100
Tie-2 (IF retina)	AF762; R&D systems	1:100
Tie-2 (WB)	sc-324; Santa Cruz	1:1000
γ-Tubulin (WB)	T5168; Sigma-Aldrich	1:5000

3.4.2 Secondary antibodies

Table 12: Secondary antibodies

Antibody	**Catalog number; Company**	**Dilution**
Rabbit anti-mouse peroxidase	A-9044; Sigma-Aldrich	1:20000
Rabbit anti-goat peroxidase	A8919; Sigma-Aldrich	1:10000
Goat anti-rabbit peroxidase	A-9169; Sigma-Aldrich	1:40000
Goat anti rabbit Alexa Fluor 488	A-11008; Life technologies	1:200
Goat anti mouse Alexa Fluor 488	A-11001; Life technologies	1:200
Swine anti-rabbit-FITC	F0205; Dako	1:20
Donkey anti-goat-FITC conjugate	R1254F; Acris	1:1000

3.5 qPCR primers and master mix

Table 13: qPCR primers, genotyping primers (PCR), and master mix

Primers	**Catalog number; Company**
18S (qPCR)	Hs03003631_g1; applied biosystems

GFAT (GFPT1) (qPCR)	Hs00899865_m1; applied biosystems
OGA (MGEA5) (qPCR)	Hs00201970_m1; applied biosystems
OGT (qPCR)	Hs00269228_m1; applied biosystems
Tie-2 (Tek) (qPCR)	Hs00945155_m1; applied biosystems
Taqman Fast Advanced Master Mix	4444556; Thermofischer
Ang-2 Lac Z (reverse) (PCR)	GAG ATC AGC AGC CTC TGT TCC
Ang-2 Lac Z (forward WT) (PCR)	CTG GGA TCT TGT CTT GGC C
Ang-2 (forward mutant) (PCR)	CTT CTC TCT GTG ACT GCT TTG
NDPK-B (reverse) (PCR)	TCC CTA TAT ACC TGC TCT GCC TCA
NDPK-B (forward WT) (PCR)	CCT ATG TGG GAA ACA ATG GGT TTC
NDPK-B (forward KO) (PCR)	TTA GCA GCT CTG GAG CTT GCA GCC
Mastermixes for PCR	M7501; Promega PEQL01-1399; PeQLab
HotShot lysis buffer	10 ml dH_2O; 14 µl 50% NaOH; 14 µl 0.5M EDTA, pH 8.0
HotShot neutralization buffer	40 mM Tris-HCl

3.6 Consumables

Table 14: Consumables

Consumables	**Company**	**Catalog number**
3-way stopcock	BD Connecta TM	394600

Cell counting chamber	Marienfeld	0640010
Cell culture plate (24 well, 12 well, 6 well)	Sarstedt	83.3922, 83.3921, 83.3920
Cell culture dish (6 cm, 10 cm, 15 cm)	Sarstedt	83.3901, 83.3902, 83.3903
Cell culture flask (T25, T75)	Sarstedt	83.3910.002, 83.3911.002
Cell scraper	Sarstedt	83.1830
Cover slips	Carl Roth GmbH	41021070
Gel combs	Bio-rad	1653359
Cryotube	Sarstedt	72.377
Eppendorf tubes (1.5 ml, 2 ml)	Eppendorf	0030 120.086
Eppendorf tips (1000 µl, 200 µl, 10 µl)	Eppendorf	70.760.002, 70.1130, 70.762
Falcon tubes (15 ml, 50 ml)	Sarstedt	62.554.502, 62.547.254
Microscope slides	R. Langenbrinck	03-0002; 2642672
Nitrocellulose membrane	Häberle	6267735
Pipettes	Sarstedt	86.1253.001, 86.1254.001, 86.1685.001
Parafilm	Parafilm'M'	PM-996

Whatman paper	VWR	514-8013
Filtropur S 0.2	Sarstedt	31046103
Syringe	Seidel Medipool	301229
Syringe needle 30G	BD Microlance	30400

3.7 Kits

Table 15: Kits

Kits	**Catalog number; Company**
Lumi-Light Western Blotting	12015200001; Roche
Super Signal West Femto Maximum Sensitivity Substrate	34095; Thermo Scientific
Bio-Rad turbo blotting supplements	10026938; Bio-Rad
Subcellular Fractionation Kit	78840; Thermo scientific
Seahorse Glycolysis Stress Test Kit	103020-100; Agilent
Seahorse Mito Stress Test Kit	103015-100; Agilent
Ang-2 ELISA	DY623, R&D Systems
OGA Activity Kit	E-130; BMR services

3.8 Apparatus

Table 16: Apparatus

Apparatus	**Company**

Laminar flow bench	Herasafe, Heraeus
Water bath	ThermoScientific
Incubator (37 ℃, 5% CO_2)	Memmert
Centrifuge	Eppendorf Hettich Toxixa/K
Shaker	Neolab
Vortex	Janke & Kunkel
Dounce homogenizer	B.Braun Biotech International
Weighing machine	Sartorius
Pipettor	Eppendorf
Multi-pipettor	Eppendorf
Microprocessor pH meter	WTW
Heating block	Thermomix comfort, Eppendorf
Electrophoresis chamber and apparatus	Bio-Rad
Bio-Rad turbo blotter	1704150
Mini-PROTEAN casting module	Bio-Rad
Voltmeter	Biometra
Gel imager	Alpha Imager 2200
Spectrophotometer	Thermolabsystems Multiscan EX
Quantitative PCR	Quantstudio 3; Applied biosystems

Stereomicroscope	Eschenbach
Fluorescence microscope	Olympus
Confocal microscope model TCS SP2	Leica
Fluorescence microscope DMRE	Leica
Millipore water machine	Milli-QR
High temperature sterilizer	Systec
-20 ℃ freezer	Bosch/ Liebherr
-60 ℃ freezer	Revco
-80 ℃ freezer	Hera
ELISA plate reader	AlphaImager® Innotech
Envision 2102 multilabel reader	Perkin-Elmer
Seahorse XF96 analyzer	Agilent Technologies
Imager	Vilber

3.9 Software

Table 17: Software

Software	**Company**
Image J	NCBI
Fluorescence microscope software	Leica
Confocal microscope software	Leica microsystems version 2.16

Statistics	Graph Pad Prism 6 software
References	Endnote V4

4. Methods

4.1 In vivo methods

4.1.1 Maintenance of the animals

The use of mice in the study was approved by the local ethics committee (Medical Faculty Mannheim, Heidelberg University, Germany). The care and experimental use of animals were in accordance with institutional guidelines and in compliance with the Association for Research in Vision and Ophthalmology (ARVO) statement. All animal experiments in this study were approved by the local ethics committee (Regierungspräsidium Karlsruhe, Germany). The mice were housed in a separate building and artificial lighting was maintained on a 12 h:12 h light-dark cycle. Room temperature was kept constant at 21 ℃. The mice received tap water for drinking and were fed normal chow diet (ssniff R/M-H) containing 9% fat, 33% protein, and 58% carbohydrate. NDPK-$B^{-/-}$ mice were generated as previously described [196]. Ang-2 +/- were generated as previously described [91]. The NDPK-$B^{-/-}$/Ang-$2^{+/-}$, NDPK-$B^{-/-}$/Ang-$2^{+/+}$, NDPK-$B^{+/+}$/Ang-$2^{+/-}$ and NDPK-$B^{+/+}$/Ang-$2^{+/+}$ mice were generated by breeding the NDPK-$B^{+/-}$/Ang-$2^{+/-}$ and NDPK-$B^{+/-}$/Ang-$2^{+/+}$ mice. The mice were numbered marked with 2 mm diameter ear clips. The ear clip tissue taken from the mice was used for determination of the genotype by PCR, described in Section 4.1.2.

4.1.2 Polymerase Chain Reaction (PCR) to determine the genotype of animals

- **DNA sample preparation**

Ear clips or tail tips from mice were lysed in 75 µl HotShot lysis buffer containing NaOH and incubated at 95 ℃ for 1 h. Afterwards, 75 µl HotSh ot neutralizing buffer containing HCl was added to neutralize the lysate. The lysates were used for the following PCR procedure. Unused lysates were stored at -20 ℃ for later use.

- **PCR**

PCR procedures to amplify Wildtype (WT) and Knockout (KO) sequences were done separately. Promega 2× PCR master mix was used for NDPK-B WT PCR, Ang-2 WT PCR, and KO PCR; and PeQLab 2× PCR master mix was used for NDPK-B KO PCR. The 2× master mixes contain DNA polymerase, dNTPs, magnesium, and buffer. **Table 19** gives an

overview of the reactions, and the PCR program for the specific genes are illustrated below in **Table 18**.

Table 18: NDPK-B WT and KO genotyping PCR

NDPK-B PCR cycle	**Ang-2 PCR cycle**
94 ℃ 3 min	94 ℃ 4 min
35 cycles: 94 ℃ 30 s	40 cycles: 94 ℃ 1 min
62 ℃ 30 s	59 ℃ 30 s
72 ℃ 60 s	72 ℃ 30 s
72 ℃ 10 min	72 ℃ 8 min
WT: ~500bp	WT: 380bp
KO: 650~700bp	Mutant: 240bp

The master mixes, primers, and water were mixed in a tube and added to the PCR tubes followed by the addition of DNA to the respective tubes. The components were mixed by pipetting or flicking the tubes and transferred to a thermal cycler, which runs the PCR program.

Table 19: NDPK-B WT and KO genotyping PCR

	WT PCR (µl)	**KO PCR (µl)**
Nuclease free water	7.5	7.5
2× MM	10	10
WT primer (20 µM)	0.25	-
KO primer (20 µM)	-	0.25
Reverse primer (20 µM)	0.25	0.25
DNA lysate	2	2
Total	20	20

4.1.3 Agarose gel electrophoresis

The PCR amplicons were separated by gel electrophoresis on a 1% agarose gel containing ethidium bromide. Agarose was weighed then mixed with TAE buffer in a glass flask and dissolved by heating up the flask in a microwave until the buffer started to boil and a clear solution formed. Once the flask was warm to touch, 0.5 µg/ml of ethidium bromide was added. The mixture was swirled then poured into a gel-forming cassette with combs and allowed to polymerize for 20 to 30 min. Once solidified, the combs were carefully removed without disturbing the DNA loading wells. The gel was completely immersed in TAE buffer in the electrophoresis chamber. The DNA samples mixed with loading buffer were loaded in the wells and run for 1 h at 120 V. The DNA bands were visualized using a UV light imager. Amplicons for only WT PCR or KO PCR were determined to be WT or KO mice respectively. Amplicons for both WT PCR and KO PCR were determined to be heterozygous (HE) mice. **Fig. 15** shows the results of an NDPK-B WT PCR and KO PCR.

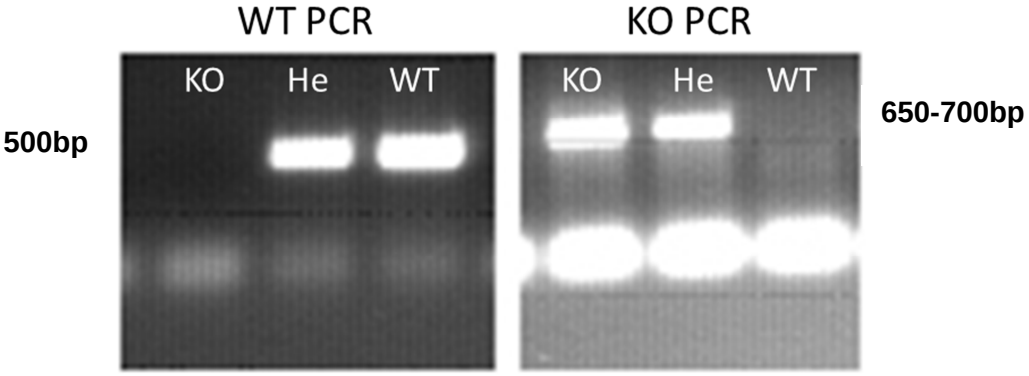

Fig. 15: Examples of an NDPK-B WT PCR and an NDPK-B KO PCR. *The left panel demonstrates results of a WT PCR and the right panel a KO PCR. WT and KO samples show positive bands for WT PCR (500bp) and KO PCR (650-700bp), respectively and HE samples show positive results for both WT PCR and KO PCR.*

4.1.4 Retinal digestion and quantitative retinal morphometry

Frozen eyes were fixed in 4% Formalin for 48 h. The eyes were then placed under a loupe microscope and dissected. The retina was exposed by removing the lens and vitreous then the retina was carefully extracted. The isolated retina was incubated at 37 ℃ in water for 30 min, and subsequently incubated at 37 ℃ for 2.5 h in 3% trypsin dissolved in 0.2M Tris-HCl buffer (pH 7.0). The retina was then transferred onto a glass object slide and carefully washed with droplets of dH_20 from a Pasteur pipette until the pure retinal vasculature could

be visualized under the microscope. After the vasculature was dried on the object slide, it was stained with Period-Acid-Schiff (PAS). The PAS staining was performed as follows:

dH_2O	5 min
1% Periodic acid	10 min
dH_2O	Brief immersion
Schiff's reagent	10 min
Running tap water	5 min
ddH_2O	Brief immersion
Mayer's Hemalum	30 s
Running tap water	7 min
ddH_2O	Brief immersion
70% ethanol	Brief immersion
80% ethanol	Brief immersion
96% ethanol	5 min
100% ethanol	5 min
Roti®-histol ×3	5 min each

Embed with Entellan®

The slides stained with PAS were observed under the microscope and photos of 40× magnification were taken. The numbers of pericytes and acellular capillaries were quantified. For the quantification of pericytes, 10 microscopic fields with 40× magnification were randomly selected in the middle one-third of the retina, and the pericytes as well as ECs were counted. The cell numbers were recorded and normalized to the relative capillary density (quantity of cells per mm^2 of capillary area). The capillary area was measured by using image analyzing software (AnalysisPro; Olympus Optical, Hamburg, Germany). The acellular capillaries were quantified using an integration ocular with a grid of 100 squares. The quantity of squares containing acellular capillary segments were counted in 10 randomly selected microscopic fields of 40× magnification in the middle one-third of the retina.

4.2 In vitro methods

4.2.1 Cell culture

The use of Human Umbilical Vein Endothelial Cells (HUVECs) was approved by the local medical ethics committee (Medical Faculty Mannheim, Heidelberg University, Germany; Approval number: 2012-388N-MA).

4.2.1.1 Isolation of HUVECs

HUVECs were isolated from the umbilical cords of newborn infants with the informed consent of their mothers according to a previously described protocol [198]. One end of the cord was clamped closed and the other end attached to a 3-way stopcock allowing a bi-directional flow of fluid through the vein, which is the largest vessel in the umbilical cord. The vein was then washed with pre-warmed low glucose DMEM until blood no longer visibly drained from it. 10X Dispase II was diluted in DMEM to yield 1X DMEM-Dispase II, which was then applied to the vein through the stopcock. The cord was then placed in a humidified incubator (37 ℃, 5% CO_2) for 30-40 min. The detached cells were collected in a falcon tube and mixed with 4 ml of FCS to halt the enzymatic digestion. The vein was massaged gently to dislodge undetached cells and once again perfused with DMEM. The collected flow was centrifuged (5 min; 1000 rpm) and the cell pellet resuspended in ECGM (**Table 2**) containing 10% FCS. To enable the attachment of the cells, they were cultured in ECGM 10% FCS on a 1% gelatin-coated cell culture dish in a humidified incubator (37 ℃, 5% CO_2) for 2 h followed by a gentle media change to remove remaining red blood cells. The attached HUVECs were maintained in fresh ECGM 10%FCS.

4.2.1.2 Culture and passaging of HUVECs, HMECs and HRMVECs

Freshly isolated HUVECs, known as passage 0 (p0), were cultured with ECGM supplemented with 10% FCS in a humidified incubator (37 ℃, 5% CO_2). The medium was replaced every two days. Cells from one umbilical cord were placed in a flask and regarded as one isolation. Once the cells reached confluency, they were detached from the flask via trypsin digestion. Once detached, the trypsin digestion was neutralized with 10% FCS ECGM. The cells were then passaged to p1 at the ratio 1:3 and cultured to confluency. All experiments were performed using cells from p1 to p4.

Human Retinal Microvascular Endothelial Cells (HRMVECs) and Human Microvascular Endothelial Cells (HMECs) were cultured in the microvascular ECGM (ECGM MV) supplemented with 10% FCS. Cell passaging, culture, freezing, thawing, and experimental procedures with HRMVECs and HMECs were identical to those for HUVECs.

4.2.1.3 Freezing and thawing of HUVECs

HUVECs at p0 or p1 were detached by trypsinization and pelleted by centrifugation. The pellet was gently resuspended in chilled ECGM supplemented with 10% FCS and 10% DMSO. The cell suspension was then transferred to sterile cryotubes and placed in a pre-chilled closed isopropanol reservoir. Every isolation was divided equally between 2 cryotubes. The reservoir was then transferred to -60 ℃. On the following day, the cryotubes were transferred to a liquid nitrogen tank and stored at -190 ℃.

To thaw the HUVECs, the required isolation was extracted from the liquid nitrogen tank and thawed rapidly in a 37 ℃ water bath. Once partiall y thawed, the cells were resuspended in pre-warmed ECGM supplemented with 10% FCS until fully thawed and then centrifuged at 1000 rpm for 5 min. The pellet was resuspended in ECGM with 10% FCS and placed in a 1% gelatin-coated dish. The culture media was replaced the next day to remove excess DMSO and the cells were cultured to confluency before use in experiments.

4.2.1.4 Isolation and culture of murine brain microvascular endothelial cells (MBMECs)

- **Preparation of rat-tail collagen**

2-3 rat tails were incubated in 70% Ethanol for 15-20 min. With a pair of sterile forceps and scissors, the tails were skinned, the vertebrae were broken and the collagen thread extracted. The collagen thread was then placed in ethanol and subsequently dried in a closed Petri dish for 2 h. The dried collagen was then transferred to a closed sterile container of 500 ml 0.1% acetic acid solution and incubated for 48 h at 4 ℃. The suspension was then placed into centrifuge tubes, weighed, and centrifuged at 17,000 rpm for 90 min. The supernatant containing the collagen suspension was collected, aliquoted and stored at 4 ℃ for future use.

- **MBMEC isolation**

MBMECs were isolated from 10-15-week-old male mice. The mice were euthanized with a brief isoflurane application followed by cervical dislocation. The intact brains were extracted and placed in cold DMEM. The forebrain cortex was surgically isolated, rolled on sterile autoclaved Whatman filter paper to remove the meninges and placed in cold DMEM. The brains were minced first by pipetting through a 25 ml pipette and then subsequently through a 10 ml pipette. The minced solution was homogenized with 10 strokes of a Dounce homogenizer. The pink homogenate was centrifuged at 400 g for 10 min at 4 ℃. Subsequently, the supernatant was discarded and the pellet was digested in a 0.75%

collagenase II solution rocked at 300-400 rpm for 1 h at 37 ℃. The digested tissue was centrifuged at 400 g for 5 min and the supernatant was carefully discarded without disturbing the pellet. The pellet was then dissolved by tapping in sterile 20% BSA-DMEM solution. The solution was centrifuged in a swing bucket rotor at 2000 g for 30 min at 4 ℃. The separated myelin layer was removed with a Pasteur pipette and the pellet was digested in DMEM containing 1 mg/ml Collagenase/Dispase and 1 µg/ml DNaseI at 300-400 rpm for 30 min at 37 ℃. The suspension was centrifuged at 400 g for 5 min and the pellet was resuspended in ECGM MV supplemented with 10% FCS. The cells were seeded on a plate coated with rat-tail collagen and incubated at 37 ℃ in a humidifie d incubator. On the following day, the media was replaced with ECGM with 10% FCS containing 4 µg/ml of puromycin to eliminate non-endothelial cell types. Puromycin treatment was continued until day 3 post-isolation. The cells were cultured to confluency. The MBMECs were detached using trypsin. Detached cells were centrifuged at 1000 rpm for 5 min then resuspended in growth media and passaged at a density of no more than 1:2. Cells were characterized by immunofluorescence and used only up to p1.

4.2.2 siRNA transfection

Cells were seeded according to the cell numbers mentioned in **Table 20** in order to allow them to attach to the coated dish overnight at 37 °C.

Table 20: Cell seeding in culture plates / dishes for siRNA transfection

Dish / plate	**Surface area per well / dish (mm^2)**	**Cell number well / dish**	**Medium (ml)**
24 well	200	50,000	0.5
12 well	401	100,000	1
6 well	962	250,000	2
6 cm	2827	550,000	4
10 cm	7854	1000,000	8

The siRNA of choice was diluted in OptiPROSFM, as was lipofectamine RNAiMAX (the respective volume of reagents is shown in **Table 21**). All procedures were carried out in a

sterile manner. The siRNA/OptiPROSFM complex was mixed with the lipofectamine/OptiPROSFM complex by pipetting up and down carefully. The mixture was incubated for 20 min at RT. Meanwhile, the cells were washed twice with PBS, and the required volume of warm OptiPROSFM was pipetted into the respective dishes/plates. The siRNA/lipofectamine mixture was then added in a drop-wise manner to the culture dishes/plates. The plates were incubated for 4 h at 37 ℃ followed by a media change to ECGM 10% FCS. The transfected cells were then used for assays from 24 to 96 hpt.

Table 21: Reagent volumes for siRNA-mediated knockdown in ECs

Culture plates	**OptiPRO™SFM for RNAiMAX (µl)**	**Lipofectamine RNAiMAX (µl)**	**OptiPRO™SFM for siRNA (µl)**	**Amount (pmol)**	**OptiPRO™ SFM (µl)**
12 well	100	2	100	100	800
6 well	250	5	250	250	2000
10 cm	1000	20	1000	1000	10000

4.2.3 Stimulation of ECs

On the day following the transfection, HUVECs were starved in ECGM 0.5% FCS for 24 h followed by further stimulation with the respective reagents (high glucose (HG) 30 mM 4 h, sTie-2 5 µg/ml 24 h, TMG 10µM 24 h). For HMECs and HRMVECs, on the day following the transfection, the cells were starved in ECGM MV with 0.5% FCS for 48 h followed by harvesting for analysis.

4.2.4 Adenovirus-mediated overexpression of human Ang-2

HUVECs were transfected with NDPK-B siRNA then starved in ECGM 0.5% FCS for 24 h, followed by infection with Ad-Ang-2 [158] in ECGM 0.5% FCS for 24 h. ECs infected with Ad-GFP served as the control. Infected cells were monitored for GFP expression. The cell supernatant was collected for confirmation of Ang-2 overexpression using the Ang-2 ELISA DuoSet kit. The pelleted cells were harvested then analyzed for protein expression by western blotting.

4.2.5 Adenovirus-mediated overexpression of NDPK-B and H118N kinase-dead mutant

HUVECs were transfected with NDPK-B siRNA, then starved in ECGM 0.5% FCS for 24 h, followed by infection with recombinant adenovirus encoding green fluorescent protein (Ad-GFP) and overexpression of WT NDPK-B (Ad-NDPK-B-GFP) or overexpression of NDPK-B kinase dead mutant (Ad-H118N-GFP) [217] in ECGM 0.5% FCS for 24 h. Cells were monitored for GFP expression for successful and identical transfection in groups and then harvested in RIPA buffer for the analysis of protein expression via WB or for the assessment of OGA activity.

4.2.6 Mass spectrometric analysis

4.2.6.1 Preparation of HUVECs and retinae for mass spectrometric analyses

HUVECs were seeded and cultured in 15-cm dishes and subjected to NDPK-B knockdown via siRNA. 24 hpt, the cells were starved in 0.5% FCS ECGM for 48 h, then washed with 150 mM ammonium acetate. The dishes were flash-frozen in liquid nitrogen and stored at -80 ℃ for further mass spectrometric analysis. The retinae from 5-month-old mice were isolated and flash-frozen in liquid nitrogen and stored at -80 ℃ for further mass spectrometric analysis.

4.2.6.2 Determination of metabolite levels via UPLC-PDA

Determination of nucleotides and sugar-nucleotides was adapted from Kochanowski et al [217]. Either HUVEC cell pellets ($10x10^6$ cells per sample) or one mouse retina were lysed and extracted in 0.37 ml ice-cold 0.5 M perchloric acid with sonication on ice. Samples were neutralized with 86 µl ice-cold neutralization solution (2.5 M KOH in 1.5 M K_2HPO_4) after 5 min sonication. To remove precipitated potassium perchlorate neutralized samples were centrifuged at 4 ℃ and 16,400 g for 10 min and filtered with 0.2 µm filters. Nucleotides and sugar-nucleotides were immediately analyzed and separated via ion-pair reverse phased chromatography using an Acquity HSS T3 column (150 mm x 2.1 mm, 1.7 µm, Waters) connected to an Acquity H-class UPLC system. The column temperature was set to 40℃ and the column was equilibrated with solvent A (50 mM potassium phosphate buffer, 8 mM tetrabutylammonium hydrogen sulfate, pH 6.5) at a flow rate of 0.45 ml/min. Autosampler temperature was maintained at 6 ℃. The elution gradient was as follows: after 2.6 min 0% B (30 % acetonitrile in 70 % solvent A) to 17 min 77% B, hold for 1 min at 77% B, followed by return to 0% B and conditioning of the column to initial conditions for 10 min. Nucleotides were detected by Acquity PDA detector (Waters, 260 nm) and quantified using ultrapure

standards (Sigma). Data acquisition and processing was performed with the Empower3 software suite (Waters).

4.2.7 Seahorse analyses

Seahorse cartridges were hydrated on the day prior to the assay according to the instruction manual. HUVECs were detached and seeded into pre-coated 96-well plates and allowed to adhere for 2 h in a humidified incubator at 37 ℃. The cells were then washed and starved in non-buffered serum-free Seahorse medium in a CO_2-free incubator for 1 h. The hydrated cartridges were prepped with the inhibitors and stimulators provided in the kit and placed on the 96-well plate containing the starved HUVECs. The cartridge-plate combination was then placed in the Seahorse XFe 96 Analyzer and assessed using the protocol for Glycolysis Stress Test or Mito Stress Test. Respective catalog numbers can be found in **Table 15**. The glycolytic stress test injects glucose, oligomycin, and 2-deoxy-D-glucose (2DG) at 20 min intervals on the EC monolayer to measure short-term changes in glycolysis, glycolytic capacity, and additional glycolytic reserve potential, respectively. Extracellular acidification rate (ECAR) is the measure of changes in pH due to lactate production at the end of anaerobic glycolysis. The Mito stress test injects oligomycin, FCCP, and electron transport chain inhibitors Antimycin A and Rotenone at 20 min intervals on the EC monolayer to measure the basal and spare respiratory capacity in real-time. Oxygen consumption rate (OCR) is used as the read out for mitochondrial respiration by oxidative phosphorylation. Results were analyzed with the Wave software and the Seahorse Report Generator.

4.3 Immunofluorescence staining

4.3.1 Seeding and fixation of cells on coverslips

Coverslips were briefly sterilized with 75% ethanol and subsequently with 100% ethanol. They were then placed in 24-well plates, dried off and coated with 1% gelatin or 1mg/ml rat-tail collagen. HUVECs were seeded on the coverslips, then treated according to the experimental conditions. HRMVECs/MBMECs were seeded in a 24-well plate containing coverslips and cultured in ECGM MV with 10% FCS. Then the cells were washed in PBS fixed with 4% Roti®-Histofix (fixation solution) for 15 min at RT. Then, the cells were washed thrice with PBS to remove excess Histofix.

4.3.2 Immunofluorescence staining and quantification

On the day of staining, the cells were permeabilized and blocked with 2.5% BSA and 0.3% Triton X-100 for 1 h. After blocking, the cells were incubated with the primary antibody at 4 ℃ overnight. The following day, the cells were washed thrice with PBS to remove unbound antibody and incubated at RT for 1 h in secondary antibodies. After 3 washes with PBS, the

cells were incubated at RT for 15 min with DAPI, followed by 3 more washes with PBS. The coverslips were then carefully picked out from the wells with forceps and mounted on an object slide with mounting medium (Roti®-Mount FluorCare). Photos were taken by confocal laser scanning microscopy (Leica Microsystems, Germany).

For immunofluorescence staining, staining intensity was quantified with Image J (NIH, USA). Pixel densities were analyzed by drawing a line across the cell (line scan), such that the cell membrane, nuclear and cytoplasmic regions were marked. Approximately 10 cells were analyzed per experimental group. This method was used for the quantification of membrane protein expression in immunofluorescence staining. The concentrations of the primary and secondary antibody are mentioned in **Table 11** and **12**, respectively.

4.3.3 Retinal whole mount immunofluorescence staining for Tie-2

For whole mount staining, mouse eyes were fixed in 4% PFA for 15 min. After dissection, the retinae were cut into four leaves at the periphery, and fixed in methanol for 15 min. Next, the retinae were washed with PBS and incubated with permeabilization/blocking solution (2% BSA, 0.5% Triton X dissolved in PBS) for 1 h at room temperature. Post-incubation, the retinae were incubated with anti-Tie-2 antibody and anti-Lectin-TRITC overnight at 4 ℃. The retinae were then washed and incubated for 1 h at RT with the donkey anti-goat-FITC secondary antibody. Finally, the retinae were mounted on glass slides with Roti-mount. Photos were taken by confocal laser scanning microscopy (Leica Microsystems, Germany). The concentrations of the primary and secondary antibody are mentioned in **Table 11** and **12**, respectively.

4.4 Protein biochemical methods

4.4.1 Protein extraction from the retina

All procedures were performed on ice. The retina from a frozen and unfixed eye was quickly extracted under the microscope and placed in an Eppendorf containing 120 µl of ice-cold RIPA buffer. Each retina was thoroughly homogenized by passing the suspension through syringe needles of descending diameters (22G, 25G, 27G, 30G). The homogenate was then centrifuged at 13,000 rpm at 4 ℃ for 30 min. The supernatant was moved to a fresh Eppendorf for further analysis.

4.4.2 Protein extraction from cells

All procedures were performed on ice. The cells were washed thrice with ice-cold PBS and lysed in chilled RIPA buffer. The volume of buffer per dish is shown in **Table 22**. Once the RIPA buffer was added to the cells, they were harvested from the dish with the help of a cell

scraper. The collected suspension was transferred to a pre-cooled Eppendorf and incubated on ice for 20-30 min. The suspension was then centrifuged at 13000 rpm for 15 min at 4℃. The supernatant containing the cell contents was collected in a fresh tube. Protein amounts were subsequently quantified and equalized before use.

Table 22: Optimization of lysis buffer

***Wells per*Culture plates / dishes**	**Seeding density**	**Confluence**	**Lysis buffer (µl)**
24 well	50,000	$0.5x10^5$	30
12 well	100,000	$1.2x10^5$	60
6 well	250,000	$4.0x10^5$	150
6 cm	550,000	$3.0x10^6$	300
10 cm	1000,000	$6.0x10^6$	500

4.4.3 Estimation of protein amount using BCA assay

Bicinchoninic Acid (BCA) assay is a colorimetric technique used to estimate protein amount prior to SDS-PAGE and other experiments. Peptide bonds in proteins reduce the copper ion in $CuSO_4.5H_2O$ which then chelates to the Bicinchoninic acid resulting in a color change from green to purple. The amount of protein is directly proportional to the optical density (OD) of the final product which can be detected at 565 nm.

The assay was performed in flat-bottomed 96-well plates. BSA with concentrations 0, 0.25, 0.5, 1, and 2 µg/µl were used to generate a standard curve as shown below. 10 µl of whole or diluted protein lysate was pipetted in duplicates. 100 µl of BCA solution was added to each well. The BCA solution was prepared as follows:

BCA A: Dissolve in 40 ml H_2O 3.420 g Na_2CO_3, 0.800 g NaOH, 0.132 g Na. K-tartrate.$4H_2O$, adjust the pH to 11.25 with $NaHCO_3$, adjust the volume to 50 ml with H_2O

BCA B: Dissolve in 4 ml H_2O 0.2 g BCA.Na_2, adjust the volume to 5 ml with H_2O

BCA C: Dissolve in 5 ml H_2O 0.2 g $CuSO_4.5H_2O$

Final BCA mixture: 50% BCA A + 48% BCA B + 2% BCA C

The plate was covered and incubated at 60 ℃ for 30 min. The OD for the samples were then read using a spectrometer at 595 nm. A standard curve was created by making linear regression of the OD values against the concentrations. The protein concentrations of the samples were extrapolated from the standard curve (**Fig. 16**). Protein amount was equalized with RIPA buffer and further denatured prior to SDS-PAGE or for storage.

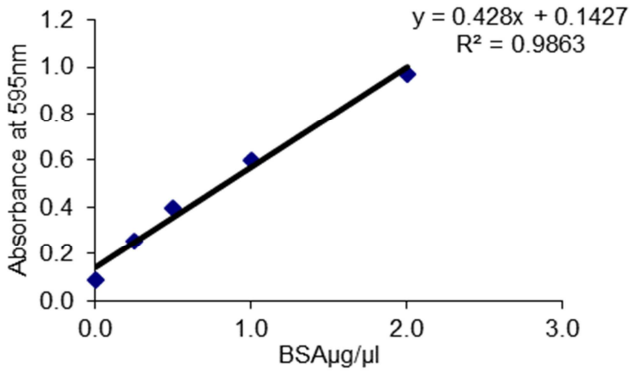

Fig. 16: Standard curve of a BCA assay. *The curve was generated using different concentrations of BSA and the corresponding OD. The protein concentrations of the samples were extrapolated from the standard curve.*

4.4.4 Protein denaturation

Prior to investigation via SDS-PAGE, the protein lysates from cells and retinae were denatured with 4X SDS loading buffer (Laemmli buffer) and boiled at 95 ℃ for 5 min on a heating block. The mixture was then cooled on ice and used for SDS-PAGE or directly stored at -20 ℃ until further analysis. If the lysates were used to detect N1-phospho-histidine, then after addition of Laemmli buffer, the lysates were denatured by incubating overnight at 4 ℃.

4.4.5 Western blotting/immunoblotting

4.4.5.1 SDS-polyacrylamide gel electrophoresis (SDS-PAGE)

SDS-PAGE is a technique used to separate polypeptides according to their sizes. The polypeptides travel along the SDS polyacrylamide gel through an electricity gradient that separates the peptides according to their sizes, the largest migrating the slowest. The separated proteins were then blotted onto a nitrocellulose membrane, where they were stained with antibodies specific to the target protein. Further visualization, analysis, and

quantification of the amount of protein bound to the membrane is indicative of the expression of target proteins.

4.4.5.2 Gel casting

An SDS-PAGE gel consists of a stacking gel and a separating gel. The size of the target protein decides the percentage of polyacrylamide in the gels as seen in **Table 23**. The reagents for making the stacking and separating gels are shown in **Table 24** and **25**. The two solutions were carefully prepared and pipetted between glass plates held together on a gel-casting stand; the stacking gel was layered above the separating gel. The separating gel was allowed to polymerize for 20-30 min before adding the stacking gel. A gel comb was used to create wells in the stacking gel for protein loading. The stacking gel polymerized in 15 min. The whole gel was either used immediately or stored at 4 ℃.

Table 23: Size of proteins and gel percentage

Size of protein (KDa)	**Gel percentage (%)**
20	15
20-40	12
40-80	10
80-100	8
100-200	5-6

Table 24: Components and volumes for casting of separating gels (ml)

Components	**5%**	**6%**	**8%**	**10%**	**12%**	**15%**
H_2O	5.6	5.3	4.6	4.0	3.3	2.3
30% polyacrylamide	1.7	2.0	2.7	3.3	4.0	5.0
1.5 M Tris (pH 8.8)	2.5	2.5	2.5	2.5	2.5	2.5

10% SDS	0.1	0.1	0.1	0.1	0.1	0.1
10% APS	0.1	0.1	0.1	0.1	0.1	0.1
TEMED	0.01	0.008	0.006	0.004	0.004	0.004

Table 25: Components and volumes for casting of stacking gels (ml)

Components	**4%**	**5%**
H_2O	7.2	6.8
30% polyacrylamide	1.3	1.7
1 M Tris (pH 6.8)	1.25	1.25
10% SDS	0.1	0.1
10% APS	0.1	0.1
TEMED	0.01	0.01

4.4.5.3 Gel loading and protein separation

The fully polymerized SDS-PAGE gel was mounted on a gel cassette and placed in an electrophoresis chamber with 1X SDS running buffer. The comb separating the wells was removed and the denatured protein lysates and a suitable protein marker were applied to the sample-loading wells. The anode and cathode were correctly connected to a power source. A voltage of 90 V was applied until the proteins were past the stacking gel. The voltage was then increased to 120 V to separate the proteins according to their molecular size. The protein separation was stopped when the bromophenol blue staining of the lysates reached the end of the separating gel. The proteins were then transferred to a membrane.

4.4.5.4 Transfer of proteins onto a nitrocellulose membrane

Following SDS-PAGE, the proteins were transferred from the gel to a nitrocellulose membrane. The materials required were pre-soaked in western transfer buffer and stacked according to **Fig. 17**. The gel was extracted from between the glass plates and placed together with the nitrocellulose membrane in a sandwich between pre-soaked Whatman's filter paper. The combination was smoothed with a roller to eliminate air bubbles between the membrane and the gel. The sandwiched transfer stack was placed in the cassette in a chamber filled with 1X Transfer buffer. The sandwich was organized as follows: anode side - sponge - Whatman paper X 2 - nitrocellulose membrane - gel - Whatman paper X 2 - sponge - cathode side. An ice cooling unit was placed beside the transfer stack to prevent overheating of the transfer assembly. The unit was connected to a power source and the transfer was conducted at 100 V for 60 min. Post-transfer, the membrane was extracted from the sandwich and stained with 0.2% Ponceau S solution to confirm the successful transfer of protein. The membranes were washed with 1X TBST and blocked for 1 h in 1X Roti®-Block at RT.

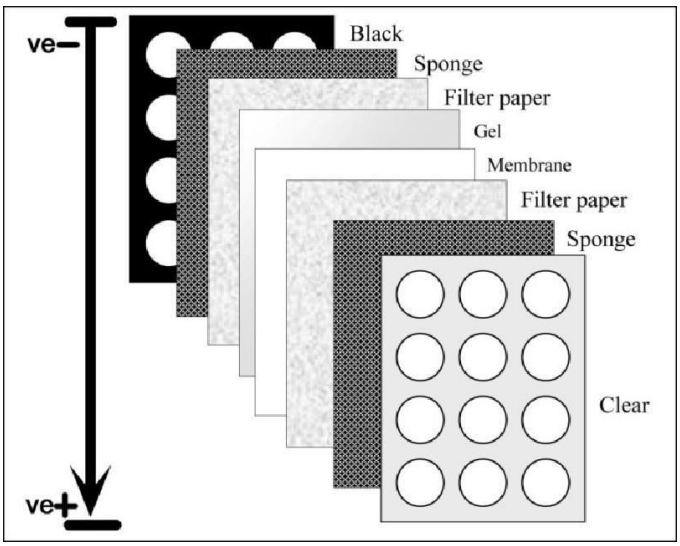

Fig. 17: Assembly of the transfer stack sandwich

4.4.5.5 Antibody incubation

After blocking, the blots were washed shortly in TBST buffer and incubated with primary antibody specific to the protein of interest. The incubation was performed at 4 ℃ overnight. After incubation, the membrane was washed thrice in 1X TBST and incubated on a shaker

for 1 h at RT with the secondary antibody specific to the host of the primary antibody. The secondary antibody was usually HRP-conjugated. The membranes were washed thrice with 1X TBST and were ready to be visualized. The dilution of the primary antibodies and secondary antibodies were as mentioned in **Table 11** and **12**.

4.4.5.6 Protein visualization

The immunoreactive proteins were visualized with enhanced chemiluminescent substrate in an imager (Vilber). Highly expressed proteins were visualized by the Lumi-Light Western Blotting Substrate and weakly expressed proteins with the Super Signal West Femto Maximum Sensitivity Substrate. The obtained images were analyzed and quantified with Image J software.

4.5 Tie-2 immunoprecipitation

Cells seeded on 10 cm dishes were washed with ice-cold PBS and harvested by scraping in 400µl lysis buffer (50 mM Tris-HCl pH 7.4, 150 mM NaCl, 1% Triton X-100) containing protease inhibitor 1 tablet/10 ml protease inhibitor (Roche, Germany) and PhosStop (phosphatase inhibitor, 1 tablet/10 ml Sigma Aldrich, Germany). The lysate was incubated on ice for 20-30 min and centrifuged at 13000g for 15 min at 4 ℃. The supernatant was collected and 60 µl of the supernatant was set aside as Input control. The remainder was incubated with the Tie-2 antibody (AF313, 2 µg per IP) on a rotator at 4 ℃ for 2 h. For each sample, 40 µl beads were washed with lysis buffer. The beads were added to the lysate antibody mixture and incubated on a rotator overnight at 4 ℃. After the incubation, the beads were collected by centrifugation, and washed with lysis buffer containing PhosStop. The immune complexes on the beads were then denatured with 1X Laemmli buffer and the lysates were investigated by western blotting. Detection of Tie-2 was performed with rabbit-anti-Tie-2 (Santa Cruz, 1:500) and phosphorylation with mouse-anti-pTyrosine 4G10 (Millipore, 1:1000).

4.6 Precipitation of O-GlcNAcylated proteins with sWGA beads

Succinylated WGA-conjugated agarose beads were implemented to precipitate the O-GlcNAcylated proteins according to the manufacturer's instructions. In brief, HUVECs in 10cm dishes were harvested in 400 µl WGA lysis buffer (50 mM Tris-HCl pH 7.4, 100 mM NaCl, 1% TritonX-100) containing a protease inhibitor (1 tablet/10 ml, Roche). The lysate was incubated on ice for 20-30 min and centrifuged at 13000g for 15 min at 4 ℃. The

supernatant was collected and 60 µl of the supernatant was set aside as Input control. For each precipitation, 40 µl beads were washed with WGA washing buffer (50 mM Tris-HCl pH 7.4, 100 mM NaCl, 0.1% TritonX-100). The remainder of the lysate was mixed with the prepped beads and incubated on a rotator at 4 ℃ ov ernight. Post-incubation, the beads were collected by centrifugation and washed thrice with WGA washing buffer. The beads were then suspended in 1X Laemmli buffer, and denatured for 5 min at 95 ℃ to extract the immunocomplexes for the analysis by western blotting.

4.7 Experimental analyses with kits

4.7.1 Cell fractionation kit

Fractionation of cells was performed with a commercially available kit (78840, ThermoFischer Scientific, Germany). HUVECs were cultured and treated accordingly. The cells were trypsinized and subjected to cytoplasm, nuclear, and membrane isolation buffer as described in the manufacturer's protocol. After separation, the respective fractions were dissolved in 4x Laemmli sample buffer and denatured at 95 ° C for 5 min. The obtained fractions were used for further western blotting.

4.7.2 Ang-2 ELISA

HUVECs were treated as illustrated in the results. The supernatants were collected and centrifuged to exclude cellular debris. These cleared supernatants were then used to detect secreted Ang-2 using the human Angiopoietin-2 DuoSet kit (DY623, R&D Systems, Germany) according to the manufacturer's instructions.

4.7.3 OGA activity

OGA activity was measured with a commercially available O-GlcNAcase assay kit (E-130, BMR Service, SUNY, Buffalo, USA). 5 retinae per genotype were each homogenized in 120 µl of an SDS-free buffer provided with the kit. Similarly, NDPK-B deficient HUVECs were harvested from 6 cm dishes in 200 µl buffer and homogenized. The homogenates were centrifuged, and the supernatant was incubated for 5 min on ice with intermittent agitation and centrifuged for 15 min. The homogenate was then centrifuged, and the supernatant was collected. 10 µl of the supernatant was used to measure OGA activity according the manufacturer's instructions.

4.7.4 NDP kinase activity assay

HUVECs and retinae were lysed in RIPA buffer and immediately subjected to the NDP kinase activity assay (**Fig. 18**). The test utilizes NDPK catalytic activity to transfer the

phosphate in GTP to ADP, generating ATP. The ATP is measured by the Kinase-GLo kit, in which ATP catalyzes the conversion of D-Luciferin to Oxyluciferin in the presence of the enzyme luciferase. The luminescent signal recorded correlates with the amount of ATP produced and is in turn proportional to the NDP kinase activity. A standard curve was generated using different concentrations of ATP (0.5 - 10 µM) dissolved in water. The NDP kinase activity in lysates was measured in a 384-well plate. Lysates were diluted in assay buffer (50 mM Tris-HCl, pH 7.5, 2 mM MgCl2, 1 mM DTT, 0.01% BSA) constituting the reaction mixture. Lastly, an ATP dependent luciferase was added to the reaction mixture and incubated at RT for 5 min. The luminescence was measured with a multiplate reader.

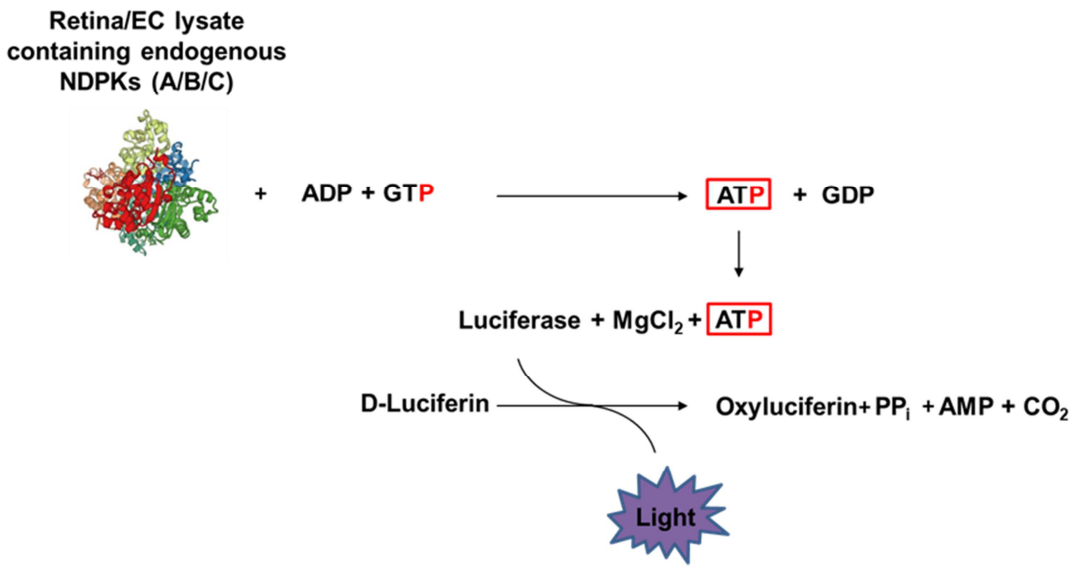

Fig. 18: Working principle of the NDP kinase activity assay

4.8 Quantitative PCR

4.8.1 Isolation of RNA from HUVECs

On the day of isolation, the HUVECs were washed thrice in ice-cold PBS and scraped in Trizol reagent. The Trizol reagent containing the cells was homogenized by pipetting up and down. Chloroform was then used to extract the RNA from the homogenate and the mixture was centrifuged at 12000 g for 15 min at 4 ℃. The aqueous layer containing the RNA was carefully removed and placed in a fresh Eppendorf. The RNA was then precipitated with an equal volume of isopropyl alcohol and centrifuged at 12000 g for 10 min at 4 ℃. The supernatant was siphoned off and replaced with 75% ethanol to purify and wash the RNA extract. The suspension was centrifuged at 9000 g for 5 min at 4 ℃. The purified pellet was

allowed to air dry and dissolved in RNase-free H_2O for 10 min at 60 ℃ with shaking. The pellet was either used for RNA estimation or stored at -80 ℃ for further use.

4.8.2 Preparation of cDNA and qPCR

RNA concentration was measured with a Nanodrop machine. Recorded RNA concentrations were used to create a suspension containing at least 1 µg of RNA. A reaction mixture was created with RNA, 4 µl of Superscript VILO cDNA synthesis reagent, and volume made up to 20 µl with RNase-free H_2O. Program for cDNA synthesis is as follows:

25 ℃ 10 min → 42 ℃ 60 min →85 ℃ 5 min

cDNA was used in the dilution 1:5 with H_2O for qPCR. 2 µl of cDNA was pipetted into the Microwell qPCR plates. A reaction mixture containing Taqman Fast advanced mastermix, the respective primers, and H_2O was assembled and 18 µl of the mixture was pipetted into the wells containing cDNA. The plate was then briefly centrifuged and placed in the Quantstudio 3 (Applied Biosystems) for qPCR. The C_T values obtained were used for analysis by the comparative C_T ($\Delta\Delta C_T$) method [218].

4.9 Data quantification and statistical analysis

For western blot analysis, the images from protein visualization were used for quantification. Images were loaded in Image J software and individual bands were selected using the 'Select tool'. The area of the select tool was adjusted in a way to allow the maximum amount of the band and the minimum amount of the background to be selected. The 'measure' function was used to measure the density of the selected band. Keeping the 'Area' parameter the same, successive bands on the same membrane were measured. 'Median' measurement was used for all quantification purposes.

All of the experiments were then analyzed statistically using the GraphPad Prism 6 software (GraphPad Software, La Jolla). For statistical analysis, data were presented as mean±SD. Statistical significance was established with paired/unpaired Student's t-test or Analysis of Variance (ANOVA) with Tukey's post-test. p values < 0.05 were considered statistically significant.

5. Results

Most of the data shown are also part of two submitted manuscripts. This is stated here to acknowledge this correctly.

5.1 The importance of Ang-2-Tie-2 signaling in HG and NDPK-B deficiency-mediated vasoregression

5.1.1 Ang-2 mediates NDPK-B deficiency-induced vascular regression

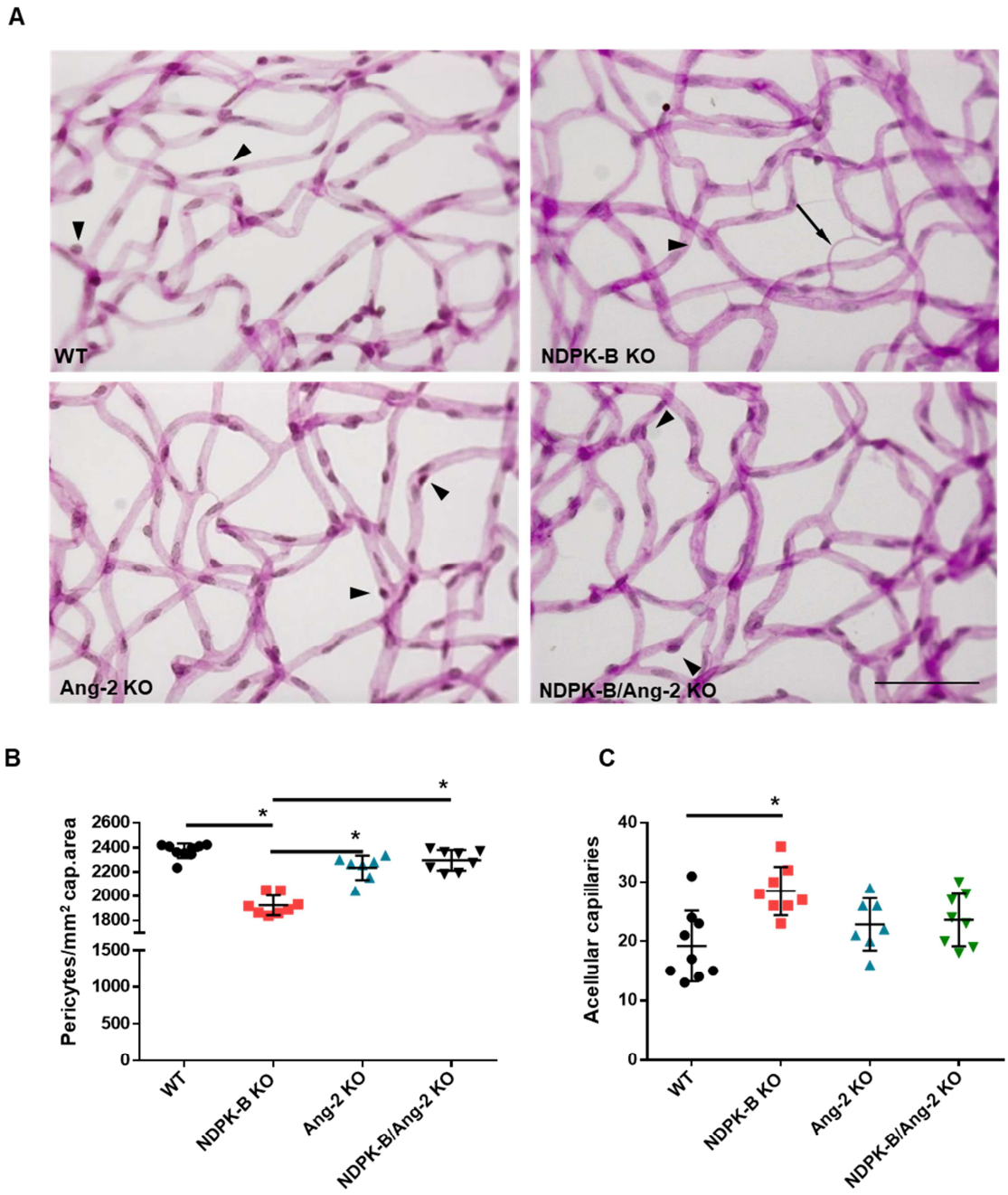

Fig. 19: Ang-2 is the mediator of NDPK-B deficiency-induced vasoregression. *Retinal vasculature was visualized by retina digestion method and PAS staining. PCs and AC were assessed*

*using quantitative retinal morphometry. A: Representative retinal digestion preparations from retinae. PCs and AC are indicated by arrowheads and arrows respectively. B: Quantification of PC numbers, (n=9, 8, 7, 8). C: Quantification of AC numbers, (n=9, 8, 7, 8). Cap. area: capillary area. Results are displayed as mean±SD. * p<0.05. Magnification: 40×. Scale bar: 50 µm.*

As illustrated in published findings, NDPK-B deficient retinae exhibited DR-like pathology accompanied by an elevation of Ang-2 [213]. Early morphological changes in DR are mediated by an elevated expression of Ang-2. In order to investigate if upregulation of Ang-2 is responsible for the DR-like pathology observed in NDPK-B deficient retinae, we crossbred the NDPK-B deficient mice with Ang-2 deficient mice to obtain NDPK-$B^{-/-}$/Ang-$2^{+/-}$ mice. 8-month-old mice from groups NDPK-$B^{+/+}$/Ang-$2^{+/+}$ (WT), NDPK-$B^{-/-}$/Ang-$2^{+/+}$ (NDPK-B KO), NDPK-$B^{+/+}$/Ang-$2^{+/-}$ (Ang-2 KO), and NDPK-$B^{-/-}$/Ang-$2^{+/-}$ (NDPK-B/Ang-2 KO) were sacrificed and their retinae were isolated. The isolated retinae were then digested, and the vasculature was assessed by retinal morphometry, where the PCs and the number of AC were quantified (**Fig. 19A**). In agreement with prior findings, NDPK-B KO retinae demonstrated significant loss in PC coverage (**Fig. 19B**) and increase in AC (**Fig. 19C**) than the WT controls. Ang-2 KO (Ang-2 haplodeficiency) yielded no observable morphological changes in the retinae. Interestingly, NDPK-B/Ang-2 KO mice reversed the vasoregression seen in NDPK-B KO retinae. 50% deletion of Ang-2 in the NDPK-B/Ang-2 KO animals was sufficient to rescue the PC dropout seen in NDPK-B KO. These data indicate that NDPK-B deficiency induces retinal vasoregression via elevated Ang-2.

5.1.2 Tie-2 is upregulated in NDPK-B deficient retinae

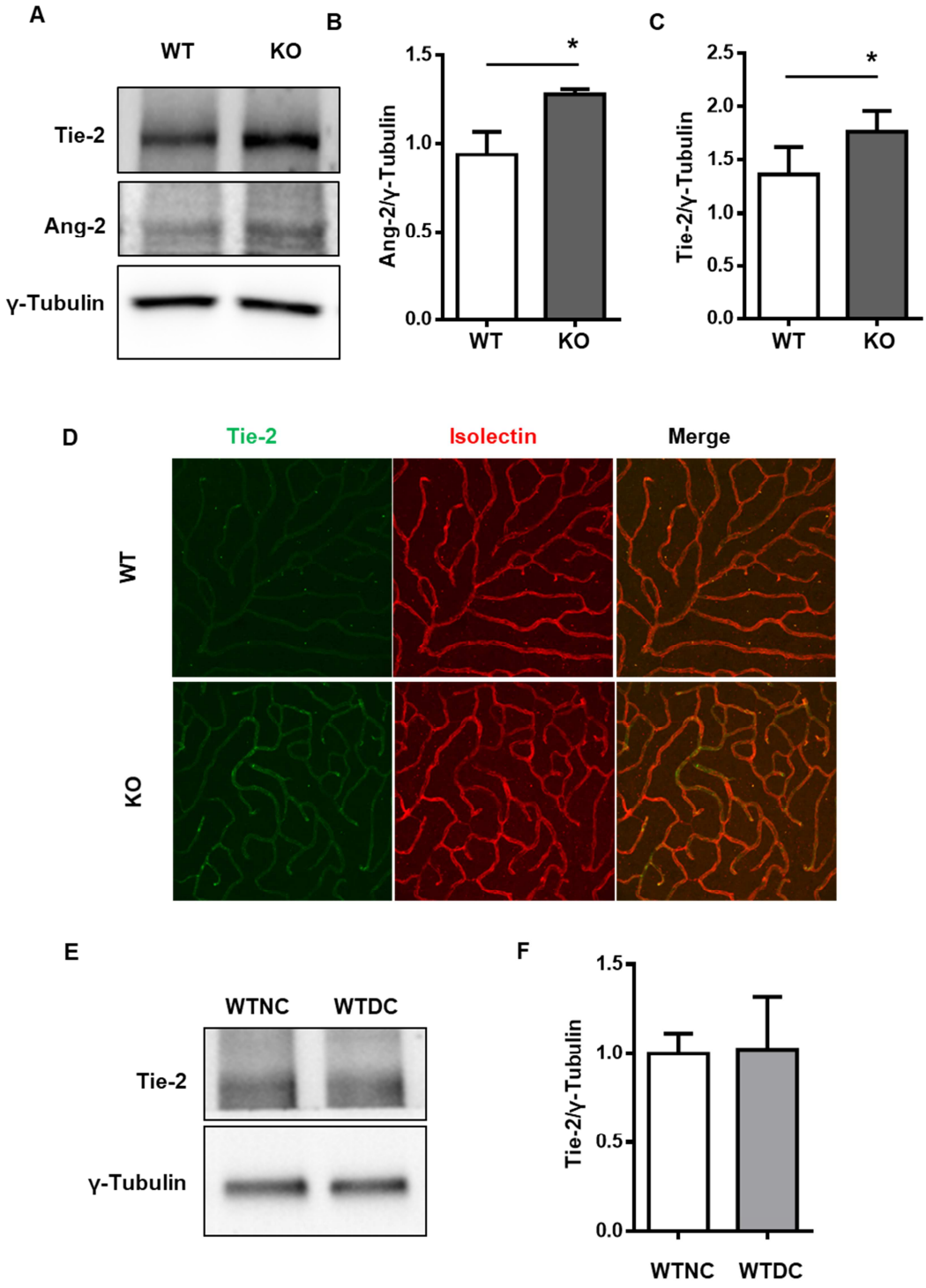

Fig. 20: Tie-2 is upregulated in NDPK-B deficient but not in diabetic retinae. *A: Representative immunoblots of Tie-2, Ang-2, and γ-Tubulin in NDPK-B$^{-/-}$ retinal lysates. B and C: Quantification of Ang-2 and Tie-2, respectively, normalized to γ-Tubulin (n=5). D: Expression of Tie-2 (green) and Isolectin (red) in the deep capillary layer of WT and KO retinae. The pictures shown are*

*representative of staining from the 3 animals in each group. E: Representative immunoblots of Tie-2 and γ-Tubulin in diabetic and non-diabetic retinal lysates. F: Quantification of Tie-2 normalized to γ-Tubulin (n=5). Results are displayed as mean±SD. WT: wild type, KO: NDPK-B$^{-/-}$, WTNC: wild type non-diabetic, WTDC: Wild type diabetic. * p<0.05.*

To address a potential role of Tie-2 in Ang-2 signaling in the context of NDPK-B deficiency, we investigated the expression of Tie-2 in 5-month-old NDPK-B$^{-/-}$ (KO) mouse retinae by immunoblot. Similar to prior findings, Ang-2 was significantly upregulated in KO retinae compared to WT by about 30% (**Fig. 20A and B**). Similarly, the level of Tie-2 in the KO retinae was also about 30% higher than in the WT retinae (**Fig. 20A and C**). To verify that this increase occurs in the endothelium, we assessed the localization of Tie-2 in the retina via whole mount immunofluorescence staining. Isolectin staining distinguished the vasculature from the surrounding retinal tissue (**Fig. 20D**). Tie-2 was predominantly expressed in the vasculature. Its expression was unaltered in the KO and WT arterioles, venules, as well as in the superficial capillary layer (data not shown). However, in the deep capillary layer, where vasoregression commonly originates, higher Tie-2 expression was observed in the KO than in the WT retinae (**Fig. 20D**). Taken together, the data show that Tie-2 is upregulated in the KO retinae, especially in the deep capillary layer, suggesting a potential contribution of Tie-2 signaling to the upregulation of Ang-2. NDPK-B KO retinae largely mimic diabetic retinae in regards to the upregulation of Ang-2 and the subsequent development of vasoregression [213]. To determine whether Tie-2 expression in diabetic retinae resembled the NDPK-B KO retinae, 3-month-old diabetic mouse retinal lysates were assessed by immunoblot. Tie-2 expression in the retina was not altered in the diabetic retinae (**Fig. 20E and F**). Thus, the phenotype of NDPK-B KO retinae apparently differs from that of diabetic retinae regarding Tie-2 expression levels.

5.1.3 NDPK-B depletion but not high glucose induces upregulation of endothelial Tie-2

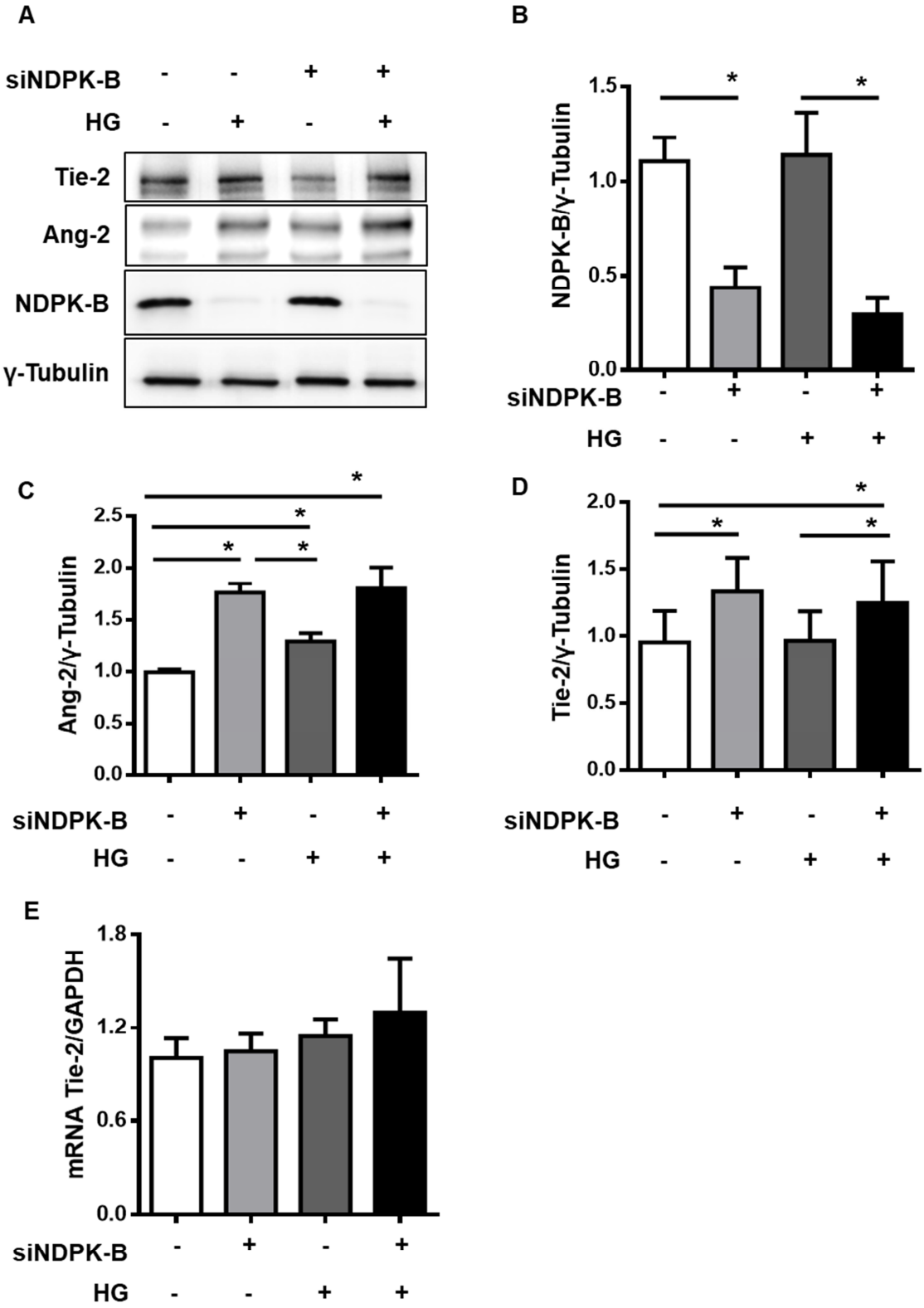

Fig. 21: NDPK-B depletion upregulates endothelial Tie-2 but high glucose does not. *HUVECs were transfected with either scrambled control (-) or siRNA against NDPK-B (siNDPK-B, +). A: Representative immunoblots of Tie-2, Ang-2, NDPK-B, and γ-Tubulin in NDPK-B depleted HUVECs*

*treated for 24 h with (HG, -) or without high glucose (HG, +). B, C, and D: Quantification of NDPK-B, Ang-2, and Tie-2, respectively, normalized to γ-Tubulin (n=4). E: Tie-2 mRNA expression in NDPK-B depleted HUVECs with and without HG treatment normalized to GAPDH (n=4). Results are displayed as mean±SD. * p<0.05.*

To further compare the Ang-2-Tie-2- axis in NDPK-B depletion and high glucose, we treated cultured ECs (HUVECs), in which an efficient siRNA-mediated NDPK-B knockdown was established (**Fig. 21A and B**, [213]), with and without high glucose (HG). HG had no influence on NDPK-B levels (**Fig. 21B**). In accordance with published data, an upregulation of Ang-2 occurred in NDPK-B depleted as well as HG ECs (**Fig. 21A and C**). The increase in Ang-2 levels was however more pronounced in NDPK-B depleted than in HG-treated ECs. As reported before [213], the combination of NDPK-B depletion and HG treatment did not further increase Ang-2 levels. In accordance with the data obtained from NDPK-B-deficient and diabetic retinae, Tie-2 was significantly elevated upon NDPK-B knockdown, however it remained unaltered upon HG treatment (**Fig. 21A and D**). HG treatment of NDPK-depleted ECs did not further alter Tie-2 levels. To determine whether Tie-2 upregulation upon NDPK-B knockdown occurs due to transcriptional regulation we analyzed its mRNA expression. Neither NDPK-B depletion nor HG treatment altered Tie-2 mRNA content (**Fig. 21E**). Taken together, these findings show that the elevation of Ang-2 in NDPK-B deficiency is distinctly higher than in HG. This enhanced Ang-2 upregulation in NDPK-B knockdown in ECs is associated with an increase in endothelial Tie-2 levels.

5.1.4 NDPK-B depletion widely upregulates Ang-2 and Tie-2 in microvascular endothelial cells

To verify that the increase in Tie-2 levels is dependent on NDPK-B depletion and a common regulation in ECs, two microvascular EC cell lines were analyzed. Human microvascular ECs (HMECs) are commercially available immortalized microvascular ECs of dermal origin. Like in HUVECs, NDPK-B was successfully depleted in HMECs via siRNA-mediated gene knockdown. Ang-2 levels were increased by 1.75-fold in NDPK-B depleted HMECs (**Fig. 22A and B**). Concomitant with the Ang-2 elevation, Tie-2 expression increased by about 2-fold. (**Fig. 22A and C**). To further corroborate these findings, NDPK-B was also depleted in human retinal microvascular ECs (HRMVECs). Unlike HMECs, HRMVECs are a non-immortalized primary cell population isolated from the retina of a single donor. HRMVECs used at late passages were characterized by staining with the endothelial marker PECAM-1 and found to be 100% endothelial in nature (**Fig. 22D**). NDPK-B knockdown induced a

significant elevation of Ang-2 and Tie-2 compared to the control group (**Fig. 22E, F and G**). Our findings indicate that NDPK-B depletion regulated Ang-2 and Tie-2 in ECs of different origins.

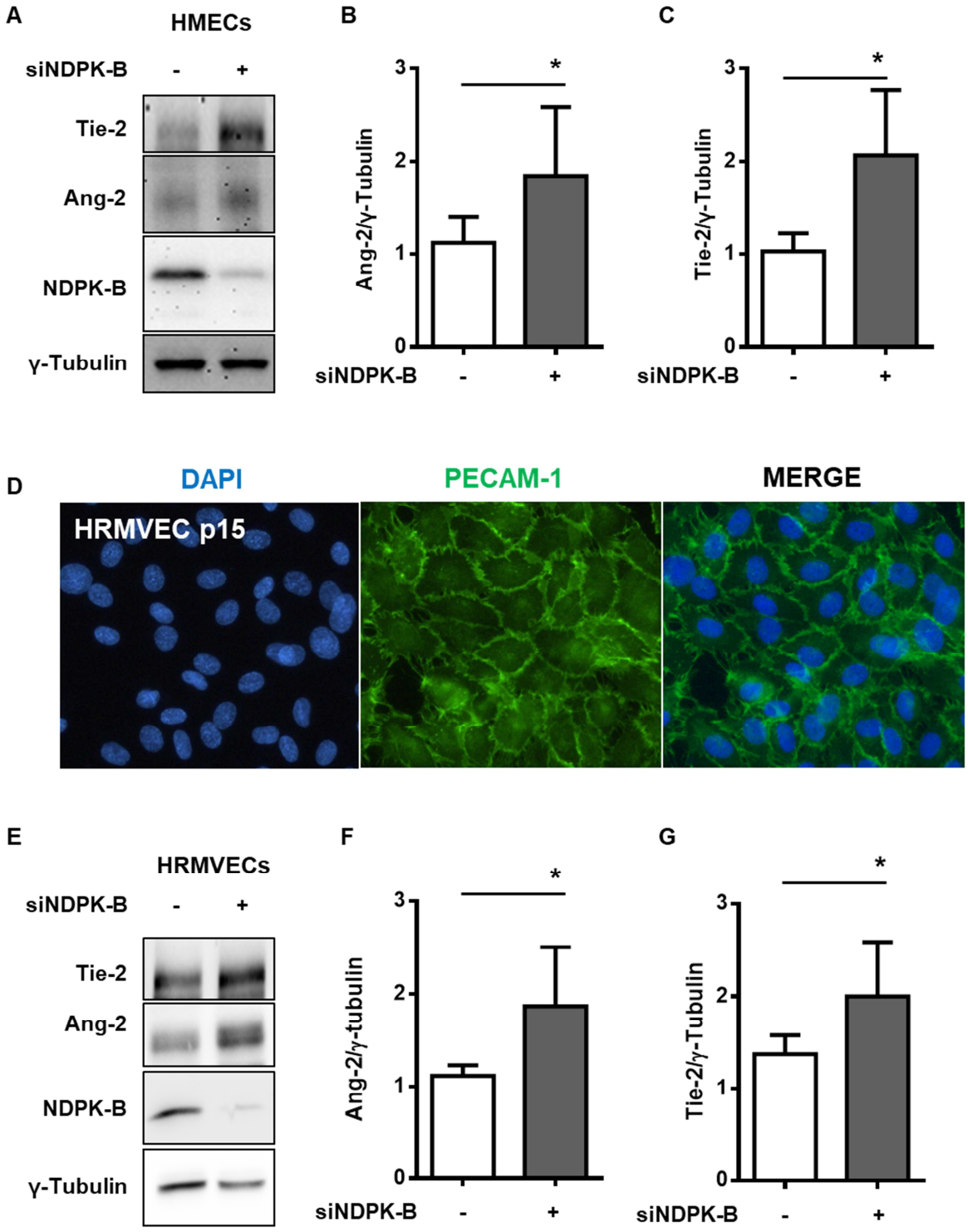

Fig. 22: NDPK-B depletion upregulates Ang-2 and Tie-2 in HMECs and HRMVECs. *HMECs and HRMVECs were transfected with either scrambled control (-) or siRNA against NDPK-B (siNDPK-B, +). A: Representative immunoblots of Tie-2, Ang-2, NDPK-B, and γ-Tubulin in NDPK-B depleted HMECs. B and C: Quantification of Ang-2 and Tie-2, respectively, normalized to γ-Tubulin (n=3). D: Expression of PECAM-1 (green) and DAPI (blue) in the HRMVECs at passage 15. The pictures shown are representative of staining from the 2 independent experiments. E: Representative immunoblots of Tie-2, Ang-2, NDPK-B, and γ-Tubulin in NDPK-B depleted HRMVECs. F and G: Quantification of Ang-2 and Tie-2, respectively, normalized to γ-Tubulin (n=5). Results are displayed as mean±SD. * p<0.05.*

5.1.5 NDPK-B depletion enriches Tie-2 localization at the cell membrane

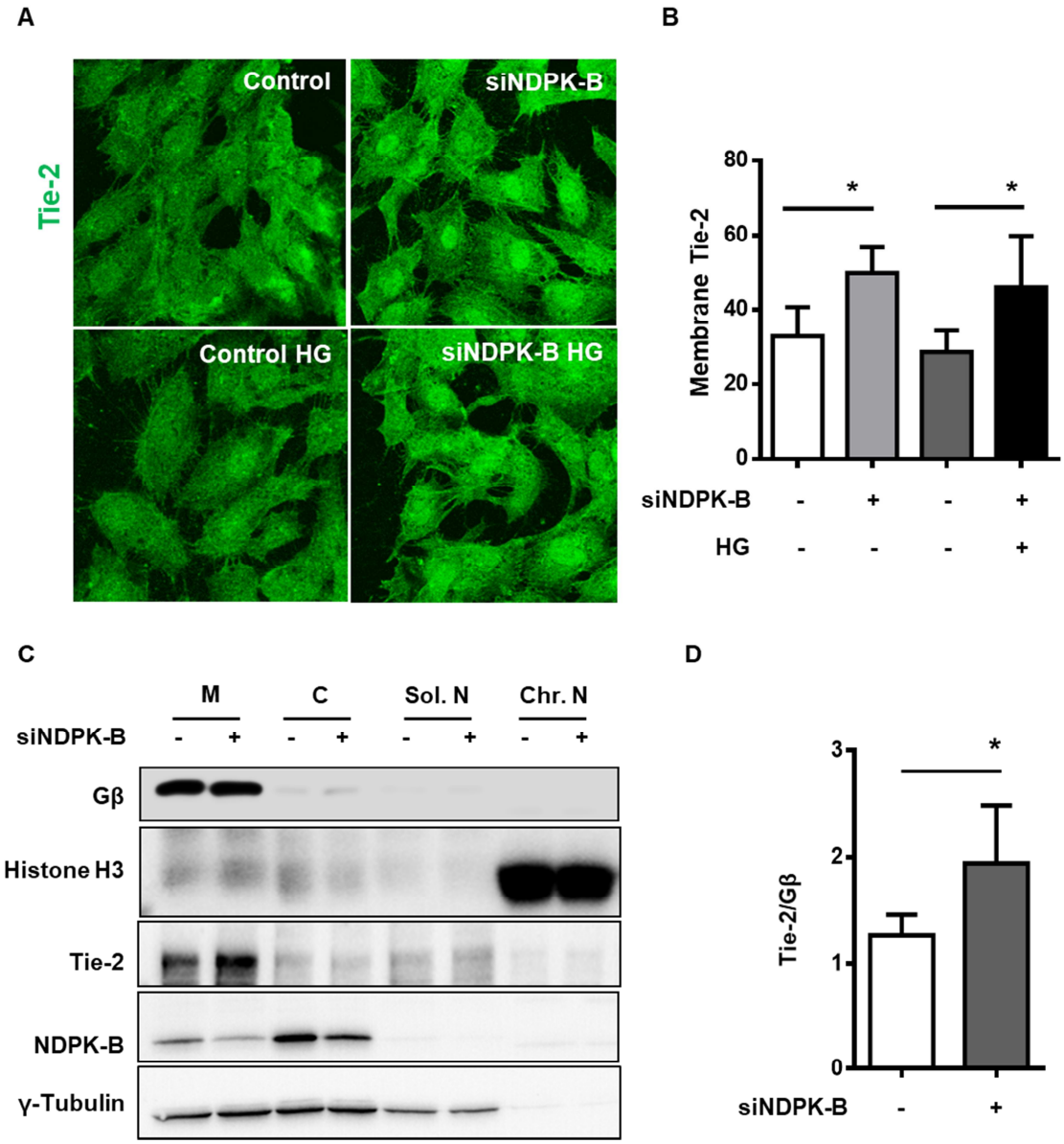

Fig. 23: NDPK-B depletion promotes Tie-2 localization at the cellular membrane. *HUVECs were transfected with either scrambled control (-) or siRNA against NDPK-B (siNDPK-B, +) and treated for 24 h with (-) or without high glucose (HG, +), as indicated. A: Representative immunofluorescence images of Tie-2 expression in NDPK-B depleted ECs with and without HG treatment. B: Quantification of membrane Tie-2 as pixel density in panel A. C: Membrane (M), Cytosolic (C), soluble nuclear (Sol. N), and chromatin nuclear (Chr. N) fractions were assessed to show the subcellular localization of Tie-2. D: Tie-2 was quantified relative to membrane protein Gβ (n=4). Results are displayed as mean±SD * p<0.05.*

Subsequently, we investigated the localization of endothelial Tie-2. Immunofluorescent staining showed that Tie-2 was localized at the cell membrane as well as in intracellular compartments (**Fig. 23A**). After NDPK-B knockdown, the overall Tie-2 content appeared elevated throughout EC, especially at the plasma membrane. HG treatment did not unambiguously alter the subcellular localization of Tie-2. The quantification of Tie-2 levels showed a significant increase at the plasma membrane by about 1.5-fold upon NDPK-B knockdown, but no alteration was detected upon HG treatment (**Fig. 23B**). To substantiate these findings, we performed subcellular fractionation to analyze the Tie-2 content in different cellular compartments of control and NDPK-B depleted ECs by immunoblot. As shown in **Fig. 23C**, the identity of the membrane fraction was validated by Gβ and the chromatin containing nuclear fraction by Histone H3. As expected, γ-Tubulin was present in the membrane, cytoplasmic and soluble nuclear fraction. NDPK-B was detected largely in the cytoplasmic fraction and partially at the membrane. Its knockdown reduced its expression in both of these cellular compartments. Tie-2 was predominantly detected at the membrane and to a much lesser extent in the other fractions. Tie-2 was also detected in the nuclear fractions. In accordance with the immunostainings, the membrane content of Tie-2 was increased about 1.8-fold in NDPK-B depleted cells (**Fig. 23D**), suggesting that NDPK-B knockdown caused the enrichment of Tie-2 at the plasma membrane.

5.1.6 NDPK-B depletion and high glucose reduce Tie-2 phosphorylation

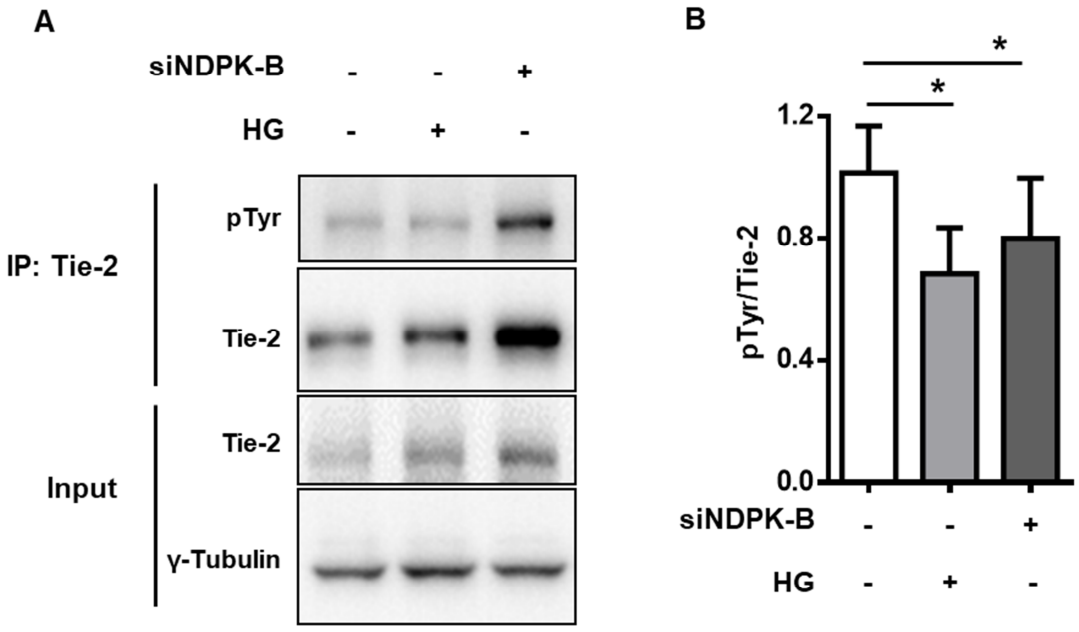

Fig. 24: NDPK-B depletion and high glucose lower Tie-2 phosphorylation. *HUVECs were transfected with either scrambled control (-) or siRNA against NDPK-B (siNDPK-B, +) or were treated for 15 min with (-) or without high glucose (HG, +), as indicated. A: Representative immunoblots of tyrosine phosphorylation (pTyr) of Tie-2 after immunoprecipitation (IP), Tie-2, and γ-Tubulin content in whole cell lysates (Input) are also shown. B: Quantification of Tie-2 phosphorylation relative to the total amount of precipitated Tie-2 (n=3). Results are displayed as mean±SD * p<0.05.*

At the plasma membrane Tie-2 functions as a receptor for the angiopoietins. Its activity can be monitored by the autophosphorylation of Tie-2 on tyrosine residues [109]. Therefore, Tie-2 was immunoprecipitated and its phosphorylation was detected by immunoblot with a phospho-tyrosine (pTyr) specific antibody (**Fig. 24A**). Also, upon immunoprecipitation the increase in total Tie-2 levels after NDPK-B depletion was detected, whereas no significant change was caused by HG treatment. Similarly, the total phosphorylation of Tie-2 was elevated after NDPK-B depletion. However, the relative Tie-2 phosphorylation (pTyr/Tie-2), which monitors the proportion of activated receptors, revealed an approximate 40% decrease upon HG treatment and a 25% decrease after NDPK-B depletion (**Fig. 24A and B**). These data indicate a decreased activation of Tie-2 receptors despite the higher amount of membranous Tie-2 after NDPK-B depletion. As Ang-2 is generally believed to act as antagonist of Tie-2, such a reduction could be caused by an enhanced Ang-2 secretion by the NDPK-B depleted ECs.

5.1.7 NDPK-B depletion in ECs elevates Ang-2 secretion

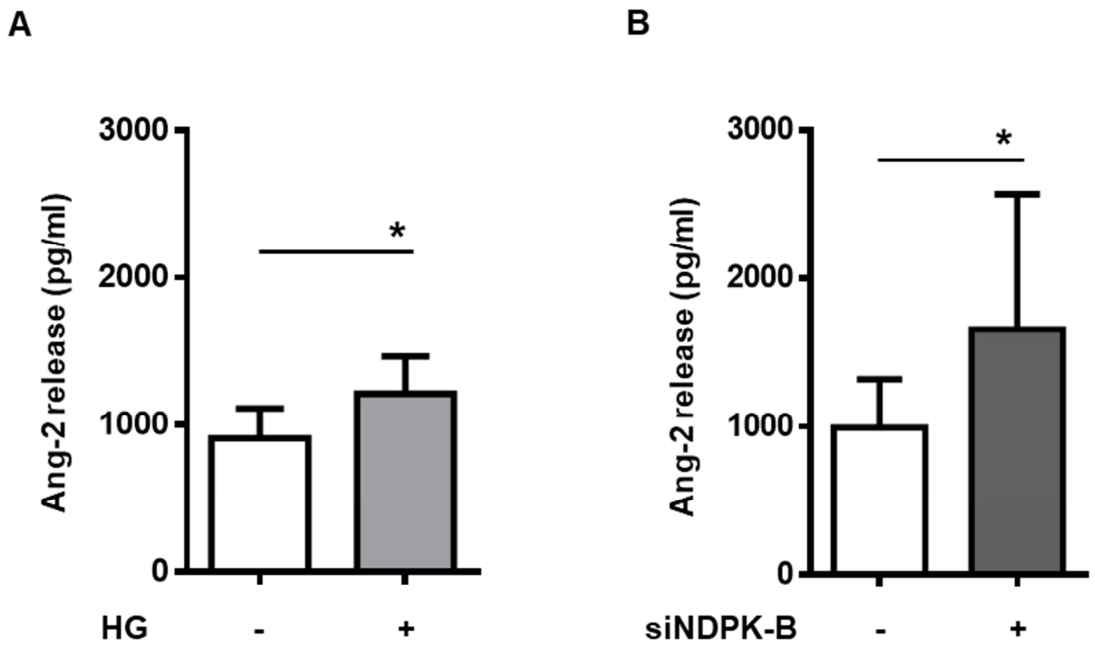

Fig. 25: NDPK-B depletion and HG in ECs promotes secretion of Ang-2. *HUVECs were transfected with either scrambled control (-) or siRNA against NDPK-B (siNDPK-B, +) or treated for 24 h with (-) or without high glucose (HG, +). A and B: Detection of secreted Ang-2 via ELISA in the supernatant of HG-treated (n=7) and NDPK-B depleted ECs (n=5), respectively. Results are displayed as mean±SD * p<0.05.*

As a mediator of vascular remodeling, endothelial Ang-2 is stored in Weibel-Palade bodies and secreted rapidly upon stimulation [113]. To investigate whether the increase in the cellular content of Ang-2 levels is reflected in its secretion, we quantified Ang-2 in the supernatants of cultured ECs by ELISA. HG treatment caused a 1.25-fold increase in Ang-2 secretion compared to low glucose treated controls (**Fig. 25A**). Similarly, NDPK-B knockdown induced an elevation in Ang-2 secretion. In accordance with the data on the increase in total Ang-2 levels in NDPK-B depleted cells (**see Fig. 21C**), the secreted Ang-2 levels in the supernatant were about 1.6-fold higher than in the supernatant of control transfected cells (**Fig. 25B**). The amount of Ang-2 secreted from NDPK-B knockdown ECs was approximately 300 pg/ml higher than in HG-stimulated ECs.

5.1.8 Ligand-Tie-2 interaction is not required for HG-induced Ang-2 upregulation

In order to examine the importance of this increase in extracellular Ang-2 levels for the Tie-2 receptor function in HG-treated ECs, we interrupted the binding of Ang-2 to membranous

Tie-2- by adding soluble Tie-2-Fc (sTie-2), the naturally occurring ectodomain of the Tie-2 receptor. It acts as a scavenger of extracellular angiopoietins, thus blocking the activation and phosphorylation of membranous Tie-2 [219]. Addition of sTie-2 had no effect on Ang-2 levels in control ECs (**Fig. 26**). As shown before, HG treatment induced a 1.5-fold increase in Ang-2 expression (**Fig. 26A and B**). sTie-2 treatment did not alter HG-induced increase in Ang-2 (**Fig. 26B**).

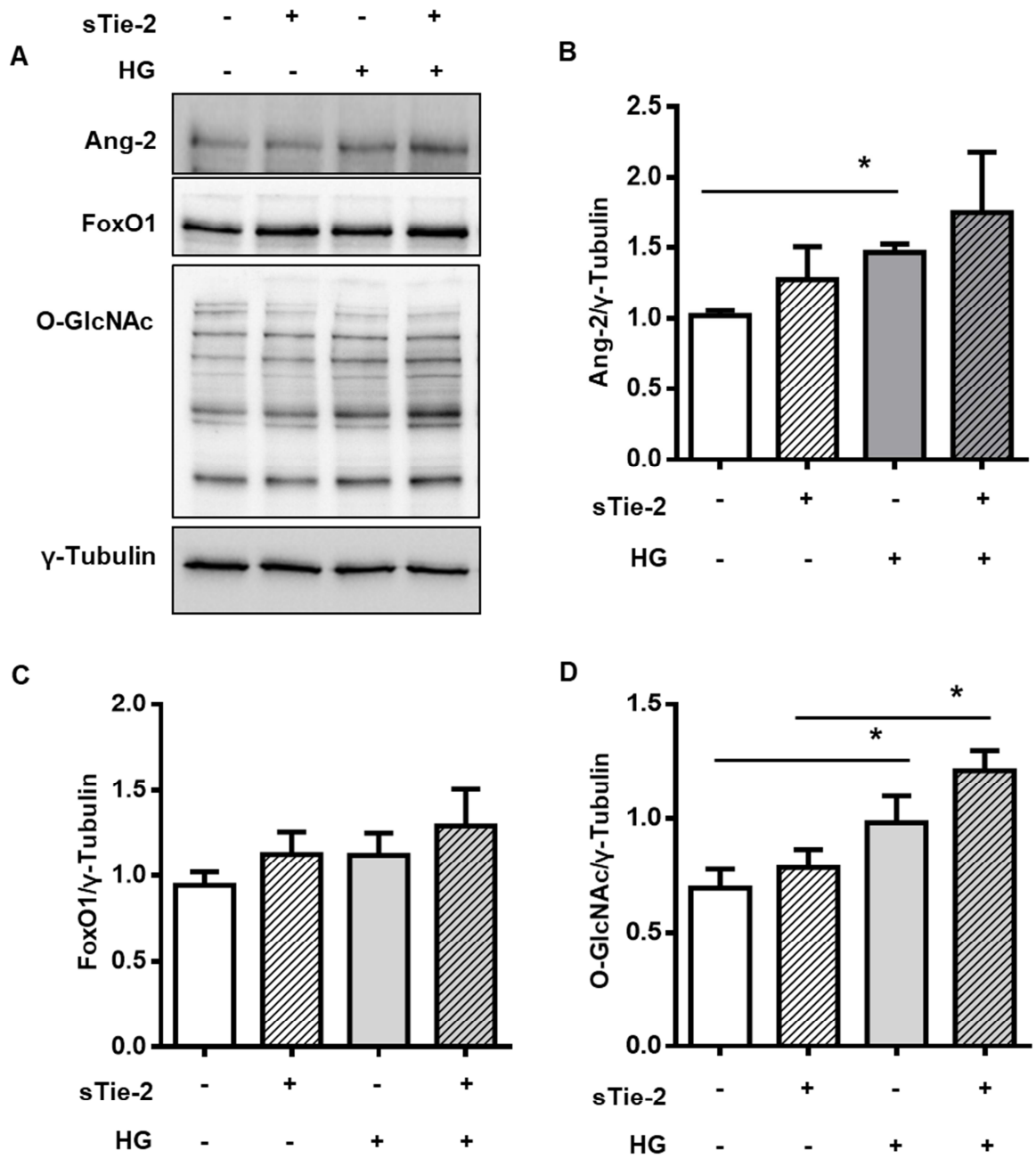

Fig. 26: ***Tie-2 receptor function is not required for HG-induced Ang-2 upregulation.*** *HUVECs were treated with (-) or without high glucose (HG, +) and without (-) and with sTie (+) for 24 h. A:*

*Representative immunoblots for Ang-2, FoxO1, O-GlcNAc,, and γ-Tubulin, as indicated B, C, and D: Quantification of Ang-2, FoxO1, and O-GlcNAc,, respectively, normalized to γ-Tubulin (n=4). Results are displayed as mean±SD *p<0.05.*

These data imply that membrane Tie-2 receptor function has no role in Ang-2 upregulation induced by HG. According to prior work, Ang-2 expression is regulated by FoxO1 [216]. Enhanced protein O-GlcNAcylation upon a loss of NDPK-B increases Ang-2 via O-GlcNAcylation of FoxO1. Therefore, we assessed the involvement of Tie-2 in FoxO1 and O-GlcNAc-mediated regulation of Ang-2. FoxO1 was neither altered by HG nor by sTie-2 treatment (**Fig. 26C**). O-GlcNAc modifications is an off shoot of glucose metabolism and hence susceptible to changes in glucose levels [102, 213]. In accordance with published reports, protein O-GlcNAcylation was significantly increased by HG treatment (**Fig. 26D**). However, sTie-2 had no influence on HG-induced protein O-GlcNAcylation.

5.1.9 Ligand-Tie-2 interaction is required for NDPK B-related Ang-2 upregulation

In order to examine the importance of the increase in extracellular Ang-2 levels for the Tie-2 receptor function in NDPK-B depleted ECs, we interrupted the binding of Ang-2 to membranous Tie-2- by adding soluble Tie-2-Fc (sTie-2). NDPK-B depletion in ECs was achieved via siRNA-mediated knockdown (**Fig. 27A and B**). Addition of sTie-2 had no effect on Ang-2 levels in control ECs (**Fig. 27C**). Tie-2 expression was again elevated in the knockdown ECs but not altered in the presence of sTie-2 (**Fig. 27A and D**). Interestingly, sTie-2 altered the upregulation of Ang-2 upon NDPK-B depletion. Whereas NDPK-B knockdown induced the previously described 2-fold increase in Ang-2 levels, this increase was abrogated in the presence of sTie-2 (**Fig. 27A and C**). These data imply that membrane Tie-2 receptor function contributes to Ang-2 upregulation upon NDPK-B depletion. According to prior work, FoxO1 was significantly elevated in NDPK-B depleted ECs and sTie-2 treatment did not influence this increase in FoxO1 (**Fig. 27A and E**). In line with the findings in Qiu et al., protein O-GlcNAcylation was also elevated in NDPK-B depleted ECs (**Fig. 27A and F**) [213]. Similar to FoxO1, O-GlcNAc elevation was unaffected by sTie-2 treatment indicating that the Tie-2-mediated regulation of Ang-2 in NDPK-B depleted ECs does not involve FoxO1 and O-GlcNAcylation.

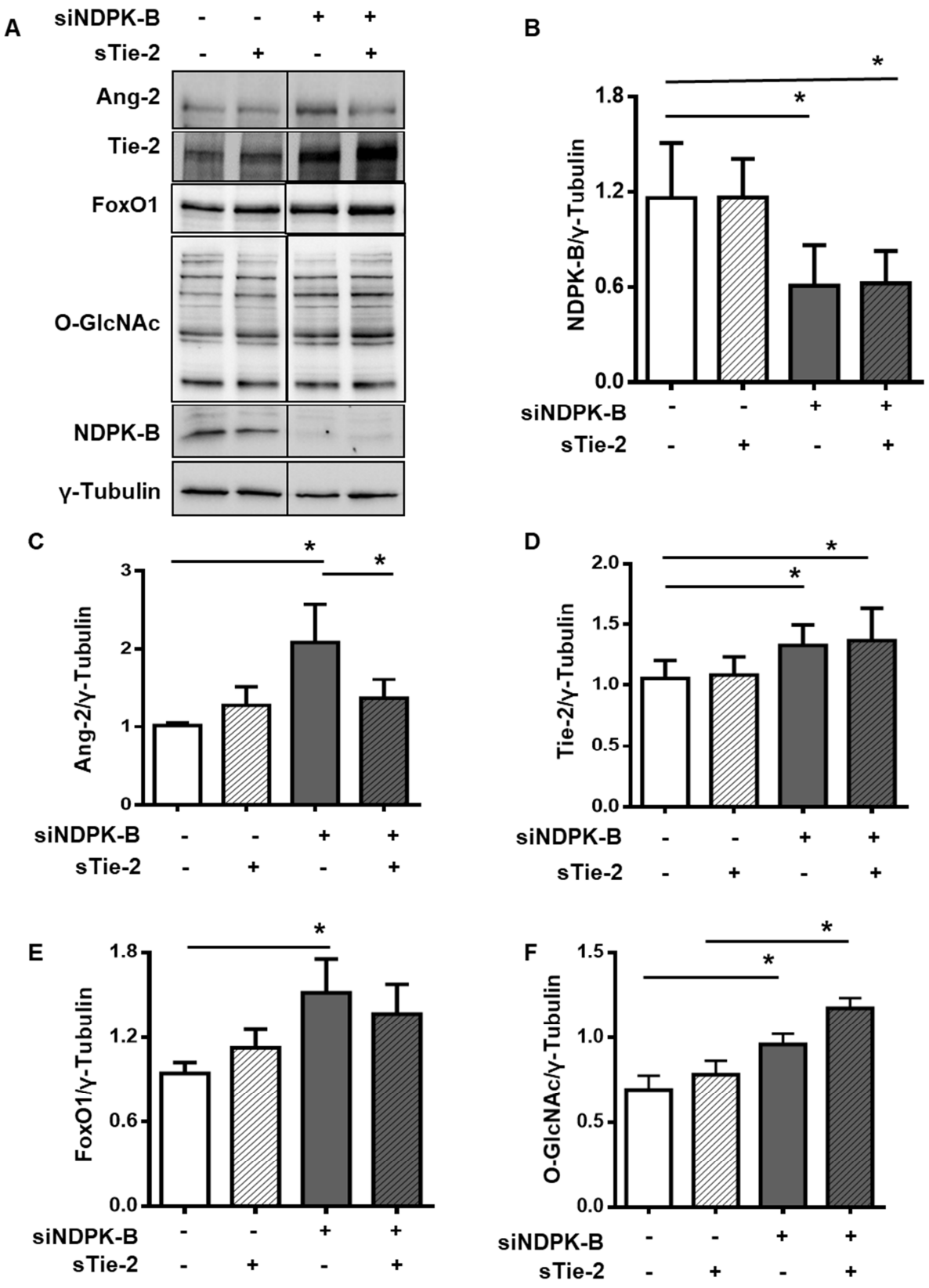

Fig. 27: Tie-2 receptor function is required for NDPK B-related Ang-2 upregulation. *HUVECs were transfected with either scrambled control (-) or siRNA against NDPK-B (siNDPK-B, +), and treated without (-) or with sTie (+) for 24 h. A: Representative immunoblots for Ang-2, Tie-2, FoxO1,*

*O-GlcNAc, NDPK-B, and γ-Tubulin, as indicated. B, C, D, E and F: Quantification of NDPK-B, Ang-2, Tie-2, FoxO1, and O-GlcNAc, respectively, normalized to γ-Tubulin (n=4). Results are displayed as mean±SD *p<0.05.*

5.1.10 Tie-2 receptor expression is required for NDPK-B-induced Ang-2 upregulation

To verify the requirement of Tie-2 for NDPK-B knockdown induced Ang-2 upregulation, we also suppressed Tie-2 levels in ECs via siRNA-mediated gene depletion. NDPK-B was depleted via siRNA (**Fig. 28A and B**). Tie-2 was diminished significantly by about 40% upon knockdown (**Fig. 28A and C**). In the Tie-2-depleted cells, the NDPK-B knockdown-induced elevation of Tie-2 was completely suppressed (**Fig. 28A and C**), suggesting an essential role of Tie-2. Although the Tie-2 depletion had no effect on the basal levels of Ang-2, it effectively inhibited the NDPK-B knockdown-induced elevation of Ang-2 (**Fig. 28A and D**). Taken together, the data indicate that the expression of membrane Tie-2 contributes to the upregulation of Ang-2 in NDPK-B depleted ECs.

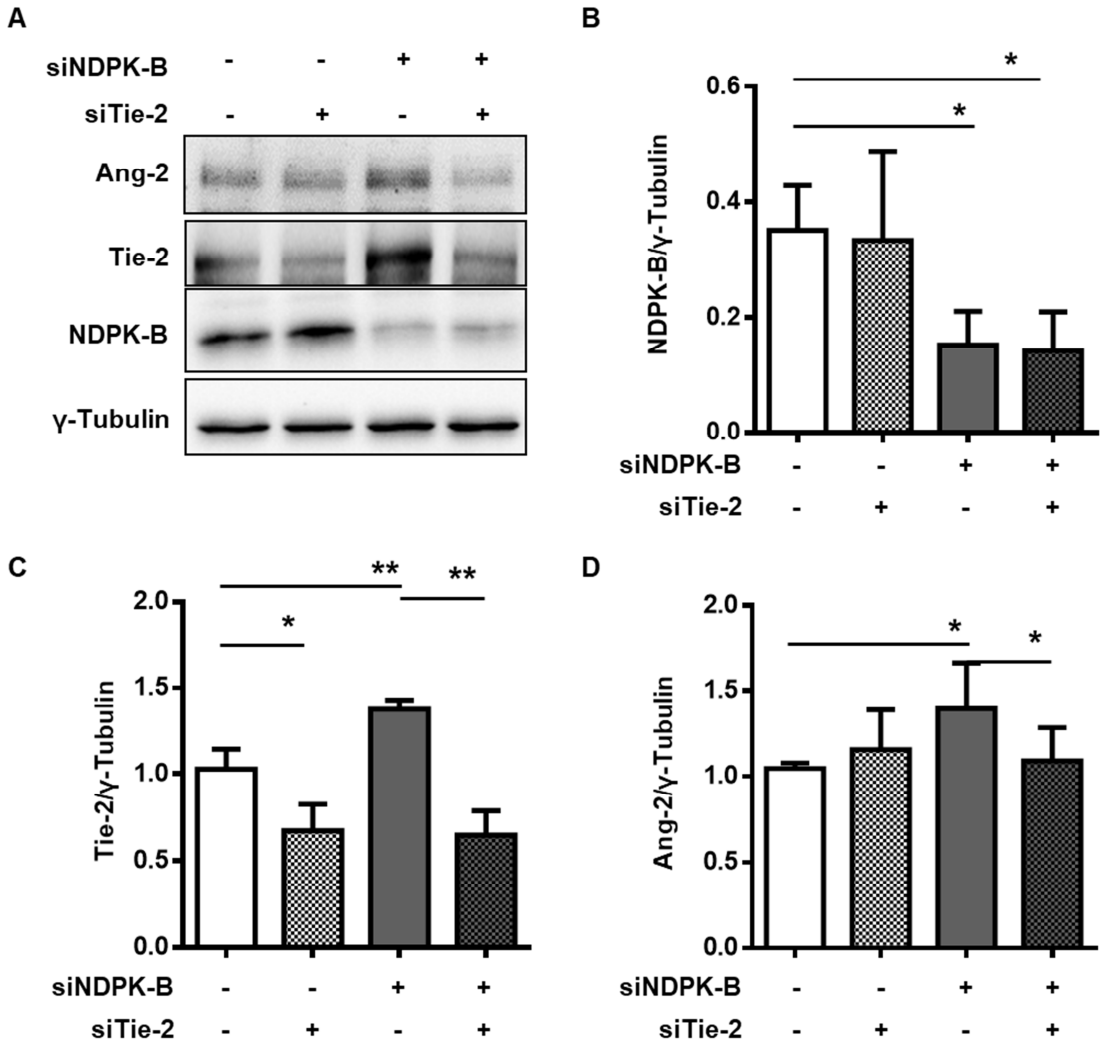

Fig. 28: Tie-2 expression is required for NDPK-B deficiency-induced Ang-2 upregulation. *HUVECs were transfected with either scrambled control (-) or siRNA against NDPK-B (siNDPK-B, +) or Tie-2 (siTie-2, +). A: Representative immunoblots for Ang-2, Tie-2, NDPK-B, and γ-Tubulin in cells depleted of NDPK-B and Tie-2. B, C, and D: Quantification of NDPK-B, Tie-2, and Ang-2, respectively, normalized to γ-Tubulin (n=4). Results are displayed as mean±SD * p<0.05.*

5.1.11 An excess of secreted Ang-2 promotes upregulation of Tie-2

As proof of concept that the upregulation of Tie-2 upon NDPK-B depletion occurs in response to an increase in Ang-2 secretion, we mimicked this condition by adenoviral overexpression. As shown in **Fig. 29A**, Ang-2 was robustly overexpressed 24 h post-infection. The quantification of Ang-2 by ELISA confirmed about 80-fold higher Ang-2 levels in the supernatant of infected ECs (**Fig. 29B**). Interestingly, Tie-2 was elevated to a similar extent in ECs overexpressing Ang-2 as in those with NDPK-B-depletion (**Fig. 29A and C**). Collectively, our findings prove that Tie-2 upregulation is mediated by increasing extracellular levels of Ang-2. As shown in **Fig. 21** and **25**, the expression and secretion of Ang-2 is more pronounced after NDPK-B depletion than in HG. The strongly secreted Ang-2 drives Ang-2-Tie-2 signaling via the elevation of membrane Tie-2, specifically when NDPK B expression is suppressed.

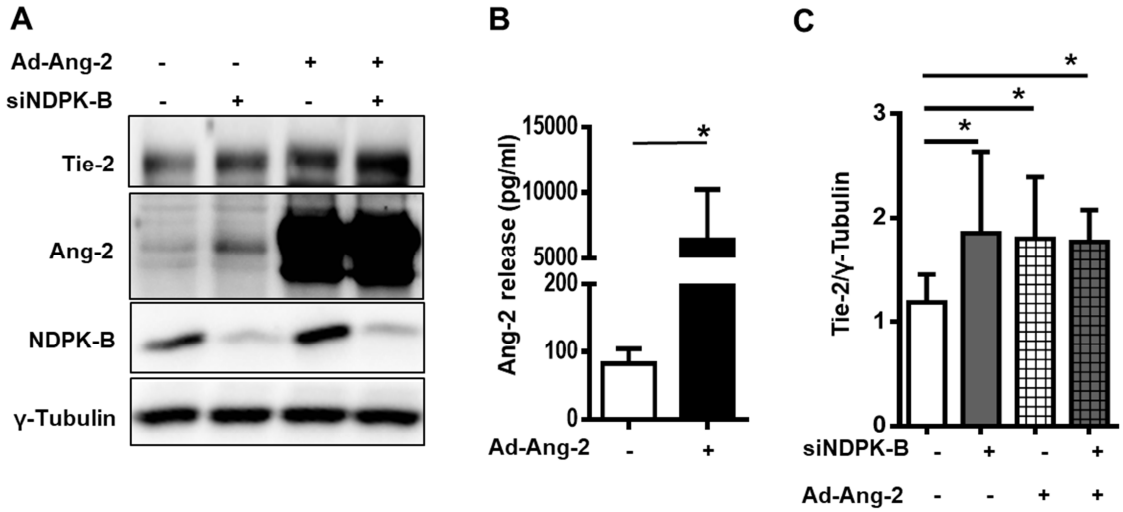

Fig. 29: An excess of extracellular Ang-2 upregulates Tie-2. *HUVECs were transfected with either scrambled control (-) or siRNA against NDPK-B (siNDPK-B, +) and infected with an Ang-2 overexpressing adenovirus (Ad-Ang-2, +) or Ad-GFP (-) as control. A: Representative immunoblots of Tie-2, Ang-2, NDPK-B, and γ-Tubulin in NDPK-B depleted cells without and with Ang-2 overexpression. B: Quantification of secreted Ang-2 in cells without and with Ang-2 overexpression*

*(Ad-Ang-2, n=4). C: Quantification of Tie-2 normalized to γ-Tubulin (n=6). Results are displayed as mean±SD * p<0.05.*

5.2 The importance of protein O-GlcNAcylation in NDPK-B deficiency

5.2.1 Loss of NDPK-B activates the HBP in ECs by elevating UDP-GlcNAc

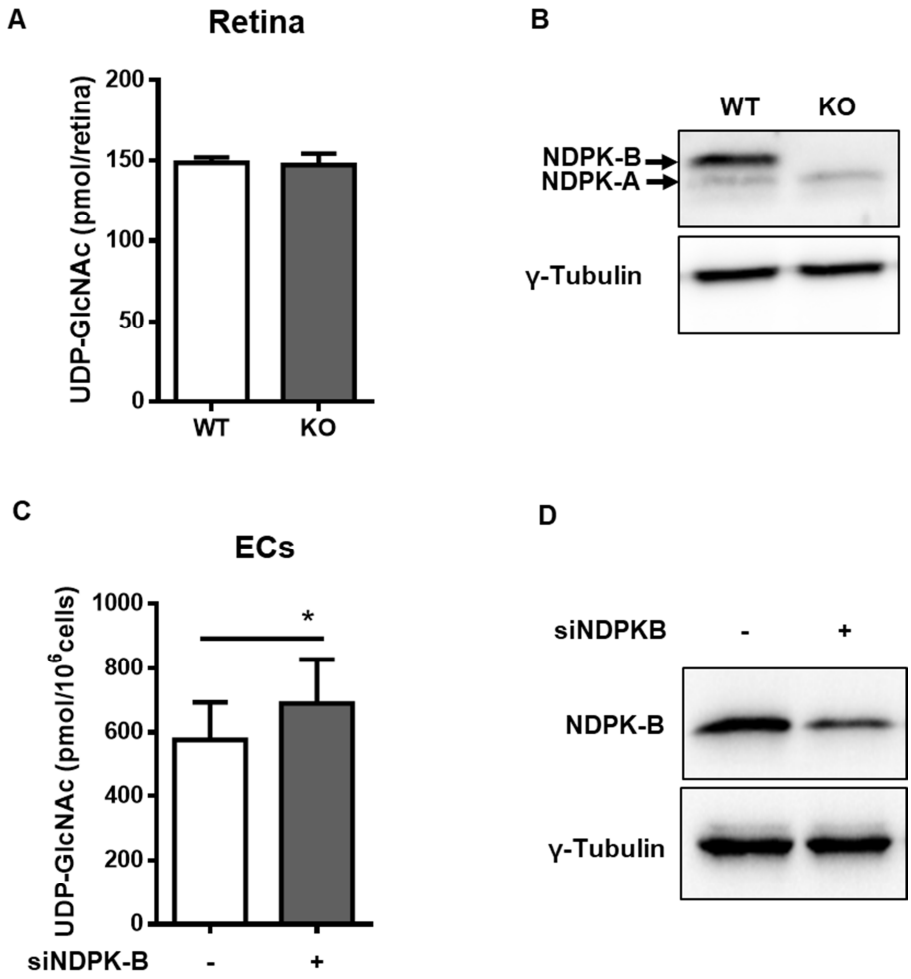

Fig. 30: NDPK-B deficiency activates the HBP in ECs by elevating UDP-GlcNAc. *NDPK-B WT and KO retinae isolated from 5-month-old male mice and HUVECs transfected with either scrambled control (-) or siRNA against NDPK-B (siNDPK-B, +) were assessed via mass spectrometry (MS) for UDP-GlcNAc. A: MS quantification of UDP-GlcNAc in the retinae (n=5 mice per genotype). B: Confirmation of NDPK-B knockout via western blotting. C: Quantification of UDP-GlcNAc in NDPK-B depleted and control ECs (n=3). D: Confirmation of NDPK-B knockdown via western blotting. Results are displayed as mean±SD. *p<0.05.*

To study the possible regulation of the HBP by NDPK-B, we first examined the HBP end product, UDP-GlcNAc, in control and NDPK-B deficient retinae as well as in control and

NDPK-B depleted ECs by mass spectrometry. Successful knockout and knockdown of NDPK-B in the retina and ECs, respectively, was confirmed by western blotting (**Fig. 30B and D**). Approximately 150 pmol of UDP-GlcNAc was detected per retina. This UDP-GlcNAc level was not altered in KO retinae compared with WT retinae (**Fig. 30A**). In cultured ECs, i.e. HUVECs, about 580 pmol UDP-GlcNAc was detected per 10^6 cells. NDPK-B knockdown significantly increased UDP-GlcNAc levels by about 20% (**Fig. 30C**). Since the retina is a complex organ consisting of many cell types of which ECs are a small subset, the data indicate that NDPK-B deficiency might activate the HBP in a cell-type-specific manner.

5.2.2 Loss of NDPK-B in ECs causes a shift in glucose metabolism from glycolysis to the HBP

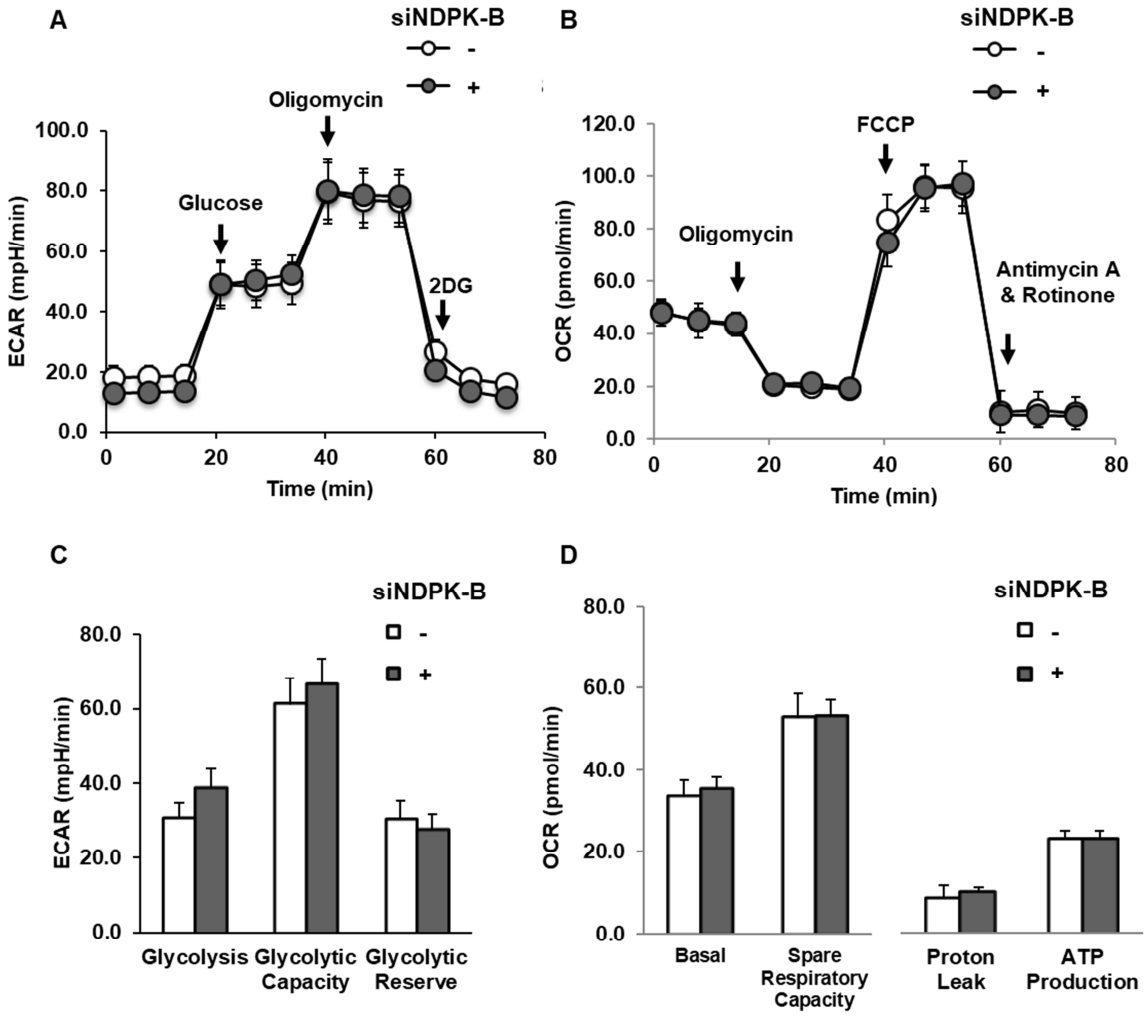

Fig. 31: NDPK-B depletion in ECs does not influence glycolysis or mitochondrial respiration. *HUVECs were transfected with either scrambled control (-) or siRNA against NDPK-B (siNDPK-B, +) and assessed for glycolytic rate and mitochondrial respiration. A: Glycolysis measured as ECAR*

(mpH/min) (n=7). B: Mitochondrial respiration measured as OCR (pmol/min) (n=7). C: Quantification of glycolysis, glycolytic capacity, and glycolytic reserve. D: Quantification of basal respiration, spare respiratory capacity, proton leak, and ATP production. ECAR: Extracellular acidification rate; OCR: Oxygen consumption rate. Results are displayed as mean±SD.

As increased flux through glycolysis also elevates HBP flux [101, 102], we measured glycolysis and mitochondrial respiration in control and NDPK-B deleted ECs. As shown in **Fig. 31A**, addition of glucose increased the extracellular acidification rate (ECAR) as a surrogate for the glycolytic activity. The subsequent addition of oligomycin, which inhibits mitochondrial respiration, maximized the glycolytic output. Addition of 2-DG, a glucose mimetic unmetabolized by glucose-6-phosphate isomerase, terminated glycolysis. NDPK-B depleted ECs acted similar to control cells and did not exhibit altered glycolysis, glycolytic capacity, or reserve (**Fig. 31A and C**). Mitochondrial respiration was monitored as oxygen consumption rate (OCR). Control ECs showed a basal respiration at around 50 pmol/min (**Fig. 31B**). Addition of oligomycin largely inhibited respiration. This was overcome by adding the ionophore FCCP which maximized respiration after 10-20 min. As expected, subsequent addition of antimycin A and rotenone completely blocked mitochondrial oxygen consumption. The difference in OCR before and after oligomycin addition is a surrogate for ATP production. The difference in OCR between oligomycin and antimycin A/rotenone addition corresponds to the proton leak and is used as indication of mitochondrial damage. NDPK-B depletion did not alter basal respiration, respiratory capacity, proton leak, or mitochondrial ATP production as compared with the controls (**Fig. 31B and D**). Collectively, these data show that NDPK-B depletion in ECs did not alter glycolysis and mitochondrial respiration but resulted in an elevation of UDP-GlcNAc (as seen in **Fig. 30C**). This indicates a shift in glucose metabolism from glycolysis to the HBP independent of the glycolytic flux.

5.2.3 Loss of NDPK-B in EC alters nucleotide metabolism without changing NTP levels

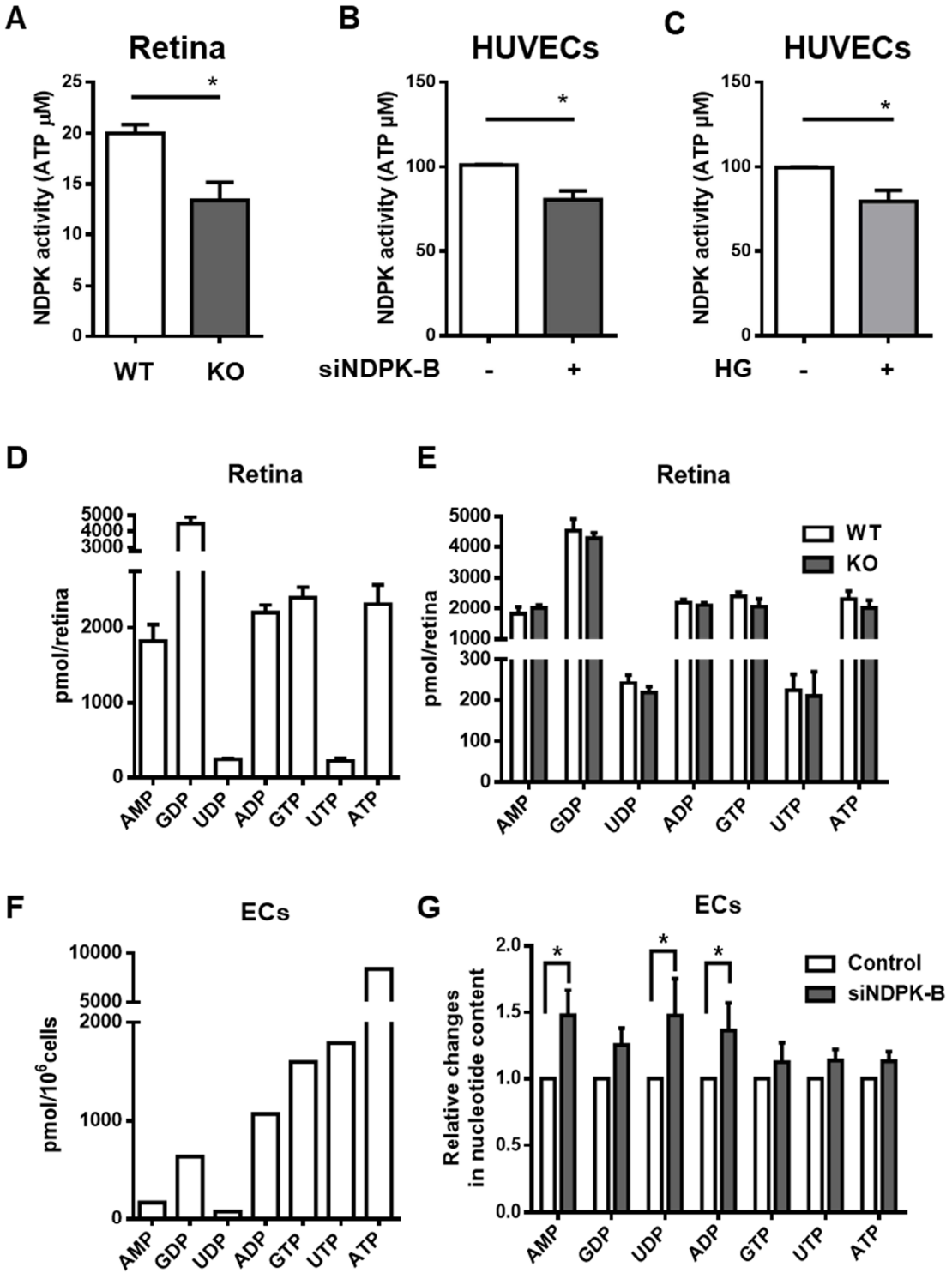

Fig. 32: Loss of NDPK-B in EC alters nucleotide metabolism but does not change NTP levels. *NDPK-B WT and KO retinae isolated from 5-month-old male mice, HUVECs transfected with either scrambled control (-) or siRNA against NDPK-B (siNDPK-B, +), and HUVECs treated without (-) or with HG (HG, +) were assessed for NDP kinase activity and for nucleotide metabolism via mass spectrometry (MS). A: Overall NDP kinase activity for NDPK-B KO and WT retinae (n=10, 6), B:*

*NDPK-B depleted ECs (n=8), and C: HG treated ECs (n=9). D: MS analysis of the retinae showing absolute nucleotide values measured as pmol/retina. E: MS quantification and comparison of nucleotides between KO and WT retinae (n=5 per genotype). F: MS analysis of ECs showing absolute values for nucleotides in pmol/million cells. G: MS quantification and comparison of relative change in nucleotide content of NDPK-B depleted ECs (n=3). AMP: Adenosine monophosphate; UDP: Uridine monophosphate; ADP: Adenosine diphosphate. Results are displayed as mean±SD. *p<0.05.*

The HBP combines elements of glucose, amino acid, fatty acid, and nucleotide metabolism. For example, UTP formed from ATP and UDP in nucleotide metabolism is required for the synthesis of UDP-GlcNAc in the HBP. As NDPKs catalyze the formation of NTPs, including UTP, we analyzed the influence of NDPK-B deficiency in the retina or depletion in ECs on the overall NTP/NDP transphosphorylase, i.e. NDPK activity and nucleotide levels. Although NDPK-B is completely absent in the retina of KO mice and largely reduced in its expression upon siRNA-mediated knockdown in ECs (siNDPK-B) (see **Fig. 30B and D**), the overall NDPK activity was reduced only by about 35% in the KO retina (**Fig. 32A**) and by 20% in the siNDPK-B-treated ECs (**Fig. 32B**). This is in agreement with the presence of other NDPK isoforms, e. g. NDPK-A, in the retina and ECs [198, 213]. Previous publications indicate a diminished activity of NDPKs in pancreatic islets β-cells of diabetic rats by >50% [205]. HG treated ECs lost 21% overall NDPK activity compared to controls (**Fig. 32C**). The reduction of overall NDPK activity in HG indicates a role of NDPKs also under HG, but it does not allow conclusion on a specific function of NDPK-B.

To determine whether NDPK-B depletion activates HBP via changing nucleotide metabolism, we performed analyses by mass spectrometry in the NDPK-B deficient retinae and NDPK-B depleted ECs. In the retina, the highest nucleotide levels of GDP were observed at around 4500 pmol/retina and GTP at 2500 pmol/retina (**Fig. 32D**). This likely reflects the important role guanine nucleotides in signal transduction in the photoreceptors of the retina [220]. Retinae contain rather low amounts of UTP/UDP compared to GTP/GDP. No differences in nucleotide content of KO retinae compared to WT retinae were detected (**Fig. 32E**). As shown in **Fig. 32F**, cultured ECs exhibit a completely different nucleotide content pattern than the total retina. They contain much more NTPs, in particular the general energy donor ATP, at approximately 7500 pmol/million cells, followed by UTP and GTP at 1500-1800 pmol/million cells (**Fig. 32F**). ADP and GDP were present at levels below 1000 pmol/million cells. UDP and AMP were also detected, but only at very low levels. NDPK-B knockdown ECs did not show differences in NTP levels but displayed a relative increase in AMP, UDP, and ADP levels by about 50% (**Fig. 32G**). This accumulation of NDPs indicates a slower nucleotide metabolism due the loss of one of the major NDPK isoforms.

Nevertheless, as the NTP pool was unchanged, the data also demonstrate that NDPK-B depletion in ECs can be compensated by other isoforms at least for the upkeep of NTP formation from ATP and the respective NDP. This includes UTP, an important co-factor for the formation of UDP-GlcNAc.

5.2.4 NDPK-B deficiency activates the HBP by elevating GFAT expression and activity

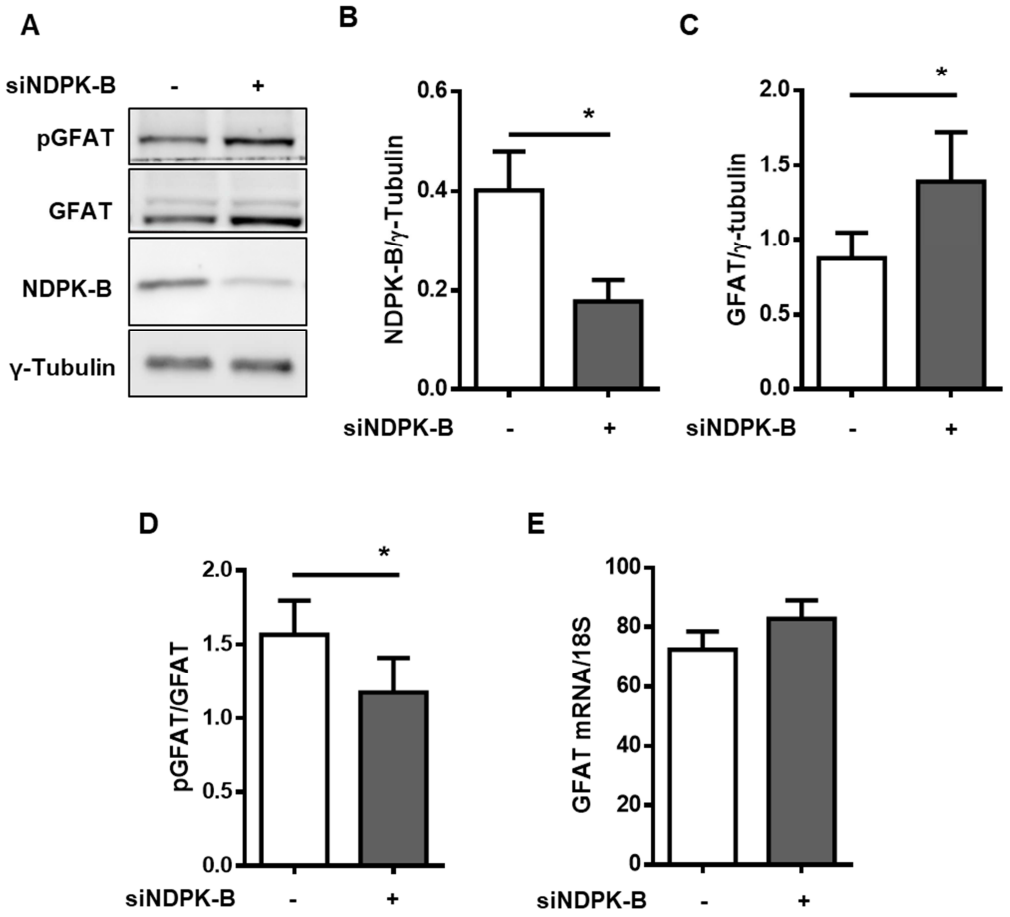

Fig. 33: NDPK-B deficiency elevates GFAT expression and activity. *A: HUVECs were transfected with either scrambled control (-) or siRNA against NDPK-B (siNDPK-B, +) were assessed by western blotting for GFAT and pGFAT and γ-Tubulin. B and C: Quantification of NDPK-B and GFAT, respectively, normalized to γ-Tubulin. D: Quantification of pGFAT/GFAT. E: qPCR quantification of GFAT mRNA expression relative to 18S. Results are displayed as mean±SD (n=5). *p<0.05.*

GFAT is a rate limiting enzyme in the HBP, catalyzing the conversion of fructose-6-phosphate to glucosamine-6-phosphate, an important precursor of UDP-GlcNAc. To investigate the role of GFAT, we first examined its protein content in NDPK-B knockdown ECs (**Fig. 33A**). NDPK-B depletion was performed via siRNA mediated knockdown (**Fig. 33B**). GFAT was upregulated nearly 1.7-fold in NDPK-B depleted ECs compared to the controls (**Fig. 33A and C**). It has recently been reported that increased phosphorylation of

endothelial GFAT at serine 243 diminishes its enzymatic activity and results in reduced protein O-GlcNAcylation [73, 74]. In the NDPK-B depleted cells, GFAT phosphorylation was significantly reduced by about 35% compared to the controls, indicating an enhancement of GFAT activity (**Fig. 33A and D**). The amount of mRNA encoding GFAT, measured via qPCR, was however not altered (**Fig. 33E**), pointing to a post-transcriptional mechanism causing the elevation of GFAT levels upon NDPK-B knockdown. Taken together, the data indicate that the upregulation of GFAT content and activity likely account for the increase in the UDP-GlcNAc level upon NDPK-B depletion shown above.

5.2.5 NDPK-B depletion in ECs does not alter the expression of O-GlcNAc cycling enzymes OGT and OGA

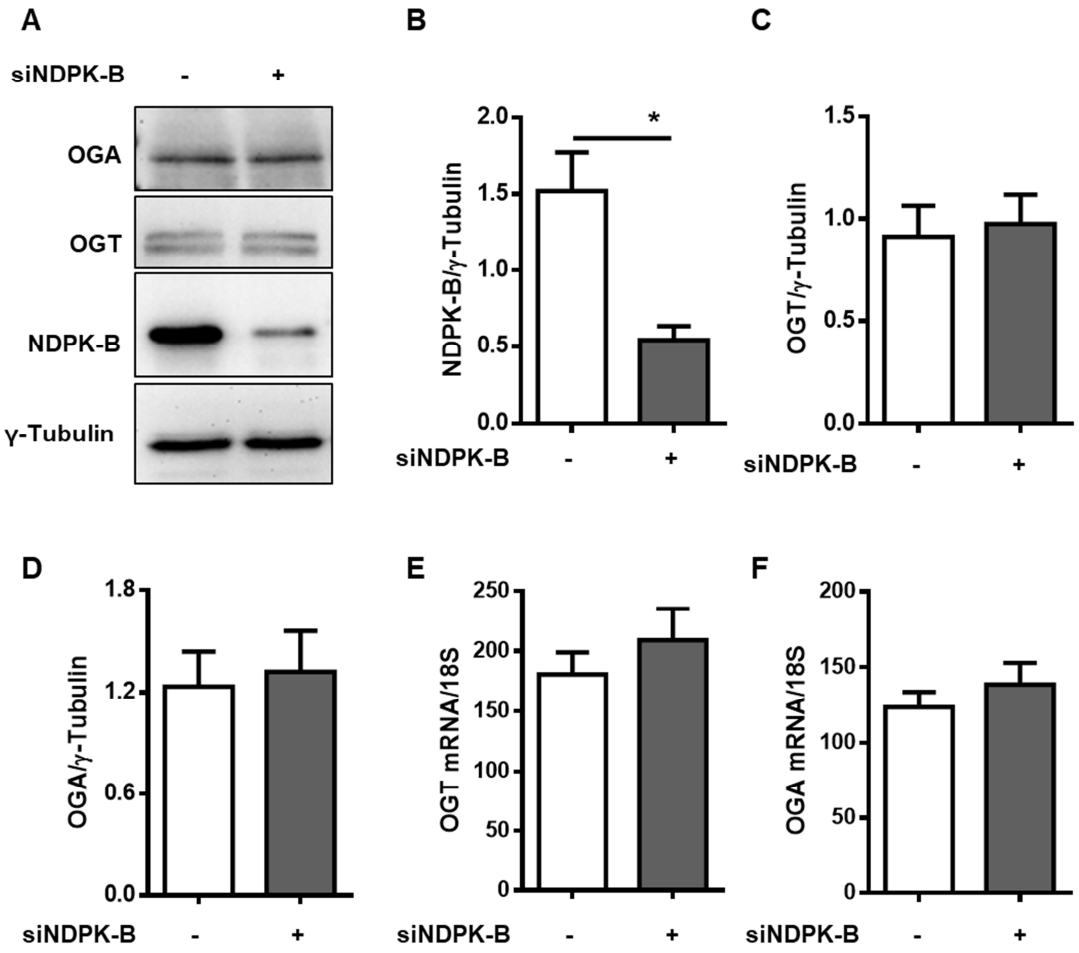

Fig. 34: NDPK-B depletion in ECs does not alter the expression of OGT and OGA. *A: HUVECs were transfected with either scrambled control (-) or siRNA against NDPK-B (siNDPK-B, +) were assessed by western blotting for OGT, OGA, and NDPK-B and γ-tubulin. B, C, and D: Quantification of NDPK-B, OGT, and OGA, respectively, normalized to γ-tubulin (n=9). E and F: qPCR results show mRNA levels of OGT and OGA relative to 18S (n=6). Results are displayed as mean±SD. *p<0.05.*

UDP-GlcNAc is the substrate for OGT in the protein O-GlcNAcylation cycle controlled by the enzymes OGT and OGA. OGA removes O-GlcNAc moieties from Serine and Threonine residues of modified proteins. We therefore assessed the content of OGT and OGA in control and NDPK-B depleted ECs (**Fig. 34A**). NDPK-B depletion was again performed by siRNA mediated knockdown (**Fig. 34B**). OGT and OGA protein levels were unaltered between knockdown and control ECs (**Fig. 34C and D**). Similarly, qPCR data showed that the content in mRNA encoding OGT or OGA was not changed in NDPK-B depleted ECs compared to control cells (**Fig. 34E and F**).

5.2.6 Reduced OGA activity enhanced protein O-GlcNAcylation in NDPK-B depleted ECs

As the activity of OGA is not only regulated by its expression level, we further assessed the enzyme activity of OGA in KO retinae, NDPK-B knockdown ECs, and NDPK B-deficient ECs isolated from the murine brain (MBMECs). The average OGA activity in a 5-month-old mouse retina was 4 IU/L (**Fig. 35A**). MBMECs isolated from murine brains had an OGA activity of 9 IU/L (**Fig. 35C**), whereas ECs had approximately 65 IU/L activity (**Fig. 35B**). No obvious change in OGA activity was detected in the total retinal lysate NDPK-B KO and WT mice (**Fig. 35A**). In ECs, NDPK-B knockdown caused a significant reduction of roughly 12% in OGA activity compared to controls in **Fig. 35B**. In order to investigate if an NDPK-B depletion-induced alteration in OGA activity and protein O-GlcNAcylation is a general phenomenon in ECs, especially in microvascular ECs, MBMECs were isolated from NDPK-B KO mice and cultured [212]. The quality of the MBMEC preparation was validated by staining with the endothelial marker PECAM-1 and pericyte marker NG2. More than 95%-of the isolated cells were positive for PECAM-1 (**Fig. 35F**). Western blotting experiments verified the absence of NDPK-B in MBMECs isolated from the KO mouse line (**Fig. 35D**) As shown in **Fig. 35C**, KO MBMECs exhibited a significantly, lower OGA activity, approximately 12%, than WT MBMECs. Similar to NDPK-B depletion in ECs, protein O-GlcNAc was significantly higher in KO than in WT MBMECs (**Fig. 35D and E**). Taken together, these data reveal that the increased formation of UDP-GlcNAc via the HBP and a reduction of OGA activity are likely working together in the elevation protein O-GlcNAcylation upon the loss of NDPK-B in ECs.

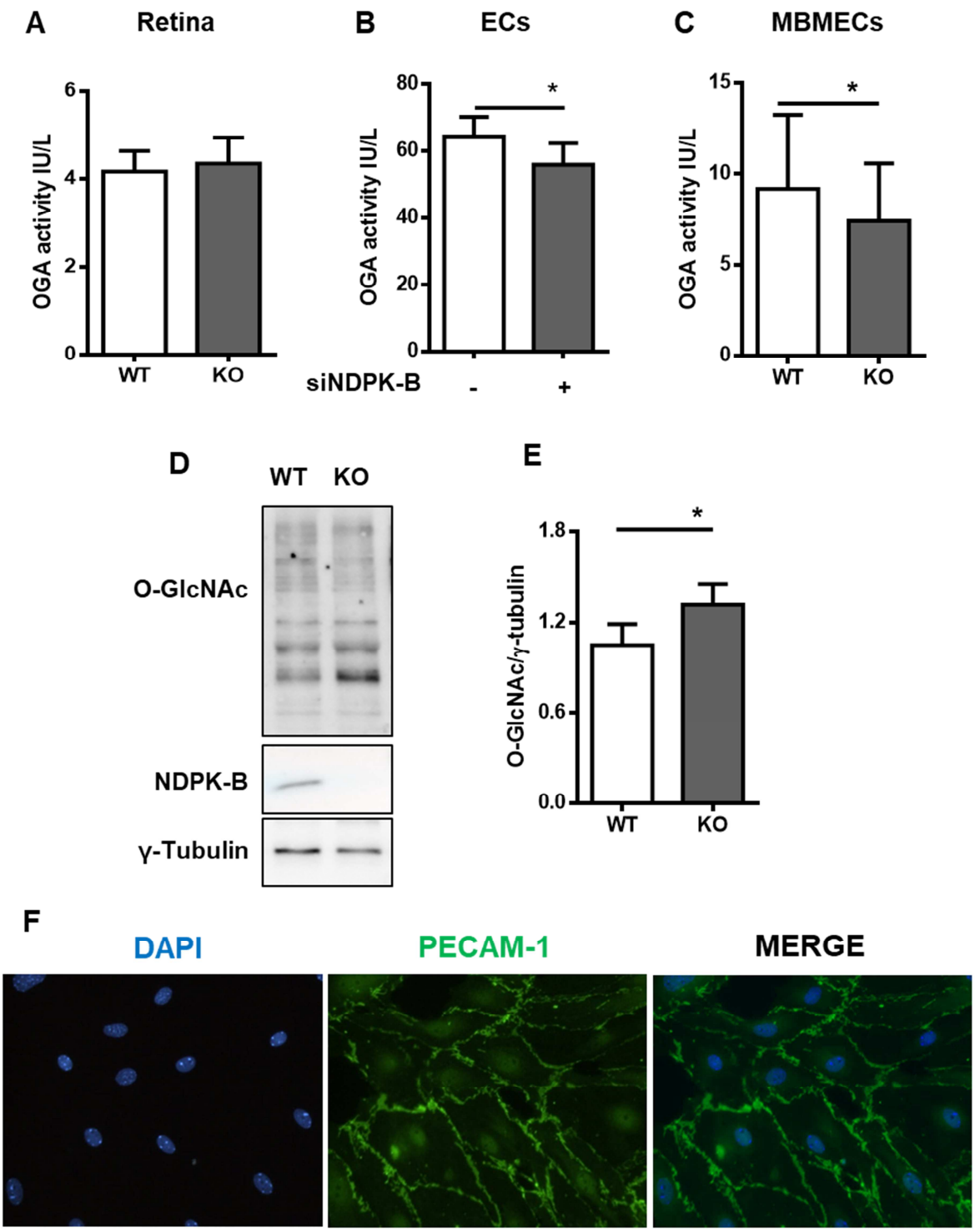

Fig. 35: Suppressed OGA contributes to elevated protein O-GlcNAcylation in upon loss of NDPK-B in ECs. *NDPK-B WT and KO retinae from 5-month-old male mice, HUVECs were transfected with either scrambled control (-) or siRNA against NDPK-B (siNDPK-B, +) and MBMECs isolated from WT and KO brains of 10-15-week-old male mice were assessed for OGA activity. A: OGA activity of KO and WT retinae (n=10, 8), B: in control and NDPK-B knockdown ECs (n=7), and C: in WT and KO MBMECs (n=60). OGA activity is expressed in IU/L. D: Western blotting analysis of WT and KO MBMECs detecting NDPK-B and O-GlcNAc and γ-Tubulin. E: Quantification of O-GlcNAc*

*normalized to γ-tubulin (n=4). F: Expression of PECAM-1 (green) and DAPI (blue) in MBMECs, depicting their endothelial nature. The pictures shown are representative of staining from the 2 independent experiments. Results are displayed as mean±SD. *p<0.05.*

5.2.7 Ang-2 is O-GlcNAcylated in WT and NDPK-B depleted ECs

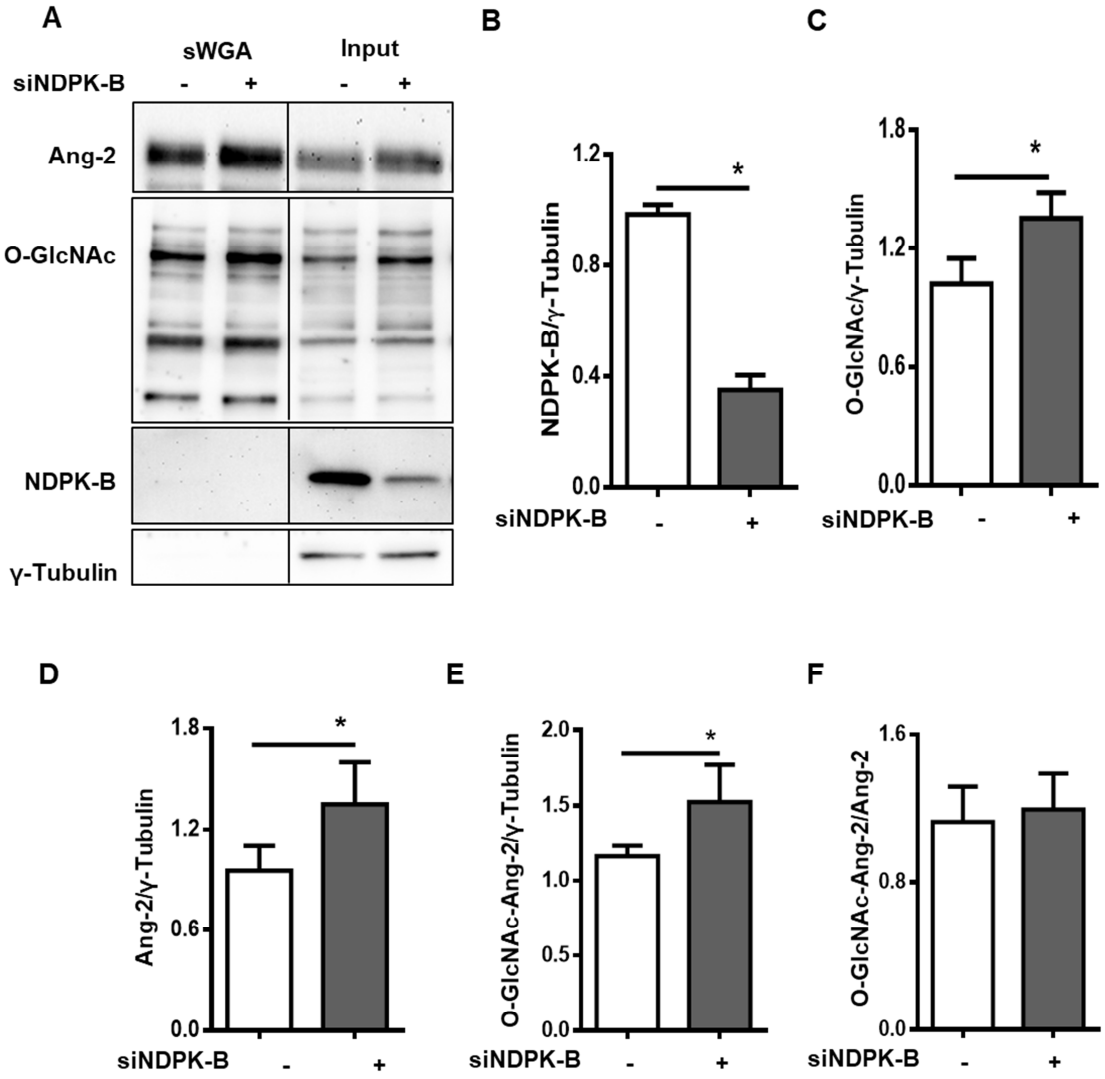

Fig. 36: Ang-2 is modified by O-GlcNAc in WT and NDPK-B depleted ECs. *HUVECs were transfected with either scrambled control (-) or siRNA against NDPK-B (siNDPK-B, +) and were assessed by precipitation of O-GlcNAcylated proteins using succinylated WGA-bound agarose beads (sWGA). A: Immunocomplexes were probed for Ang-2, O-GlcNAc, and NDPK-B and γ-Tubulin. Whole cell lysate (Input) was used to establish knockdown efficiency and probed for total Ang-2. B, C, D, and E: Quantification of NDPK-B, O-GlcNAc, Ang-2, and O-GlcNAcylated Ang-2, respectively, normalized to γ-Tubulin. F: Quantification of O-GlcNAcylated Ang-2 relative to Ang-2 in 'Input'. Results are displayed as mean±SD (n=4). *p<0.05.*

Prior findings indicate that Ang-2 is a crucial mediator of vasoregression in NDPK-B deficiency and its content is regulated by O-GlcNAcylation [213, 216]. To study whether Ang-2 itself is modified by O-GlcNAc, O-GlcNAcylated proteins were pulled out of cell lysates by succinylated-WGA-bound to agarose beads (sWGA) and subjected to SDS-PAGE and western blotting. The blots were probed with antibodies against O-GlcNAc and Ang-2 (**Fig. 36A**). NDPK-B depletion was achieved by siRNA mediated knockdown (**Fig. 36B**). In accordance with the published data, total protein O-GlcNAcylation was significantly increased in NDPK-B depleted ECs compared to control cells. O-GlcNAcylated proteins were enriched on the sWGA-beads and the overall increase in protein O-GlcNAcylation was reflected in the bound fraction (**Fig. 36A and C**). An O-GlcNAcylation of NDPK-B was not detected in ECs. In line with the reported data [213, 216], the Ang-2 content was significantly higher in NDPK-B depleted ECs than control ECs (**Fig. 36A and D**). Notably, Ang-2 turned out to be an O-GlcNAcylated protein already under basal conditions. Relative to Tubulin in the cell lysates used for enrichment, the amount of O-GlcNAcylated Ang-2 was nearly 1.5-fold higher in NDPK-B depleted ECs than in the respective controls (**Fig. 36A and E**). With respect to the total Ang-2 level in the cell lysate, the relative fraction of O-GlcNAcylated Ang-2 was not different between NDPK-B depleted and control cells (**Fig. 36F**).

5.2.8 Enhanced protein O-GlcNAcylation increased Ang-2 content

To determine if the upregulation of Ang-2 in NDPK-B depleted ECs is a result of dysregulation of the OGT/OGA, we modulated OGA activity by other means than NDPK-B depletion. When OGT was depleted from ECs by siRNA transfection to about 50%, overall protein O-GlcNAcylation was reduced (**Fig. 37A**). As shown in **Fig. 37B**, we effectively depleted OGA via siRNA-mediated knockdown. As expected, this resulted in increased protein O-GlcNAcylation. Additionally, we inhibited OGA activity with the potent inhibitor Thiamet G (TMG, 10µM for 24h). Protein O-GlcNAcylation in the OGA knockdown cells was about 1.25-fold higher compared to control siRNA treated cells (**Fig. 37C and D**). TMG treatment increased protein O-GlcNAcylation even stronger (about 2-fold, **Fig. 37D**). Interestingly, Ang-2 content was significantly upregulated in TMG and siOGA treated cells by about 1.3 - 1.5-fold (**Fig. 37E**). Ang-2 receptor Tie-2 was however unaffected by OGA knockdown and TMG treatment (**Fig. 37F**). Taken together, the data indicate that Ang-2 levels in ECs correlate to changes in the overall O-GlcNAcylation of endothelial proteins independent of the type of manipulation inducing the enhancement in protein O-GlcNAcylation.

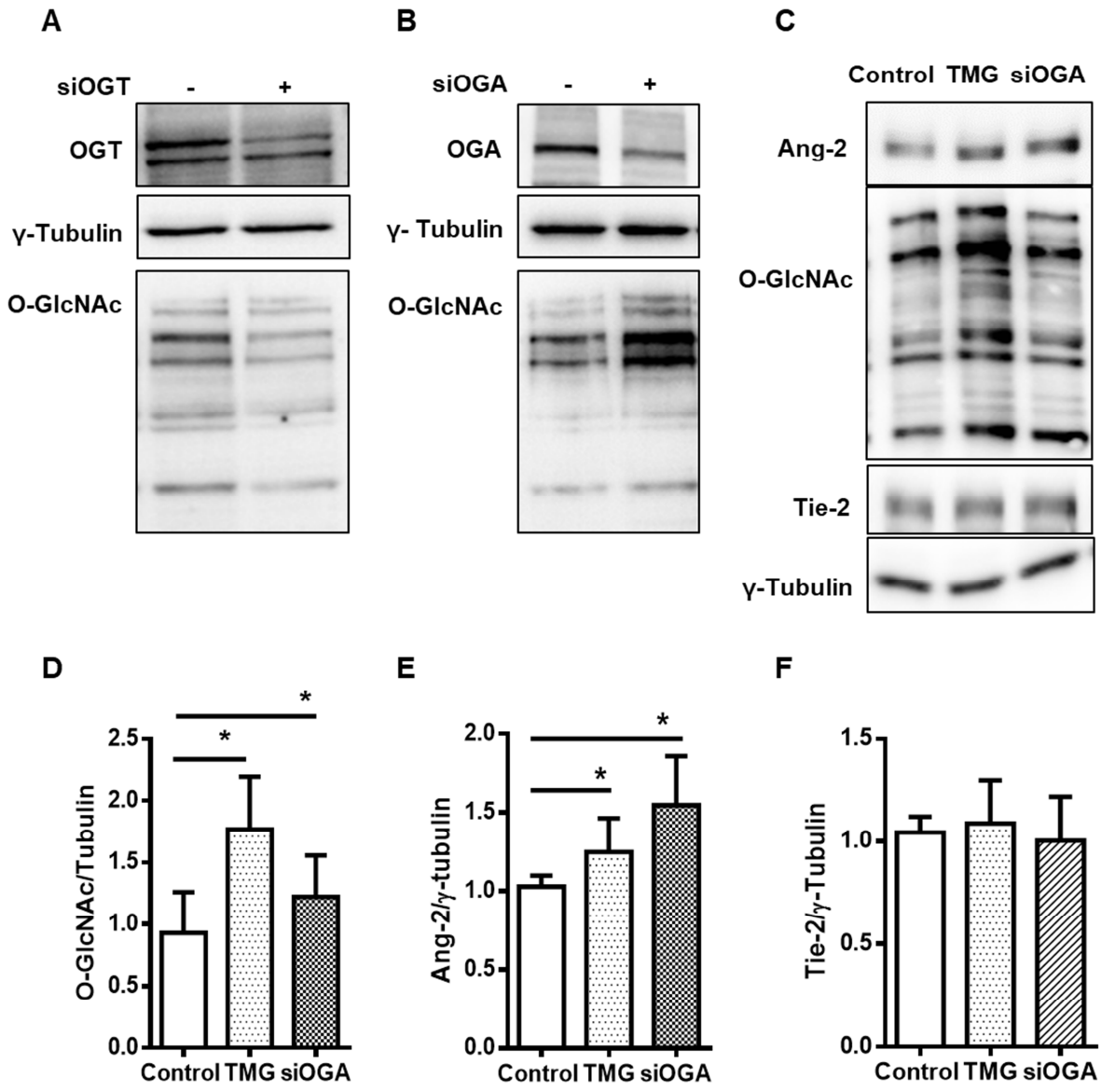

Fig. 37: Enhanced protein O-GlcNAcylation increased Ang-2 content. *ECs were depleted of OGT or OGA via siRNA-mediated gene knockdown, followed by treatment with Thiamet G (TMG: OGA inhibitor) at 10µM and assessed by western blotting. A: Detection of OGT and O-GlcNAc in OGT knockdown ECs. B: Detection of OGA and O-GlcNAc in OGA knockdown ECs. C: Detection of Ang-2 and O-GlcNAc and γ-Tubulin. D, E, and F: Quantification of O-GlcNAc, Ang-2 and Tie-2, respectively, normalized to γ-tubulin. Results are displayed as mean±SD (n=8). *p<0.05.*

5.2.9 The enzymatic NTP/NDP transphosphorylase and protein histidine activity of NDPK-B does not contribute to the regulation of protein O-GlcNAcylation

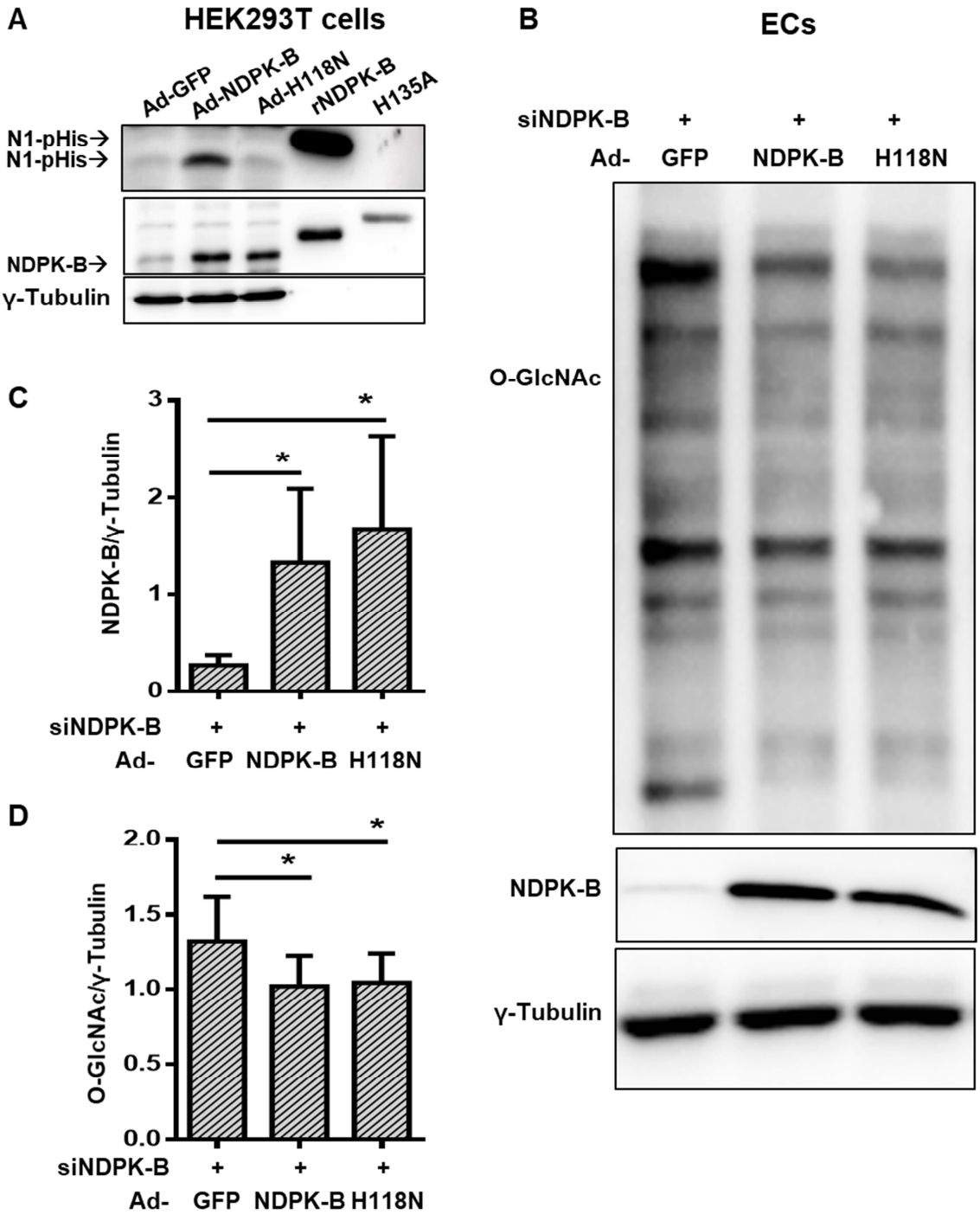

Fig. 38: The transphosphorylase and histidine activity of NDPK-B kinase does not contribute to the regulation of protein O-GlcNAcylation. *A: HEK293T cells were used to demonstrate the function of the NDPK-B overexpression constructs. The cells were transduced with adenovirus expressing GFP (Ad-GFP), overexpressing NDPK-B (Ad-NDPK-B), and the kinase dead mutant H118N (Ad-H118N). Recombinant NDPK-B (rNDPK-B with 6xHis-Tag) and recombinant NDPK-C*

*(H135A with 6xHis-Tag) were used as controls for the enzyme autophosphorylation. The lysates were investigated for N1-phospho-histidine, NDPK-B, and γ-Tubulin. B: HUVECs were transfected with siRNA against NDPK-B (siNDPK-B, +) and were transduced with Ad-GFP, Ad-NDPK-B and Ad-H118N, and examined for O-GlcNAc, NDPK-B and γ-tubulin. C and D: Quantification of NDPK-B and O-GlcNAc, respectively, normalized to γ-tubulin. All results are represented as mean±SD (n=8). *p<0.05, **p<0.01.*

Besides its NTP/NDP transphosphorylase [165] and its protein histidine kinase activity [221], which are both dependent on the presence of a histidine residue in position 118 (H118), NDPK-B can function as a scaffold protein, regulating for example caveolae formation in ECs [198, 212]. To determine whether enzymatic activities of NDPK-B are required for the regulation of protein O-GlcNAcylation in ECs, we performed experiments with adenoviral re-expression of either wild type NDPK-B or an enzymatic inactive mutant H118N after siRNA-mediated depletion. As the autophosphorylation H118 is part of its enzymatic activities [165, 221, 222], we used the detection of its autophosphorylation with an N1 phospho-histidine specific antibody (N1-pHis) to monitor the catalytic activity in NDPK-B [221]. To validate the used adenoviruses and the detection of N1-pHis, we first transduced HEK293T cells and used purified recombinant NDPKs as controls. As shown in **Fig. 38A**, similar levels of NDPK-B overexpression were achieved with Ad-NDPK-B and Ad-H118N. Recombinant NDPK-B (rNDPK-B) and a recombinant kinase activity deficient mutant of NDPK-C (H135A) served as a positive and negative control, respectively, for N1-pHis detection. In cells transfected with a control virus (Ad-GFP), the detection of N1-pHis correlated to the modest expression of endogenous NDPK-B. A strong increase in NDPK-B autophosphorylation occurred only in Ad-NDPK-B but not in Ad-H118N transduced cells. Therefore, the constructs were used to re-express NDPK-B in NDPK-B knockdown ECs. A similar overexpression of NDPK-B by more than 5-fold was achieved in Ad-NDPK-B and Ad-H118N infected cells (**Fig. 38B and C**). Both re-expression of wild type NDPK-B or its kinase deficient mutant diminished overall protein O-GlcNAcylation to a similar extent in NDPK-B depleted ECs (**Fig. 38B and D**). Taken together, these data demonstrate that the regulation of protein O-GlcNAcylation by NDPK-B is not dependent on its role in nucleotide metabolism and protein histidine phosphorylation, but likely requires its scaffolding function.

6. Discussion

Both the hyperglycemia- as well as NDPK-B ablation-induced retinopathy are initiated by the upregulation of Ang-2, causing pericyte drop out and subsequent vasoregression [213]. In this study, we investigated the contribution of Tie-2 and protein O-GlcNAcylation in high glucose- and NDPK-B deficiency-dependent Ang-2 regulation. The modulation of these pathways distinctly regulates Ang-2 in multiple ways, mediating retinal vascular regression.

6.1 Excess Ang-2 initiates retinal vasoregression in NDPK-B KO retina

Qiu et al. showed the similarities between HG and NDPK-B deficiency in the retina in terms of the development of vasoregression [213]. In the diabetic retina, dropout of PC and AC formation is mediated by hyperglycemia-induced upregulation of Ang-2 [91]. In NDPK-B KO retina, similar to DR, PC dropout and AC formation occurs in the absence of hyperglycemia. In this study, we showed that the Ang-2 upregulation in the normoglycemic NDPK-B KO retina is indeed a crucial initiator of vasoregression. Since ECs are one of the major sources of Ang-2 in the retina, it was of importance to investigate the regulation of endothelial Ang-2 in NDPK-B deficiency in more detail.

6.2 Tie-2 regulates Ang-2 in NDPK-B deficiency differently than in HG

We demonstrated that, concomitant to a stronger upregulation of Ang-2, NDPK-B deficiency but not hyperglycemia increases retinal and endothelial Tie-2 content at the plasma membrane. The upregulation of Tie-2 in the NDPK-B$^{-/-}$ retina occurred predominantly in the deep capillary layer. Therefore, the question arose whether this upregulation is specific to the microvasculature or occurs also in ECs of other origin. As NDPK-B depletion in ECs of micro- and macrovascular origin induced similar increases in the amounts of Ang-2 and Tie-2, our data suggest that the regulation of Tie-2 and Ang-2 is conserved across diverse vascular beds. Notably, the increase in Tie-2 levels occurred at the plasma membrane and was not reflected by an increase in Tie-2 gene transcription. With regard to the concomitant upregulation of Ang-2, we have already shown that this is likely linked to an enhanced O-GlcNAcylation, and therefore also the enhanced stability of the transcription factor FoxO1 [216]. In addition, we have also shown that NDPK-B depletion in ECs interferes with caveolin-1 transport and caveolae formation [189, 212]. Therefore, an increase in the membrane content of Tie-2, as detected herein, might be a result of its stabilization preventing its internalization and degradation [223]. The interpretation that more than one mechanism might be involved in the NDPK-B-depletion induced increase in Tie-2 levels is further corroborated by the notion that HG treatment, although causing enhanced protein O-GlcNAcylation, is not able to elevate Tie-2 levels. Our findings, however, support reports by

others showing the decrease in Tie-2 phosphorylation as a measure of its activity by hyperglycemia [224, 225]. This suppression of the phosphorylation of Tie-2 likely occurs via the inhibitory action of the secreted Ang-2 on Tie-2. In line with this interpretation, the fraction of phosphorylated Tie-2 was reduced upon NDPK-B depletion although the total amount of Tie-2 was increased.

As mentioned before, Ang-2 acts as an antagonist to Tie-2 by competing with the agonist Ang-1 [109].Thus, the upregulation of Ang-2 in pathological conditions is believed to be the driving force of vascular regression by inhibiting the endothelial quiescence-promoting Ang-1-Tie-2 signaling [28]. Interestingly, NDPK-B depletion induced more Ang-2 secretion than HG. As we hypothesized, this increase in Ang-2 secretion is of relevance for the observed increase in Tie-2 levels upon NDPK-B depletion. We adenovirally overexpressed Ang-2 in ECs thereby strongly increasing also the amount of secreted Ang-2. Interestingly, although the amount of secreted Ang-2 exceeded that induced by NDPK-B-depletion by far, a similar increase in Tie-2 levels was observed. The elevation of Ang-2 in HG not causing an increase in Tie-2 suggests a minimum required concentration of Ang-2 required to induce Tie-2 regulation.

Numerous studies have elaborated that the effect of Ang-2 on Tie-2 signaling is context dependent [148, 150, 151, 226]. For example, in pathological conditions, Ang-2 inhibits the survival-promoting Tie-2 activation by Ang-1, whereas under non-pathological conditions, it can act as an agonist, promoting Tie-2 phosphorylation [148]. Ang-1 is secreted from peri-endothelial cells, for example pericytes and monocytes, but was recently reported to be released from activated platelets [159-161, 227]. It is however generally believed not to secreted from ECs. Thus, we could use sTie-2 to address the role of secreted Ang-2 upon NDPK-B depletion. Interestingly, by sequestering secreted Ang-2, the increase in the amount of cellular Ang-2 upon NDPK-B depletion was prevented, whereas the smaller increase in Ang-2 levels upon HG treatment was not. This indicates that after reaching a threshold, Ang-2 might foster its own expression and secretion from ECs in a manner dependent on the Tie-2 expression level. Although Ang-2 is able to interact with other receptors on endothelial cells, such as integrins and thrombomodulin, to modulate vascular remodeling [158-161, 227], the data obtained upon Tie-2 depletion point to the Ang-2-Tie-2-interaction as major mediator of such a feed forward loop. A 40% reduction in Tie-2 expression completely suppressed the NDPK-B knockdown-induced increase in Ang-2 levels.

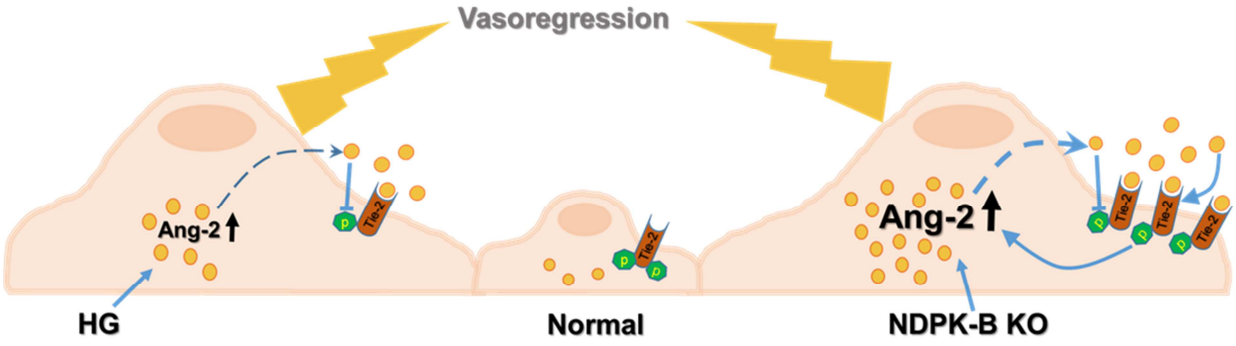

Fig. 39: Putative role of Tie-2 in the regulation of Ang-2 initiated by a loss in NDPK-B expression in comparison to HG

Our study outlines a novel modulation in the Ang-2-Tie-2 axis in endothelial cells which is induced by NDPK-B deficiency but not by hyperglycemia/HG (**Fig. 39**). Although NDPK-B and HG induce an upregulation of Ang-2, likely influencing Tie-2 signaling, only NDPK-B deficiency induces a positive feedback loop in which Tie-2 is upregulated, inducing a further enhancement of released Ang-2 that further promotes its elevation and is in accordance with the important role of Ang-2 in NDPK-B driven vasoregression [216]. Our findings identify Tie-2 as a key regulator in NDPK-B deficiency-driven vascular regression.

6.3 Protein O-GlcNAcylation is a central mediator in the regulation of Ang-2 upon the loss of NDPK-B

The connection between NDPK-B and protein O-GlcNAcylation in ECs was analyzed in detail. The data obtained collectively show that a loss in NDPK-B protein expression activates the HBP without altering glycolysis in ECs. Despite altering nucleotide metabolism in ECs, the loss of NDPK-B expression does not alter nucleotide triphosphate levels in ECs. NDPK-B depletion increases the level of the rate-limiting enzyme of the HBP, GFAT, in ECs and diminishes its inhibitory phosphorylation at Ser243; both promoting UDP-GlcNAc production. Reduced NDPK-B expression is further associated with a reduction of OGA activity. The loss of NDPK-B therefore enhances protein O-GlcNAcylation in ECs via HBP activation and the suppression of OGA activity. Enhanced protein O-GlcNAcylation in ECs is driving the upregulation of Ang-2, which itself is O-GlcNAcylated. The NTP/NDP transphosphorylase and protein kinase activity of NDPK-B are dispensable for their effect on protein O-GlcNAcylation.

It has been shown before that high glucose leads to the activation of the HBP and increased UDP-GlcNAc levels in ECs [101, 102]. As a result of the HBP activation, diabetic conditions

in animals or HG treatment of cultured ECs increase protein O-GlcNAcylation [93, 101, 213, 216]. As also confirmed herein, by directly interfering with OGA activity, the level of protein O-GlcNAcylation governs Ang-2 content in ECs and in the retina [213, 216][213, 216][213, 216][213, 216]. Enhanced protein O-GlcNAcylation and upregulation of Ang-2 upon NDPK-B depletion are apparently common to ECs of all vascular beds. Besides in HUVECs, it occurred in human microvascular ECs from the dermis and retina. Also, in MBMECs isolated from NDPK-deficient mice enhanced protein O-GlcNAcylation was clearly evident. Another feature, which became apparent in this study, is that Ang-2 is highly O-GlcNAcylated itself. O-GlcNAcylation of a protein is often associated with an increased stability of the protein due to the inhibition of proteasomal degradation [62, 228]. Therefore, a rather complex regulation of the Ang-2 levels in ECs can be envisioned. Taking into account that the upregulation of GFAT as well as the suppression the OGA activity were independent of gene transcription, many of the alterations similarly induced by hyperglycemia/high glucose or loss of NDPK-B are also caused by similar changes in post-transcriptional modification patterns.

The increase in protein O-GlcNAcylation as well as the upregulation of Ang-2, caused by NDPK-B deficiency, were detected before in whole retinal lysates [213]. The increase in UDP-GlcNAc levels, which was detected upon NDPK-B depletion in cultured ECs, was however not detected in the NDPK-B deficient retina. The retina is a complex organ consisting of many cell types of which the ECs are a small subset. Therefore, changes in such a small subset of cells may escape detection, especially when the detection method performed analyses of components which are present in any cell type such as nucleotides or their derivates. Assuming that the elevation of UDP-GlcNAc upon NDPK-B deficiency is specific for ECs and possibly Müller glia cells, another source of elevated retinal Ang-2 [229], it escaped detection in the pool of total UDP-GlcNAc in the retinal lysate. This interpretation is corroborated by the results obtained from the nucleotide content analysis. While GTP and GDP were the most prominent nucleotides in the total retinal lysates, ATP showed by far the highest level in ECs, which is line with their known high glycolysis rate, therefore producing ATP as a source of energy [230]. Moreover, none of the changes in the nucleotide pattern observed in NDPK-B depleted ECs was reflected in the NDPK-B deficient retinae.

The NDPKs are originally a family of housekeeping enzymes that replenish the NTP pool by their NTP/NDP transphosphorylase activity [165, 166]. As NDPK-B is one of the two major isoforms, its depletion in ECs diminished the overall NDP kinase activity by about 20%. The similar extent of reduction in overall NDPK activity in HG-treated ECs indicates yet another similarity between HG and NDPK-B deficiency. This finding, however, does not allow conclusions regarding the importance of NDPK-B specifically [205]. In accordance with the NDPK-B knockdown in ECs, 35% of the NDP kinase activity was missing in the NDPK-B

deficient retinae. Nevertheless, although the absence of NDPK-B altered slightly the nucleotide metabolism in ECs the measured NTP levels are not changed, indicating that the activity of the remaining NDPK family members is sufficient to hold up these levels. An altered UTP level [231] was therefore excluded as a driving force for the enhanced UDP-GlcNAc levels upon NDPK-B depletion. In line with this interpretation, the re-expression experiments with NDPK-B or its catalytically inactive mutant revealed that its enzymatic activity is not required to lower protein O-GlcNAcylation in ECs.

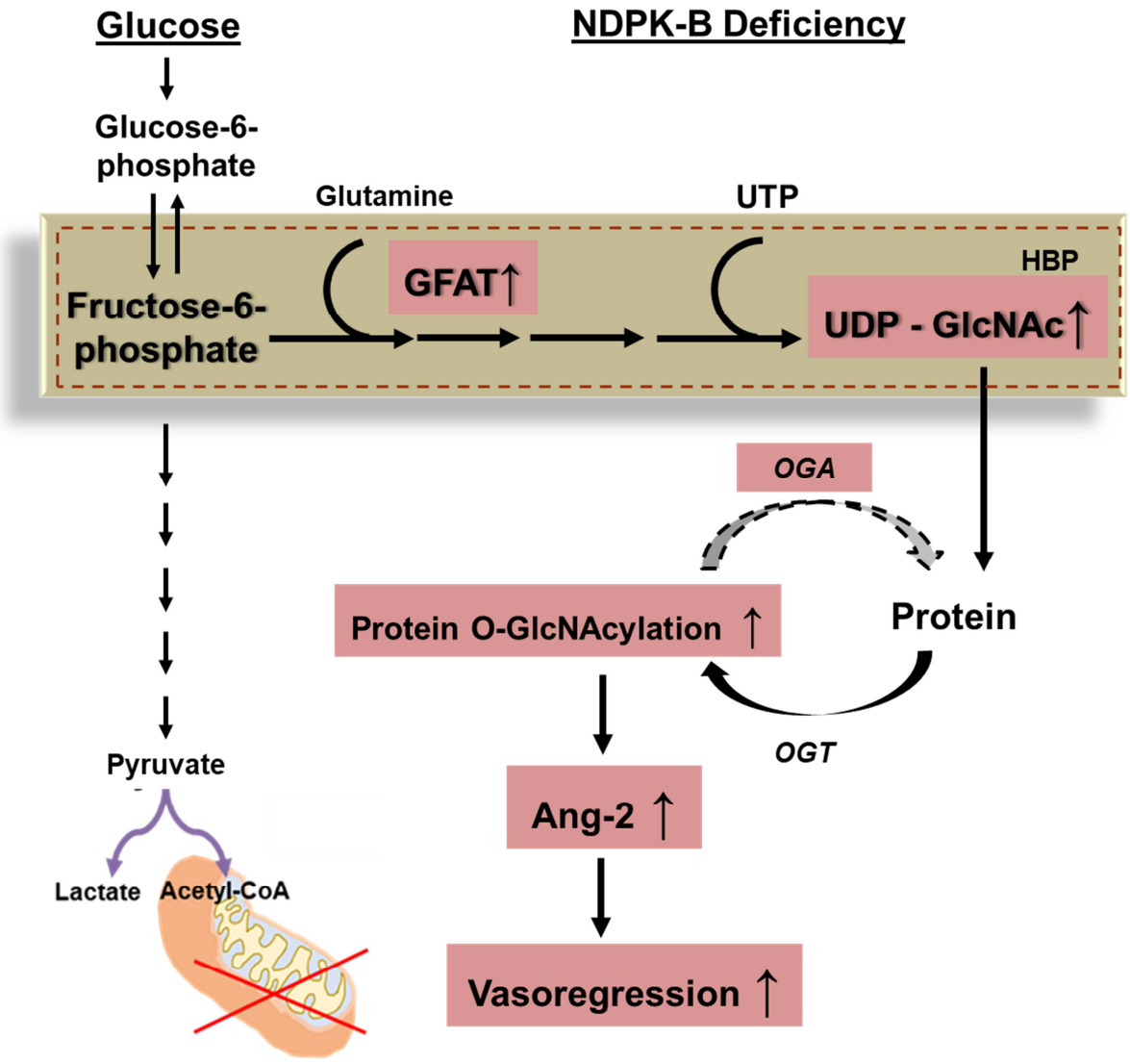

Fig. 40: The proposed mechanism of protein O-GlcNAc regulation in NDPK-B deficiency

In conclusion, the data reported herein shed light on a novel pathway by which the loss of NDPK-B in ECs causes a shift from glycolysis to the HBP. By increasing the GFAT content and suppressing OGA protein activity protein O-GlcNAcylation is generally enhanced (**Fig. 40**). This induces the upregulation of Ang-2. Taken together, these data highlight the importance of the HBP in the retinopathy caused by NDPK-B deficiency in mice [213, 216] and further validate this model for mechanistic investigations related to diabetic retinopathy in humans.

6.4 The multifaceted regulation of Ang-2 via Tie-2 and protein O-GlcNAcylation

The increase in Ang-2 content and release has been shown to be responsible for the initiation of PC dropout in the retina, the formation of AC, and thus vasoregression [28, 91, 92]. The same process has now been confirmed to occur in NDPK-B deficient mice. Several explanations as to how protein O-GlcNAcylation increases Ang-2 levels have been suggested. For instance, hyperglycemia promotes methylglyoxal modification of mSin3A in ECs, triggering the increased O-GlcNAcylation of the transcriptional regulator Sp3 via recruitment of OGT [54]. A feed forward loop involving Tie-2 in fostering Ang-2 upregulation in ECs after a reduction in NDPK-B expression has been shown herein. We and others showed that the Ang-2 expression in ECs is dependent on FoxO1, a transcription factor also stabilized by O-GlcNAcylation [162, 216]. However, interfering with Ang-2-Tie-2 signalling had no effect on FoxO1 or protein O-GlcNAcylation, indicating no discernible crosstalk between the two modes of Ang-2 regulation. In accordance, Tie-2 was unchanged upon TMG and OGA silencing-mediated increase in protein O-GlcNAcylation. Upon reaching a threshold in Ang-2 content and secretion, which is reached upon loss of NDPK-B, but not in HG, the Ang-2-Tie-2 interaction further fosters Ang-2 content and secretion in ECs. The extent to which the two mechanisms contribute to Ang-2 upregulation in NDPK-B deficiency is yet to be determined. However, several publications explore the possibility of targeting Tie-2 in vascular disorders, including diabetic retinopathy, featuring high circulating Ang-2 for therapeutic intervention [232-235]. Therefore, our data might be of relevance for several vascular diseases and provide novel insights into the mechanisms of the Ang-2-Tie-2 signaling in ECs.

6.5 Limitations of the study

However, several questions remain unanswered in this study. On ECs, Ang-2 binds the integrins to modulate vascular remodeling. Binding at low Tie-2 conditions promoted sprouting angiogenesis in developing vessels and stress fiber formation in quiescent ECs [158, 160, 161]. In normal Tie-2 conditions, Ang-2-mediated complex formation between integrins and Tie-2 at cell-cell junctions leading to integrin internalization and degradation

[236], indicating a possible mechanism for Ang-2-mediated loosening of cell-cell and cell-matrix contacts. Therefore, the possibility of the involvement of integrins in Ang-2-mediated retinal vasoregression cannot be excluded and should be investigated.

We have extensively investigated the effect of altering nucleotide metabolism in NDPK-B deficiency and excluded it as a mediator of HBP activation. The other components of the HBP, amino acid metabolism, and fatty acid metabolism also contribute to the regulation of the protein O-GlcNAc [237-239]. Alterations in these metabolic pathways, upon loss of NDPK-B, might contribute to the observed flux through the HBP and need to be analyzed. Alternately, fructose-6-phosphate is the substrate for GFAT, and as we postulated, elevated GFAT expression and activity is responsible for HBP activation. Due to the lack of reliable tools, we were unable to detect whether fructose-6-phosphate is elevated in NDPK-B depleted ECs. At the other end of the O-GlcNAcylation pathway, OGT was not regulated at the protein or mRNA level, but we did not assess its enzymatic activity which may also play an important part in O-GlcNAc cycling. In accordance, both OGT and OGA can be O-GlcNAcylated which may alter their specificity or activity [62].

The findings in this study as well as our previous publication confirm that Ang-2 is modified by O-GlcNAc [216]. However, tools such as sWGA beads have their limitations in terms of specificity. More precise methods such as mass spectrometry need to be employed in order to detect the modified residues on Ang-2 [240]. Furthermore, the consequence of Ang-2 O-GlcNAcylation needs to be addressed as well. O-GlcNAc modification may protect modified proteins from proteasomal degradation [62, 228]. An assessment of Ang-2 ubiquitination may shed light on the outcome of its modification, and whether it contributes to the function of Ang-2 as the mediator of retinal vasoregression.

Scaffold functions of NDPK-B in the regulation of protein complex formation have been reported before and are also seen for other NDPK isoforms, e. g. NDPK-C [188, 190, 191, 241]. In ECs, NDPK-B is apparently involved in caveolae formation and caveolin transport [198, 212]. Thus, the possible contribution of Cav-1 in NDPK-B-dependent vasoregression needs to be assessed, and might help to decide whether the overexpression of NDPK-B in wildtype and kinase dead mutant forms is an option to be considered to tackle the Ang-2 upregulation in the retina as a possible therapeutic approach to treat vasoregression.

6.6 Conclusion

By comparing NDPK-B with HG, this work further clarified its role in Ang-2-driven vasoregerssion in the retina. NDPK-B depletion alters the participation of the HBP in glucose metabolism via alteration of GFAT levels and suppression of OGA activity, which

subsequently further increases protein O-GlcNAcylation and upregulates Ang-2. NDPK-B deficiency additionally induces an increase in Tie-2 expression levels which supports further Ang-2 production and secretion in a positive feedback loop. As enhanced Tie-2 expression was detected on the vasculature of NDPK-B-deficient mice showing early stages of pathological vasoregression, it likely contributed, together with enhanced protein O-GlcNAcylation, to the Ang-2-driven pathology (**Fig. 41**). Therefore, interfering with protein O-GlcNAcylation and/or Tie-2 activity seems to be a key target to prevent early stages of retinal vasoregression.

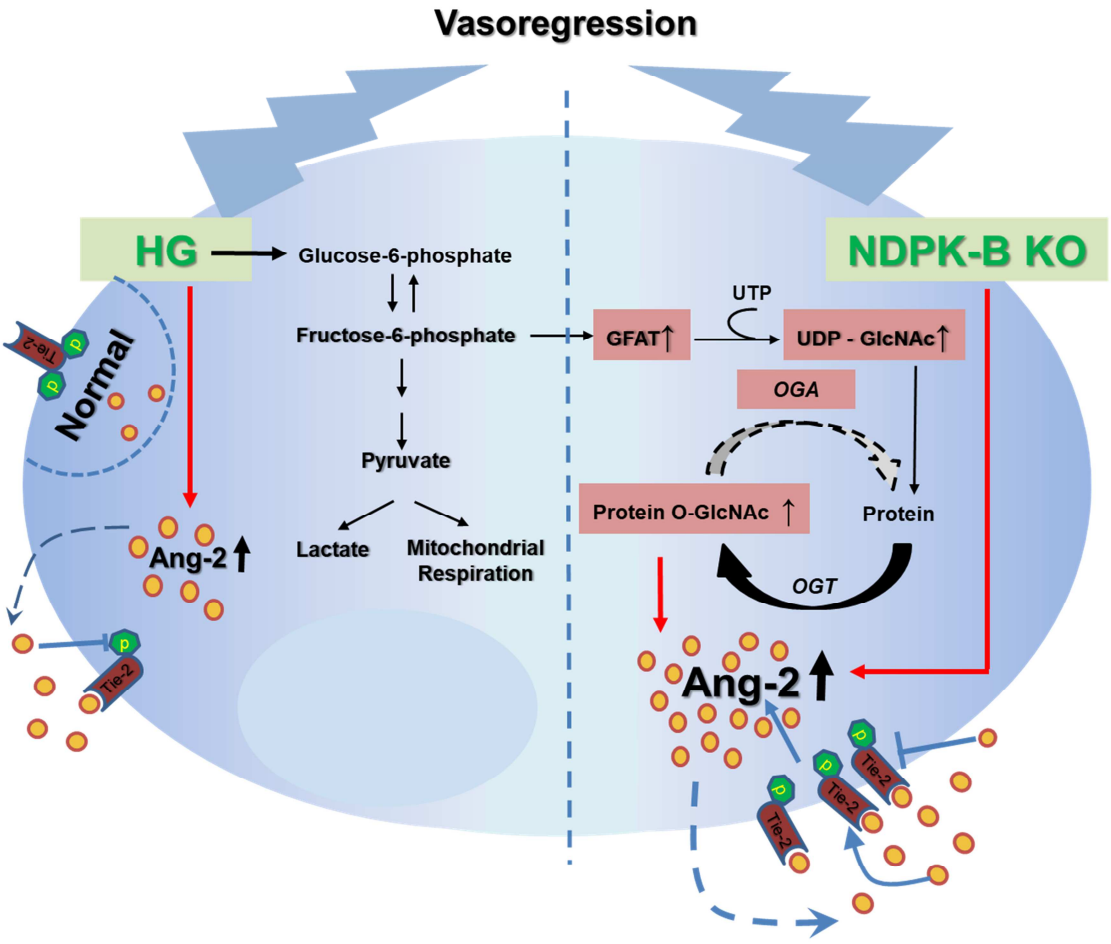

Fig. 41: The regulation of Ang-2 by Tie-2 and protein O-GlcNAcylation in ECs

References

1. DeFronzo, R.A., et al., *International Textbook of Diabetes Mellitus, 2 Volume Set*. Vol. 1. 2015: John Wiley & Sons.
2. Cho, N.H., et al., *IDF Diabetes Atlas: Global estimates of diabetes prevalence for 2017 and projections for 2045.* Diabetes Res Clin Pract, 2018. **138**: p. 271-281.
3. *Diagnosis and classification of diabetes mellitus.* Diabetes Care, 2010. **33 Suppl 1**: p. S62-9.
4. Fowler, M.J., *Microvascular and Macrovascular Complications of Diabetes.* Clinical Diabetes, 2008. **26**(2): p. 77-82.
5. Duh, E.J., J.K. Sun, and A.W. Stitt, *Diabetic retinopathy: current understanding, mechanisms, and treatment strategies.* JCI Insight, 2017. **2**(14).
6. Leasher, J.L., et al., *Erratum. Global Estimates on the Number of People Blind or Visually Impaired by Diabetic Retinopathy: A Meta-analysis From 1990-2010. Diabetes Care 2016;39:1643-1649.* Diabetes Care, 2016. **39**(11): p. 2096.
7. Hammes, H.P., *Diabetic retinopathy: hyperglycaemia, oxidative stress and beyond.* Diabetologia, 2018. **61**(1): p. 29-38.
8. Yau, J.W., et al., *Global prevalence and major risk factors of diabetic retinopathy.* Diabetes Care, 2012. **35**(3): p. 556-64.
9. *Intensive blood-glucose control with sulphonylureas or insulin compared with conventional treatment and risk of complications in patients with type 2 diabetes (UKPDS 33). UK Prospective Diabetes Study (UKPDS) Group.* Lancet, 1998. **352**(9131): p. 837-53.
10. Damato, E.M., et al., *Sight-threatening diabetic retinopathy at presentation to screening services in Fiji.* Ophthalmic Epidemiol, 2014. **21**(5): p. 318-26.
11. Ponto, K.A., et al., *Prevalence of diabetic retinopathy in screening-detected diabetes mellitus: results from the Gutenberg Health Study (GHS).* Diabetologia, 2016. **59**(9): p. 1913-9.
12. Ting, D.S., G.C. Cheung, and T.Y. Wong, *Diabetic retinopathy: global prevalence, major risk factors, screening practices and public health challenges: a review.* Clin Exp Ophthalmol, 2016. **44**(4): p. 260-77.
13. Forbes, J.M. and M.E. Cooper, *Mechanisms of diabetic complications.* Physiol Rev, 2013. **93**(1): p. 137-88.
14. Stitt, A.W., et al., *The progress in understanding and treatment of diabetic retinopathy.* Prog Retin Eye Res, 2016. **51**: p. 156-86.
15. Gardner, T.W. and J.R. Davila, *The neurovascular unit and the pathophysiologic basis of diabetic retinopathy.* Graefes Arch Clin Exp Ophthalmol, 2017. **255**(1): p. 1-6.
16. Augustin, H.G., et al., *Control of vascular morphogenesis and homeostasis through the angiopoietin-Tie system.* Nat Rev Mol Cell Biol, 2009. **10**(3): p. 165-77.
17. Fruttiger, M., *Development of the retinal vasculature.* Angiogenesis, 2007. **10**(2): p. 77-88.
18. Gariano, R.F. and T.W. Gardner, *Retinal angiogenesis in development and disease.* Nature, 2005. **438**(7070): p. 960-6.
19. Kur, J., E.A. Newman, and T. Chan-Ling, *Cellular and physiological mechanisms underlying blood flow regulation in the retina and choroid in health and disease.* Prog Retin Eye Res, 2012. **31**(5): p. 377-406.
20. Dietrich, N. and H.P. Hammes, *Retinal digest preparation: a method to study diabetic retinopathy.* Methods Mol Biol, 2012. **933**: p. 291-302.
21. *Early photocoagulation for diabetic retinopathy. ETDRS report number 9. Early Treatment Diabetic Retinopathy Study Research Group.* Ophthalmology, 1991. **98**(5 Suppl): p. 766-85.
22. *Fundus photographic risk factors for progression of diabetic retinopathy. ETDRS report number 12. Early Treatment Diabetic Retinopathy Study Research Group.* Ophthalmology, 1991. **98**(5 Suppl): p. 823-33.

23. Klein, R., et al., *The Wisconsin Epidemiologic Study of Diabetic Retinopathy. X. Four-year incidence and progression of diabetic retinopathy when age at diagnosis is 30 years or more.* Arch Ophthalmol, 1989. **107**(2): p. 244-9.
24. Klein, R., et al., *The Wisconsin Epidemiologic Study of Diabetic Retinopathy: XXII the twenty-five-year progression of retinopathy in persons with type 1 diabetes.* Ophthalmology, 2008. **115**(11): p. 1859-68.
25. Kuwabara, T. and D.G. Cogan, *Retinal vascular patterns. VI. Mural cells of the retinal capillaries.* Arch Ophthalmol, 1963. **69**: p. 492-502.
26. Korn, C. and H.G. Augustin, *Mechanisms of Vessel Pruning and Regression.* Dev Cell, 2015. **34**(1): p. 5-17.
27. Pfister, F., et al., *Pericytes in the eye.* Pflugers Arch, 2013. **465**(6): p. 789-96.
28. Hammes, H.P., et al., *Diabetic retinopathy: targeting vasoregression.* Diabetes, 2011. **60**(1): p. 9-16.
29. Hammes, H.P., et al., *Pericytes and the pathogenesis of diabetic retinopathy.* Diabetes, 2002. **51**(10): p. 3107-12.
30. Valdez, C.N., et al., *Retinal microangiopathy in a mouse model of inducible mural cell loss.* Am J Pathol, 2014. **184**(10): p. 2618-26.
31. Dietrich, N., et al., *The DPP4 Inhibitor Linagliptin Protects from Experimental Diabetic Retinopathy.* PLoS One, 2016. **11**(12): p. e0167853.
32. Robinson, R., et al., *Update on animal models of diabetic retinopathy: from molecular approaches to mice and higher mammals.* Dis Model Mech, 2012. **5**(4): p. 444-56.
33. Karlstetter, M., et al., *Retinal microglia: just bystander or target for therapy?* Prog Retin Eye Res, 2015. **45**: p. 30-57.
34. Reichenbach, A. and A. Bringmann, *New functions of Muller cells.* Glia, 2013. **61**(5): p. 651-78.
35. Arnold, T. and C. Betsholtz, *Correction: The importance of microglia in the development of the vasculature in the central nervous system.* Vasc Cell, 2013. **5**(1): p. 12.
36. Xu, Q., et al., *Vascular development in the retina and inner ear: control by Norrin and Frizzled-4, a high-affinity ligand-receptor pair.* Cell, 2004. **116**(6): p. 883-95.
37. Antonetti, D.A., R. Klein, and T.W. Gardner, *Diabetic retinopathy.* N Engl J Med, 2012. **366**(13): p. 1227-39.
38. Heilig, C.W., et al., *Overexpression of glucose transporters in rat mesangial cells cultured in a normal glucose milieu mimics the diabetic phenotype.* J Clin Invest, 1995. **96**(4): p. 1802-14.
39. Kaiser, N., et al., *Differential regulation of glucose transport and transporters by glucose in vascular endothelial and smooth muscle cells.* Diabetes, 1993. **42**(1): p. 80-9.
40. Du, X.L., et al., *Hyperglycemia-induced mitochondrial superoxide overproduction activates the hexosamine pathway and induces plasminogen activator inhibitor-1 expression by increasing Sp1 glycosylation.* Proc Natl Acad Sci U S A, 2000. **97**(22): p. 12222-6.
41. Giugliano, D., A. Ceriello, and G. Paolisso, *Oxidative stress and diabetic vascular complications.* Diabetes Care, 1996. **19**(3): p. 257-67.
42. Nishikawa, T., et al., *Normalizing mitochondrial superoxide production blocks three pathways of hyperglycaemic damage.* Nature, 2000. **404**(6779): p. 787-90.
43. Brownlee, M., *The pathobiology of diabetic complications: a unifying mechanism.* Diabetes, 2005. **54**(6): p. 1615-25.
44. Lee, A.Y. and S.S. Chung, *Contributions of polyol pathway to oxidative stress in diabetic cataract.* FASEB J, 1999. **13**(1): p. 23-30.
45. Engerman, R.L., T.S. Kern, and M.E. Larson, *Nerve conduction and aldose reductase inhibition during 5 years of diabetes or galactosaemia in dogs.* Diabetologia, 1994. **37**(2): p. 141-4.
46. McLellan, A.C., et al., *Glyoxalase system in clinical diabetes mellitus and correlation with diabetic complications.* Clin Sci (Lond), 1994. **87**(1): p. 21-9.

47. Neeper, M., et al., *Cloning and expression of a cell surface receptor for advanced glycosylation end products of proteins.* J Biol Chem, 1992. **267**(21): p. 14998-5004.
48. Schmidt, A.M., et al., *Advanced glycation endproducts interacting with their endothelial receptor induce expression of vascular cell adhesion molecule-1 (VCAM-1) in cultured human endothelial cells and in mice. A potential mechanism for the accelerated vasculopathy of diabetes.* J Clin Invest, 1995. **96**(3): p. 1395-403.
49. Shinohara, M., et al., *Overexpression of glyoxalase-I in bovine endothelial cells inhibits intracellular advanced glycation endproduct formation and prevents hyperglycemia-induced increases in macromolecular endocytosis.* J Clin Invest, 1998. **101**(5): p. 1142-7.
50. Vlassara, H., et al., *Cachectin/TNF and IL-1 induced by glucose-modified proteins: role in normal tissue remodeling.* Science, 1988. **240**(4858): p. 1546-8.
51. Hammes, H.P., et al., *Aminoguanidine treatment inhibits the development of experimental diabetic retinopathy.* Proc Natl Acad Sci U S A, 1991. **88**(24): p. 11555-8.
52. Ishii, H., et al., *Amelioration of vascular dysfunctions in diabetic rats by an oral PKC beta inhibitor.* Science, 1996. **272**(5262): p. 728-31.
53. Wells, L. and G.W. Hart, *O-GlcNAc turns twenty: functional implications for post-translational modification of nuclear and cytosolic proteins with a sugar.* FEBS Lett, 2003. **546**(1): p. 154-8.
54. Yao, D., et al., *High glucose increases angiopoietin-2 transcription in microvascular endothelial cells through methylglyoxal modification of mSin3A.* J Biol Chem, 2007. **282**(42): p. 31038-45.
55. Du, X., et al., *Inhibition of GAPDH activity by poly(ADP-ribose) polymerase activates three major pathways of hyperglycemic damage in endothelial cells.* J Clin Invest, 2003. **112**(7): p. 1049-57.
56. van den Born, J.C., et al., *Gasotransmitters in Vascular Complications of Diabetes.* Diabetes, 2016. **65**(2): p. 331-45.
57. Kolibabka, M., et al., *Dicarbonyl Stress Mimics Diabetic Neurovascular Damage in the Retina.* Exp Clin Endocrinol Diabetes, 2016. **124**(7): p. 437-9.
58. Lachin, J.M., et al., *Effect of glycemic exposure on the risk of microvascular complications in the diabetes control and complications trial--revisited.* Diabetes, 2008. **57**(4): p. 995-1001.
59. Holt, G.D. and G.W. Hart, *The subcellular distribution of terminal N-acetylglucosamine moieties. Localization of a novel protein-saccharide linkage, O-linked GlcNAc.* J Biol Chem, 1986. **261**(17): p. 8049-57.
60. Housley, M.P., et al., *O-GlcNAc regulates FoxO activation in response to glucose.* J Biol Chem, 2008. **283**(24): p. 16283-92.
61. Torres, C.R. and G.W. Hart, *Topography and polypeptide distribution of terminal N-acetylglucosamine residues on the surfaces of intact lymphocytes. Evidence for O-linked GlcNAc.* J Biol Chem, 1984. **259**(5): p. 3308-17.
62. Yang, X. and K. Qian, *Protein O-GlcNAcylation: emerging mechanisms and functions.* Nat Rev Mol Cell Biol, 2017. **18**(7): p. 452-465.
63. Hart, G.W. and Y. Akimoto, *The O-GlcNAc Modification.* 2009.
64. Hart, G.W., et al., *Cross talk between O-GlcNAcylation and phosphorylation: roles in signaling, transcription, and chronic disease.* Annu Rev Biochem, 2011. **80**: p. 825-58.
65. Dorfman, A., et al., *The biosynthesis of hyaluronic acid by group A Streptococcus. II. Origin of the N-acetylglucosamine moiety.* J Biol Chem, 1955. **212**(2): p. 583-91.
66. Ghosh, S., et al., *Glucosamine metabolism. V. Enzymatic synthesis of glucosamine 6-phosphate.* J Biol Chem, 1960. **235**: p. 1265-73.
67. Marshall, S., V. Bacote, and R.R. Traxinger, *Complete inhibition of glucose-induced desensitization of the glucose transport system by inhibitors of mRNA synthesis. Evidence for rapid turnover of glutamine:fructose-6-phosphate amidotransferase.* J Biol Chem, 1991. **266**(16): p. 10155-61.

68. Broschat, K.O., et al., *Kinetic characterization of human glutamine-fructose-6-phosphate amidotransferase I: potent feedback inhibition by glucosamine 6-phosphate.* J Biol Chem, 2002. **277**(17): p. 14764-70.
69. Copeland, R.J., J.W. Bullen, and G.W. Hart, *Cross-talk between GlcNAcylation and phosphorylation: roles in insulin resistance and glucose toxicity.* Am J Physiol Endocrinol Metab, 2008. **295**(1): p. E17-28.
70. Fantus, I.G., et al., *The Hexosamine Biosynthesis Pathway*, in *The Diabetic Kidney*, P. Cortes and C.E. Mogensen, Editors. 2006, Humana Press: Totowa, NJ. p. 117-133.
71. Zhou, J., et al., *Regulation of glutamine:fructose-6-phosphate amidotransferase by cAMP-dependent protein kinase.* Diabetes, 1998. **47**(12): p. 1836-40.
72. Chang, Q., et al., *Phosphorylation of human glutamine:fructose-6-phosphate amidotransferase by cAMP-dependent protein kinase at serine 205 blocks the enzyme activity.* J Biol Chem, 2000. **275**(29): p. 21981-7.
73. Eguchi, S., et al., *AMP-activated protein kinase phosphorylates glutamine : fructose-6-phosphate amidotransferase 1 at Ser243 to modulate its enzymatic activity.* Genes Cells, 2009. **14**(2): p. 179-89.
74. Zibrova, D., et al., *GFAT1 phosphorylation by AMPK promotes VEGF-induced angiogenesis.* Biochem J, 2017. **474**(6): p. 983-1001.
75. Lazarus, M.B., et al., *Structure of human O-GlcNAc transferase and its complex with a peptide substrate.* Nature, 2011. **469**(7331): p. 564-7.
76. Janetzko, J. and S. Walker, *The making of a sweet modification: structure and function of O-GlcNAc transferase.* J Biol Chem, 2014. **289**(50): p. 34424-32.
77. Ma, J. and G.W. Hart, *Protein O-GlcNAcylation in diabetes and diabetic complications.* Expert Rev Proteomics, 2013. **10**(4): p. 365-80.
78. Golks, A., et al., *Requirement for O-linked N-acetylglucosaminyltransferase in lymphocytes activation.* EMBO J, 2007. **26**(20): p. 4368-79.
79. Yang, X., F. Zhang, and J.E. Kudlow, *Recruitment of O-GlcNAc transferase to promoters by corepressor mSin3A: coupling protein O-GlcNAcylation to transcriptional repression.* Cell, 2002. **110**(1): p. 69-80.
80. Vosseller, K., et al., *Elevated nucleocytoplasmic glycosylation by O-GlcNAc results in insulin resistance associated with defects in Akt activation in 3T3-L1 adipocytes.* Proc Natl Acad Sci U S A, 2002. **99**(8): p. 5313-8.
81. Soesanto, Y.A., et al., *Regulation of Akt signaling by O-GlcNAc in euglycemia.* Am J Physiol Endocrinol Metab, 2008. **295**(4): p. E974-80.
82. Andrali, S.S., Q. Qian, and S. Ozcan, *Glucose mediates the translocation of NeuroD1 by O-linked glycosylation.* J Biol Chem, 2007. **282**(21): p. 15589-96.
83. Gao, Y., J. Miyazaki, and G.W. Hart, *The transcription factor PDX-1 is post-translationally modified by O-linked N-acetylglucosamine and this modification is correlated with its DNA binding activity and insulin secretion in min6 beta-cells.* Arch Biochem Biophys, 2003. **415**(2): p. 155-63.
84. Akimoto, Y., et al., *Elevation of the post-translational modification of proteins by O-linked N-acetylglucosamine leads to deterioration of the glucose-stimulated insulin secretion in the pancreas of diabetic Goto-Kakizaki rats.* Glycobiology, 2007. **17**(2): p. 127-40.
85. Akimoto, Y., et al., *Localization of the O-linked N-acetylglucosamine transferase in rat pancreas.* Diabetes, 1999. **48**(12): p. 2407-13.
86. Akimoto, Y., et al., *Increased O-GlcNAc transferase in pancreas of rats with streptozotocin-induced diabetes.* Diabetologia, 2000. **43**(10): p. 1239-47.
87. Hanover, J.A., et al., *Elevated O-linked N-acetylglucosamine metabolism in pancreatic beta-cells.* Arch Biochem Biophys, 1999. **362**(1): p. 38-45.

88. Ball, L.E., M.N. Berkaw, and M.G. Buse, *Identification of the major site of O-linked beta-N-acetylglucosamine modification in the C terminus of insulin receptor substrate-1.* Mol Cell Proteomics, 2006. **5**(2): p. 313-23.
89. Whelan, S.A., M.D. Lane, and G.W. Hart, *Regulation of the O-linked beta-N-acetylglucosamine transferase by insulin signaling.* J Biol Chem, 2008. **283**(31): p. 21411-7.
90. Yang, X., et al., *Phosphoinositide signalling links O-GlcNAc transferase to insulin resistance.* Nature, 2008. **451**(7181): p. 964-9.
91. Hammes, H.P., et al., *Angiopoietin-2 causes pericyte dropout in the normal retina: evidence for involvement in diabetic retinopathy.* Diabetes, 2004. **53**(4): p. 1104-10.
92. Pfister, F., et al., *Retinal overexpression of angiopoietin-2 mimics diabetic retinopathy and enhances vascular damages in hyperglycemia.* Acta Diabetol, 2010. **47**(1): p. 59-64.
93. Gurel, Z., et al., *Retinal O-linked N-acetylglucosamine protein modifications: implications for postnatal retinal vascularization and the pathogenesis of diabetic retinopathy.* Mol Vis, 2013. **19**: p. 1047-59.
94. Huang, Q. and N. Sheibani, *High glucose promotes retinal endothelial cell migration through activation of Src, PI3K/Akt1/eNOS, and ERKs.* Am J Physiol Cell Physiol, 2008. **295**(6): p. C1647-57.
95. Forsythe, M.E., et al., *Caenorhabditis elegans ortholog of a diabetes susceptibility locus: oga-1 (O-GlcNAcase) knockout impacts O-GlcNAc cycling, metabolism, and dauer.* Proc Natl Acad Sci U S A, 2006. **103**(32): p. 11952-7.
96. Khidekel, N., et al., *Probing the dynamics of O-GlcNAc glycosylation in the brain using quantitative proteomics.* Nat Chem Biol, 2007. **3**(6): p. 339-48.
97. Lehman, D.M., et al., *A single nucleotide polymorphism in MGEA5 encoding O-GlcNAc-selective N-acetyl-beta-D glucosaminidase is associated with type 2 diabetes in Mexican Americans.* Diabetes, 2005. **54**(4): p. 1214-21.
98. Hu, Y., et al., *Adenovirus-mediated overexpression of O-GlcNAcase improves contractile function in the diabetic heart.* Circ Res, 2005. **96**(9): p. 1006-13.
99. Hu, Y., et al., *Increased enzymatic O-GlcNAcylation of mitochondrial proteins impairs mitochondrial function in cardiac myocytes exposed to high glucose.* J Biol Chem, 2009. **284**(1): p. 547-55.
100. McClain, D.A., et al., *Altered glycan-dependent signaling induces insulin resistance and hyperleptinemia.* Proc Natl Acad Sci U S A, 2002. **99**(16): p. 10695-9.
101. Du, X.-L., et al., *Hyperglycemia-induced mitochondrial superoxide overproduction activates the hexosamine pathway and induces plasminogen activator inhibitor-1 expression by increasing Sp1 glycosylation.* Proceedings of the National Academy of Sciences, 2000. **97**(22): p. 12222-12226.
102. Hammes, H.-P., et al., *Benfotiamine blocks three major pathways of hyperglycemic damage and prevents experimental diabetic retinopathy.* Nature Medicine, 2003. **9**(3): p. 294-299.
103. Du, X.L., et al., *Hyperglycemia inhibits endothelial nitric oxide synthase activity by posttranslational modification at the Akt site.* J Clin Invest, 2001. **108**(9): p. 1341-8.
104. Musicki, B., et al., *Inactivation of phosphorylated endothelial nitric oxide synthase (Ser-1177) by O-GlcNAc in diabetes-associated erectile dysfunction.* Proc Natl Acad Sci U S A, 2005. **102**(33): p. 11870-5.
105. Taylor, R.P., et al., *Glucose deprivation stimulates O-GlcNAc modification of proteins through up-regulation of O-linked N-acetylglucosaminyltransferase.* J Biol Chem, 2008. **283**(10): p. 6050-7.
106. Taylor, R.P., et al., *Up-regulation of O-GlcNAc transferase with glucose deprivation in HepG2 cells is mediated by decreased hexosamine pathway flux.* J Biol Chem, 2009. **284**(6): p. 3425-32.
107. Risau, W., *Mechanisms of angiogenesis.* Nature, 1997. **386**(6626): p. 671-4.

108. Davis, S., et al., *Isolation of angiopoietin-1, a ligand for the TIE2 receptor, by secretion-trap expression cloning.* Cell, 1996. **87**(7): p. 1161-9.
109. Maisonpierre, P.C., et al., *Angiopoietin-2, a natural antagonist for Tie2 that disrupts in vivo angiogenesis.* Science, 1997. **277**(5322): p. 55-60.
110. Cheung, A.H., R.J. Stewart, and P.A. Marsden, *Endothelial Tie2/Tek ligands angiopoietin-1 (ANGPT1) and angiopoietin-2 (ANGPT2): regional localization of the human genes to 8q22.3-q23 and 8p23.* Genomics, 1998. **48**(3): p. 389-91.
111. Grosios, K., et al., *Assignment of ANGPT4, ANGPT1, and ANGPT2 encoding angiopoietins 4, 1 and 2 to human chromosome bands 20p13, 8q22.3-->q23 and 8p23.1, respectively, by in situ hybridization and radiation hybrid mapping.* Cytogenet Cell Genet, 1999. **84**(1-2): p. 118-20.
112. Xu, Y. and Q. Yu, *Angiopoietin-1, unlike angiopoietin-2, is incorporated into the extracellular matrix via its linker peptide region.* J Biol Chem, 2001. **276**(37): p. 34990-8.
113. Fiedler, U., et al., *The Tie-2 ligand angiopoietin-2 is stored in and rapidly released upon stimulation from endothelial cell Weibel-Palade bodies.* Blood, 2004. **103**(11): p. 4150-6.
114. Jeon Byeong, H., et al., *Tie-ing the Antiinflammatory Effect of Angiopoietin-1 to Inhibition of NF-κB.* Circulation Research, 2003. **92**(6): p. 586-588.
115. Ramsauer, M. and P.A. D'Amore, *Getting Tie(2)d up in angiogenesis.* The Journal of Clinical Investigation, 2002. **110**(11): p. 1615-1617.
116. Suri, C., et al., *Requisite Role of Angiopoietin-1, a Ligand for the TIE2 Receptor, during Embryonic Angiogenesis.* Cell, 1996. **87**(7): p. 1171-1180.
117. Thurston, G., et al., *Angiopoietin-1 protects the adult vasculature against plasma leakage.* Nat Med, 2000. **6**(4): p. 460-3.
118. Wong Adrianne, L., et al., *Tie2 Expression and Phosphorylation in Angiogenic and Quiescent Adult Tissues.* Circulation Research, 1997. **81**(4): p. 567-574.
119. Partanen, J., et al., *A novel endothelial cell surface receptor tyrosine kinase with extracellular epidermal growth factor homology domains.* Mol Cell Biol, 1992. **12**(4): p. 1698-707.
120. Dumont, D.J., et al., *Dominant-negative and targeted null mutations in the endothelial receptor tyrosine kinase, tek, reveal a critical role in vasculogenesis of the embryo.* Genes Dev, 1994. **8**(16): p. 1897-909.
121. Patan, S., *TIE1 and TIE2 receptor tyrosine kinases inversely regulate embryonic angiogenesis by the mechanism of intussusceptive microvascular growth.* Microvasc Res, 1998. **56**(1): p. 1-21.
122. Sato, T.N., et al., *Distinct roles of the receptor tyrosine kinases Tie-1 and Tie-2 in blood vessel formation.* Nature, 1995. **376**(6535): p. 70-4.
123. Takakura, N., et al., *Critical role of the TIE2 endothelial cell receptor in the development of definitive hematopoiesis.* Immunity, 1998. **9**(5): p. 677-86.
124. Puri, M.C., et al., *Interaction of the TEK and TIE receptor tyrosine kinases during cardiovascular development.* Development, 1999. **126**(20): p. 4569-80.
125. Rodewald, H.R. and T.N. Sato, *Tie1, a receptor tyrosine kinase essential for vascular endothelial cell integrity, is not critical for the development of hematopoietic cells.* Oncogene, 1996. **12**(2): p. 397-404.
126. Suri, C., et al., *Requisite role of angiopoietin-1, a ligand for the TIE2 receptor, during embryonic angiogenesis.* Cell, 1996. **87**(7): p. 1171-80.
127. Fiedler, U., et al., *Angiopoietin-2 sensitizes endothelial cells to TNF-alpha and has a crucial role in the induction of inflammation.* Nat Med, 2006. **12**(2): p. 235-9.
128. Gale, N.W., et al., *Angiopoietin-2 is required for postnatal angiogenesis and lymphatic patterning, and only the latter role is rescued by Angiopoietin-1.* Dev Cell, 2002. **3**(3): p. 411-23.
129. Goede, V., et al., *Analysis of blood vessel maturation processes during cyclic ovarian angiogenesis.* Lab Invest, 1998. **78**(11): p. 1385-94.

130. Hackett, S.F., et al., *Angiopoietin-2 plays an important role in retinal angiogenesis.* J Cell Physiol, 2002. **192**(2): p. 182-7.
131. Pitera, J.E., et al., *Dysmorphogenesis of kidney cortical peritubular capillaries in angiopoietin-2-deficient mice.* Am J Pathol, 2004. **165**(6): p. 1895-906.
132. Eklund, L. and P. Saharinen, *Angiopoietin signaling in the vasculature.* Exp Cell Res, 2013. **319**(9): p. 1271-80.
133. Kim, I., et al., *Angiopoietin-1 reduces VEGF-stimulated leukocyte adhesion to endothelial cells by reducing ICAM-1, VCAM-1, and E-selectin expression.* Circ Res, 2001. **89**(6): p. 477-9.
134. Suri, C., et al., *Increased vascularization in mice overexpressing angiopoietin-1.* Science, 1998. **282**(5388): p. 468-71.
135. Vikkula, M., et al., *Vascular dysmorphogenesis caused by an activating mutation in the receptor tyrosine kinase TIE2.* Cell, 1996. **87**(7): p. 1181-90.
136. Gurnik, S., et al., *Angiopoietin-2-induced blood-brain barrier compromise and increased stroke size are rescued by VE-PTP-dependent restoration of Tie2 signaling.* Acta Neuropathol, 2016. **131**(5): p. 753-73.
137. Daly, C., et al., *Angiopoietin-1 modulates endothelial cell function and gene expression via the transcription factor FKHR (FOXO1).* Genes Dev, 2004. **18**(9): p. 1060-71.
138. Gavard, J., V. Patel, and J.S. Gutkind, *Angiopoietin-1 prevents VEGF-induced endothelial permeability by sequestering Src through mDia.* Dev Cell, 2008. **14**(1): p. 25-36.
139. Sullivan, C.C., et al., *Induction of pulmonary hypertension by an angiopoietin 1/TIE2/serotonin pathway.* Proc Natl Acad Sci U S A, 2003. **100**(21): p. 12331-6.
140. Uemura, A., et al., *Recombinant angiopoietin-1 restores higher-order architecture of growing blood vessels in mice in the absence of mural cells.* J Clin Invest, 2002. **110**(11): p. 1619-28.
141. Fukuhara, S., et al., *Differential function of Tie2 at cell-cell contacts and cell-substratum contacts regulated by angiopoietin-1.* Nat Cell Biol, 2008. **10**(5): p. 513-26.
142. Saharinen, P., et al., *Angiopoietins assemble distinct Tie2 signalling complexes in endothelial cell-cell and cell-matrix contacts.* Nat Cell Biol, 2008. **10**(5): p. 527-37.
143. DeBusk, L.M., D.E. Hallahan, and P.C. Lin, *Akt is a major angiogenic mediator downstream of the Ang1/Tie2 signaling pathway.* Exp Cell Res, 2004. **298**(1): p. 167-77.
144. Kontos, C.D., et al., *The endothelial receptor tyrosine kinase Tie1 activates phosphatidylinositol 3-kinase and Akt to inhibit apoptosis.* Mol Cell Biol, 2002. **22**(6): p. 1704-13.
145. Papapetropoulos, A., et al., *Angiopoietin-1 inhibits endothelial cell apoptosis via the Akt/survivin pathway.* J Biol Chem, 2000. **275**(13): p. 9102-5.
146. Tsigkos, S., et al., *Regulation of Ang2 release by PTEN/PI3-kinase/Akt in lung microvascular endothelial cells.* J Cell Physiol, 2006. **207**(2): p. 506-11.
147. Hanahan, D., *Signaling vascular morphogenesis and maintenance.* Science, 1997. **277**(5322): p. 48-50.
148. Kim, M., et al., *Opposing actions of angiopoietin-2 on Tie2 signaling and FOXO1 activation.* J Clin Invest, 2016. **126**(9): p. 3511-25.
149. Teichert-Kuliszewska, K., et al., *Biological action of angiopoietin-2 in a fibrin matrix model of angiogenesis is associated with activation of Tie2.* Cardiovascular Research, 2001. **49**(3): p. 659-670.
150. Yuan, H.T., et al., *Angiopoietin 2 is a partial agonist/antagonist of Tie2 signaling in the endothelium.* Mol Cell Biol, 2009. **29**(8): p. 2011-22.
151. Daly, C., et al., *Angiopoietin-2 functions as an autocrine protective factor in stressed endothelial cells.* Proc Natl Acad Sci U S A, 2006. **103**(42): p. 15491-6.
152. Scharpfenecker, M., et al., *The Tie-2 ligand angiopoietin-2 destabilizes quiescent endothelium through an internal autocrine loop mechanism.* J Cell Sci, 2005. **118**(Pt 4): p. 771-80.

153. Benest, A.V., et al., *Angiopoietin-2 is critical for cytokine-induced vascular leakage.* PLoS One, 2013. **8**(8): p. e70459.
154. Le, C.T., et al., *Synergistic actions of blocking angiopoietin-2 and tumor necrosis factor-alpha in suppressing remodeling of blood vessels and lymphatics in airway inflammation.* Am J Pathol, 2015. **185**(11): p. 2949-68.
155. Aiello, L.P., et al., *Vascular endothelial growth factor in ocular fluid of patients with diabetic retinopathy and other retinal disorders.* N Engl J Med, 1994. **331**(22): p. 1480-7.
156. Gerhardt, H., et al., *VEGF guides angiogenic sprouting utilizing endothelial tip cell filopodia.* J Cell Biol, 2003. **161**(6): p. 1163-77.
157. Liu, H., et al., *Notch3 is critical for proper angiogenesis and mural cell investment.* Circ Res, 2010. **107**(7): p. 860-70.
158. Felcht, M., et al., *Angiopoietin-2 differentially regulates angiogenesis through TIE2 and integrin signaling.* J Clin Invest, 2012. **122**(6): p. 1991-2005.
159. Yun, J.H., et al., *Angiopoietin 2 induces astrocyte apoptosis via alphavbeta5-integrin signaling in diabetic retinopathy.* Cell Death Dis, 2016. **7**: p. e2101.
160. Hakanpaa, L., et al., *Endothelial destabilization by angiopoietin-2 via integrin beta1 activation.* Nat Commun, 2015. **6**: p. 5962.
161. Park, S.W., et al., *Angiopoietin 2 induces pericyte apoptosis via alpha3beta1 integrin signaling in diabetic retinopathy.* Diabetes, 2014. **63**(9): p. 3057-68.
162. Potente, M., et al., *Involvement of Foxo transcription factors in angiogenesis and postnatal neovascularization.* J Clin Invest, 2005. **115**(9): p. 2382-92.
163. Berg, P. and W.K. Joklik, *Transphosphorylation between nucleoside polyphosphates.* Nature, 1953. **172**(4387): p. 1008-9.
164. Krebs, H.A. and R. Hems, *Some reactions of adenosine and inosine phosphates in animal tissues.* Biochim Biophys Acta, 1953. **12**(1-2): p. 172-80.
165. Morera, S., et al., *Mechanism of phosphate transfer by nucleoside diphosphate kinase: X-ray structures of the phosphohistidine intermediate of the enzymes from Drosophila and Dictyostelium.* Biochemistry, 1995. **34**(35): p. 11062-70.
166. Tepper, A.D., et al., *Investigation of the active site and the conformational stability of nucleoside diphosphate kinase by site-directed mutagenesis.* J Biol Chem, 1994. **269**(51): p. 32175-80.
167. Bosnar, M.H., R. Bago, and H. Cetkovic, *Subcellular localization of Nm23/NDPK A and B isoforms: a reflection of their biological function?* Mol Cell Biochem, 2009. **329**(1-2): p. 63-71.
168. Lacombe, M.L., et al., *The human Nm23/nucleoside diphosphate kinases.* J Bioenerg Biomembr, 2000. **32**(3): p. 247-58.
169. Lacombe, M.L., et al., *The mitochondrial nucleoside diphosphate kinase (NDPK-D/NME4), a moonlighting protein for cell homeostasis.* Lab Invest, 2018. **98**(5): p. 582-588.
170. Gilles, A.M., et al., *Nucleoside diphosphate kinase from human erythrocytes. Structural characterization of the two polypeptide chains responsible for heterogeneity of the hexameric enzyme.* J Biol Chem, 1991. **266**(14): p. 8784-9.
171. Janin, J., et al., *Three-dimensional structure of nucleoside diphosphate kinase.* J Bioenerg Biomembr, 2000. **32**(3): p. 215-25.
172. Bilitou, A., et al., *The NM23 family in development.* Mol Cell Biochem, 2009. **329**(1-2): p. 17-33.
173. Fan, Z., et al., *Tumor suppressor NM23-H1 is a granzyme A-activated DNase during CTL-mediated apoptosis, and the nucleosome assembly protein SET is its inhibitor.* Cell, 2003. **112**(5): p. 659-72.
174. Lee, M.Y., et al., *NM23H2 inhibits EGF- and Ras-induced proliferation of NIH3T3 cells by blocking the ERK pathway.* Cancer Lett, 2009. **275**(2): p. 221-6.

175. Marino, N., J.C. Marshall, and P.S. Steeg, *Protein-protein interactions: a mechanism regulating the anti-metastatic properties of Nm23-H1.* Naunyn Schmiedebergs Arch Pharmacol, 2011. **384**(4-5): p. 351-62.
176. Mochizuki, T., et al., *Xenopus NM23-X4 regulates retinal gliogenesis through interaction with p27Xic1.* Neural Dev, 2009. **4**: p. 1.
177. Postel, E.H., et al., *Human c-myc transcription factor PuF identified as nm23-H2 nucleoside diphosphate kinase, a candidate suppressor of tumor metastasis.* Science, 1993. **261**(5120): p. 478-80.
178. Thakur, R.K., et al., *Metastases suppressor NM23-H2 interaction with G-quadruplex DNA within c-MYC promoter nuclease hypersensitive element induces c-MYC expression.* Nucleic Acids Res, 2009. **37**(1): p. 172-83.
179. Boissan, M., et al., *Increased lung metastasis in transgenic NM23-Null/SV40 mice with hepatocellular carcinoma.* J Natl Cancer Inst, 2005. **97**(11): p. 836-45.
180. Steeg, P.S., et al., *Evidence for a novel gene associated with low tumor metastatic potential.* J Natl Cancer Inst, 1988. **80**(3): p. 200-4.
181. Clapham, D.E. and E.J. Neer, *G protein beta gamma subunits.* Annu Rev Pharmacol Toxicol, 1997. **37**: p. 167-203.
182. Hamm, H.E., *The many faces of G protein signaling.* J Biol Chem, 1998. **273**(2): p. 669-72.
183. Wieland, T. and M.C. Michel, *Can a GDP-liganded G-protein be active?* Mol Pharmacol, 2005. **68**(3): p. 559-62.
184. Wieland, T., *Interaction of nucleoside diphosphate kinase B with heterotrimeric G protein betagamma dimers: consequences on G protein activation and stability.* Naunyn Schmiedebergs Arch Pharmacol, 2007. **374**(5-6): p. 373-83.
185. Cuello, F., et al., *Activation of heterotrimeric G proteins by a high energy phosphate transfer via nucleoside diphosphate kinase (NDPK) B and Gbeta subunits. Complex formation of NDPK B with Gbeta gamma dimers and phosphorylation of His-266 IN Gbeta.* J Biol Chem, 2003. **278**(9): p. 7220-6.
186. Hippe, H.J., et al., *Regulation of cardiac cAMP synthesis and contractility by nucleoside diphosphate kinase B/G protein beta gamma dimer complexes.* Circ Res, 2007. **100**(8): p. 1191-9.
187. Hippe, H.J., et al., *Activation of heterotrimeric G proteins by a high energy phosphate transfer via nucleoside diphosphate kinase (NDPK) B and Gbeta subunits. Specific activation of Gsalpha by an NDPK B.Gbetagamma complex in H10 cells.* J Biol Chem, 2003. **278**(9): p. 7227-33.
188. Hippe, H.J., et al., *Through scaffolding and catalytic actions nucleoside diphosphate kinase B differentially regulates basal and beta-adrenoceptor-stimulated cAMP synthesis.* Cell Signal, 2011. **23**(3): p. 579-85.
189. Hippe, H.J., et al., *Nucleoside diphosphate kinase B is required for the formation of heterotrimeric G protein containing caveolae.* Naunyn Schmiedebergs Arch Pharmacol, 2011. **384**(4-5): p. 461-72.
190. Abu-Taha, I.H., et al., *Nucleoside Diphosphate Kinase-C Suppresses cAMP Formation in Human Heart Failure.* Circulation, 2017. **135**(9): p. 881-897.
191. Hippe, H.J., et al., *The interaction of nucleoside diphosphate kinase B with Gbetagamma dimers controls heterotrimeric G protein function.* Proc Natl Acad Sci U S A, 2009. **106**(38): p. 16269-74.
192. Wagner, P.D. and N.D. Vu, *Phosphorylation of ATP-citrate lyase by nucleoside diphosphate kinase.* J Biol Chem, 1995. **270**(37): p. 21758-64.
193. Cai, X., et al., *Regulation of the epithelial Ca(2)(+) channel TRPV5 by reversible histidine phosphorylation mediated by NDPK-B and PHPT1.* Mol Biol Cell, 2014. **25**(8): p. 1244-50.
194. Muimo, R., et al., *Histidine phosphorylation of annexin I in airway epithelia.* J Biol Chem, 2000. **275**(47): p. 36632-6.

195. Srivastava, S., et al., *Histidine phosphorylation of the potassium channel KCa3.1 by nucleoside diphosphate kinase B is required for activation of KCa3.1 and CD4 T cells.* Mol Cell, 2006. **24**(5): p. 665-675.
196. Di, L., et al., *Nucleoside diphosphate kinase B knock-out mice have impaired activation of the K+ channel KCa3.1, resulting in defective T cell activation.* J Biol Chem, 2010. **285**(50): p. 38765-71.
197. Couet, J., M. Sargiacomo, and M.P. Lisanti, *Interaction of a receptor tyrosine kinase, EGF-R, with caveolins. Caveolin binding negatively regulates tyrosine and serine/threonine kinase activities.* J Biol Chem, 1997. **272**(48): p. 30429-38.
198. Feng, Y., et al., *Nucleoside diphosphate kinase B regulates angiogenesis through modulation of vascular endothelial growth factor receptor type 2 and endothelial adherens junction proteins.* Arterioscler Thromb Vasc Biol, 2014. **34**(10): p. 2292-300.
199. Fujita, T., et al., *Accumulation of molecules involved in alpha1-adrenergic signal within caveolae: caveolin expression and the development of cardiac hypertrophy.* Cardiovasc Res, 2001. **51**(4): p. 709-16.
200. Insel, P.A., et al., *Compartmentation of G-protein-coupled receptors and their signalling components in lipid rafts and caveolae.* Biochem Soc Trans, 2005. **33**(Pt 5): p. 1131-4.
201. Liao, W.X., et al., *Compartmentalizing VEGF-induced ERK2/1 signaling in placental artery endothelial cell caveolae: a paradoxical role of caveolin-1 in placental angiogenesis in vitro.* Mol Endocrinol, 2009. **23**(9): p. 1428-44.
202. Kowluru, A., R.A. Kowluru, and A. Yamazaki, *Functional alterations of G-proteins in diabetic rat retina: a possible explanation for the early visual abnormalities in diabetes mellitus.* Diabetologia, 1992. **35**(7): p. 624-31.
203. Kowluru, A. and R.A. Kowluru, *Subcellular localization and characterization of nucleoside diphosphate kinase in rat retina: effect of diabetes.* Biosci Rep, 1998. **18**(4): p. 187-98.
204. Kowluru, A., R. Veluthakal, and D.M. Kaetzel, *Regulatory roles for nm23/nucleoside diphosphate kinase-like enzymes in insulin secretion from the pancreatic islet beta cell.* J Bioenerg Biomembr, 2006. **38**(3-4): p. 227-32.
205. Kowluru, A., *Defective protein histidine phosphorylation in islets from the Goto-Kakizaki diabetic rat.* Am J Physiol Endocrinol Metab, 2003. **285**(3): p. E498-503.
206. Veluthakal, R., M.V. Suresh, and A. Kowluru, *Down-regulation of expression and function of nucleoside diphosphate kinase in insulin-secreting beta-cells under in vitro conditions of glucolipotoxicity.* Mol Cell Biochem, 2009. **329**(1-2): p. 121-9.
207. Arnaud-Dabernat, S., et al., *Knockout mice as model systems for studying nm23/NDP kinase gene functions. Application to the nm23-M1 gene.* J Bioenerg Biomembr, 2003. **35**(1): p. 19-30.
208. Boissan, M. and M.L. Lacombe, *Learning about the functions of NME/NM23: lessons from knockout mice to silencing strategies.* Naunyn Schmiedebergs Arch Pharmacol, 2011. **384**(4-5): p. 421-31.
209. Postel, E.H., et al., *Double knockout Nme1/Nme2 mouse model suggests a critical role for NDP kinases in erythroid development.* Mol Cell Biochem, 2009. **329**(1-2): p. 45-50.
210. Postel, E.H., et al., *Targeted deletion of Nm23/nucleoside diphosphate kinase A and B reveals their requirement for definitive erythropoiesis in the mouse embryo.* Dev Dyn, 2009. **238**(3): p. 775-87.
211. Zhou, X.B., et al., *Nucleoside diphosphate kinase B-activated intermediate conductance potassium channels are critical for neointima formation in mouse carotid arteries.* Arterioscler Thromb Vasc Biol, 2015. **35**(8): p. 1852-61.
212. Gross, S., et al., *Nucleoside diphosphate kinase B regulates angiogenic responses in the endothelium via caveolae formation and c-Src-mediated caveolin-1 phosphorylation.* J Cereb Blood Flow Metab, 2017. **37**(7): p. 2471-2484.

213. Qiu, Y., et al., *Nucleoside diphosphate kinase B deficiency causes a diabetes-like vascular pathology via up-regulation of endothelial angiopoietin-2 in the retina.* Acta Diabetol, 2016. **53**(1): p. 81-9.
214. MATSUMURA, T., et al., *Hyperglycemia increases angiopoietin-2 expression in retinal muller cells through superoxide-induced overproduction of [Alpha]-Oxoaldehyde age precursors.* Diabetes, 2000. **49**(5): p. A55-A55.
215. Qiu, Y., et al., *Mediation of FoxO1 in Activated Neuroglia Deficient for Nucleoside Diphosphate Kinase B during Vascular Degeneration.* Neuroglia, 2018. **1**(1): p. 19.
216. Shan, S., et al., *O-GlcNAcylation of FoxO1 mediates nucleoside diphosphate kinase B deficiency induced endothelial damage.* Sci Rep, 2018. **8**(1): p. 10581.
217. Kochanowski, N., et al., *Intracellular nucleotide and nucleotide sugar contents of cultured CHO cells determined by a fast, sensitive, and high-resolution ion-pair RP-HPLC.* Anal Biochem, 2006. **348**(2): p. 243-51.
218. Livak, K.J. and T.D. Schmittgen, *Analysis of relative gene expression data using real-time quantitative PCR and the 2(-Delta Delta C(T)) Method.* Methods, 2001. **25**(4): p. 402-8.
219. Findley, C.M., et al., *VEGF induces Tie2 shedding via a phosphoinositide 3-kinase/Akt dependent pathway to modulate Tie2 signaling.* Arterioscler Thromb Vasc Biol, 2007. **27**(12): p. 2619-26.
220. Arshavsky, V.Y., T.D. Lamb, and E.N. Pugh, Jr., *G proteins and phototransduction.* Annu Rev Physiol, 2002. **64**: p. 153-87.
221. Fuhs, S.R. and T. Hunter, *pHisphorylation: the emergence of histidine phosphorylation as a reversible regulatory modification.* Curr Opin Cell Biol, 2017. **45**: p. 8-16.
222. Besant, P.G. and P.V. Attwood, *Mammalian histidine kinases.* Biochim Biophys Acta, 2005. **1754**(1-2): p. 281-90.
223. Wehrle, C., P. Van Slyke, and D.J. Dumont, *Angiopoietin-1-induced ubiquitylation of Tie2 by c-Cbl is required for internalization and degradation.* Biochem J, 2009. **423**(3): p. 375-80.
224. Tuo, Q.H., et al., *Angiopoietin-1 protects myocardial endothelial cell function blunted by angiopoietin-2 and high glucose condition.* Acta Pharmacol Sin, 2011. **32**(1): p. 45-51.
225. Singh, H., N.P. Brindle, and V.A. Zammit, *High glucose and elevated fatty acids suppress signaling by the endothelium protective ligand angiopoietin-1.* Microvasc Res, 2010. **79**(2): p. 121-7.
226. Hansen, T.M., et al., *Effects of angiopoietins-1 and -2 on the receptor tyrosine kinase Tie2 are differentially regulated at the endothelial cell surface.* Cell Signal, 2010. **22**(3): p. 527-32.
227. Daly, C., et al., *Angiopoietins bind thrombomodulin and inhibit its function as a thrombin cofactor.* Sci Rep, 2018. **8**(1): p. 505.
228. Ruan, H.B., Y. Nie, and X. Yang, *Regulation of protein degradation by O-GlcNAcylation: crosstalk with ubiquitination.* Mol Cell Proteomics, 2013. **12**(12): p. 3489-97.
229. Qiu, Y., et al., *Mediation of FoxO1 in Activated Neuroglia Deficient for Nucleoside Diphosphate Kinase B during Vascular Degeneration.* Neuroglia, 2018. **1**(1): p. 280-291.
230. Potente, M. and P. Carmeliet, *The Link Between Angiogenesis and Endothelial Metabolism.* Annu Rev Physiol, 2017. **79**: p. 43-66.
231. Hawkins, M., et al., *The tissue concentration of UDP-N-acetylglucosamine modulates the stimulatory effect of insulin on skeletal muscle glucose uptake.* J Biol Chem, 1997. **272**(8): p. 4889-95.
232. Campochiaro, P.A. and K.G. Peters, *Targeting Tie2 for Treatment of Diabetic Retinopathy and Diabetic Macular Edema.* Curr Diab Rep, 2016. **16**(12): p. 126.
233. Campochiaro, P.A., et al., *Treatment of diabetic macular edema with an inhibitor of vascular endothelial-protein tyrosine phosphatase that activates Tie2.* Ophthalmology, 2015. **122**(3): p. 545-54.
234. Shen, J., et al., *Targeting VE-PTP activates TIE2 and stabilizes the ocular vasculature.* J Clin Invest, 2014. **124**(10): p. 4564-76.

235. Campochiaro, P.A., et al., *Enhanced Benefit in Diabetic Macular Edema from AKB-9778 Tie2 Activation Combined with Vascular Endothelial Growth Factor Suppression.* Ophthalmology, 2016. **123**(8): p. 1722-1730.
236. Thomas, M., et al., *Angiopoietin-2 stimulation of endothelial cells induces alphavbeta3 integrin internalization and degradation.* J Biol Chem, 2010. **285**(31): p. 23842-9.
237. Marshall, S., O. Nadeau, and K. Yamasaki, *Dynamic actions of glucose and glucosamine on hexosamine biosynthesis in isolated adipocytes: differential effects on glucosamine 6-phosphate, UDP-N-acetylglucosamine, and ATP levels.* J Biol Chem, 2004. **279**(34): p. 35313-9.
238. Weigert, C., et al., *Palmitate-induced activation of the hexosamine pathway in human myotubes: increased expression of glutamine:fructose-6-phosphate aminotransferase.* Diabetes, 2003. **52**(3): p. 650-6.
239. Cooksey, R.C. and D.A. McClain, *Increased hexosamine pathway flux and high fat feeding are not additive in inducing insulin resistance: evidence for a shared pathway.* Amino Acids, 2011. **40**(3): p. 841-6.
240. Ma, J. and G.W. Hart, *Analysis of Protein O-GlcNAcylation by Mass Spectrometry.* Curr Protoc Protein Sci, 2017. **87**: p. 24 10 1-24 10 16.
241. Chen, C.W., et al., *Two separate functions of NME3 critical for cell survival underlie a neurodegenerative disorder.* Proc Natl Acad Sci U S A, 2019. **116**(2): p. 566-574.